Title

Promoting Wound Healing by Engineering Enzyme-Responsive Delivery of Multiple Proteins and Amphiphilic Injectable Hydrogel

Author

Zhu, Suwei

Publication Date

2015

Peer reviewed|Thesis/dissertation

UNIVERSITY OF CALIFORNIA

Los Angeles

Promoting Wound Healing by Engineering Enzyme-Responsive Delivery of Multiple Proteins and Amphiphilic Injectable Hydrogel

A dissertation submitted in partial satisfaction

of the requirements for the degree Doctor of Philosophy

in Chemical Engineering

by

Suwei Zhu

2015

ABSTRACT OF THE DISSERTATION

Promoting Wound Healing by Engineering Enzyme-Responsive Delivery of Multiple Proteins and Amphiphilic Injectable Hydrogel

By

Suwei Zhu

Doctor of Philosophy in Chemical Engineering

University of California, Los Angeles, 2015

Professor Tatiana Segura, Chair

The growth of tissues and organs is regulated by orchestrated biological signals such as enzymes and growth factors (GFs). The ability to deliver biologics and small molecule drugs in response to these signals holds great promise for tissue repair and regeneration. This dissertation focuses on two aspects, enhancing angiogenesis and preventing infection, as therapeutic and prophylactic means to promoting wound healing.

Pro-angiogenic factors regulate the formation of new blood vessels and the renewal of vasculature after wounding, which is crucial for ischemic tissue repair. The mode of GF delivery has become increasingly important, as the narrow therapeutic window and threshold of GF dosage for normal angiogenesis is more and more clear. However the majority of delivery vehicles nowadays rely on hydrolysable scaffolds and thin films of protein-containing polymers

for constitutive GF release, which cannot be programmed to respond to biological signals. Here, a delivery platform based on enantiomeric protein nanocapsules is demonstrated, which enables controlled delivery of multiple proteins in response to wound proteases. Exemplified by stroke and diabetic wound healing in mice, sequential delivery of vascular endothelial GF (VEGF) and platelet-derived GF greatly enhances tissue revascularization and vessel maturation. Furthermore, the molecular mechanism for sustained released VEGF in enhancing angiogenesis was studied and revealed differential receptor activation and downstream signaling dynamics.

Meanwhile, delivery of hydrophobic drugs to diseased tissue (e.g. antibiotics to an infected wound) is a common therapeutic approach, although little has been done to combine hydrophobic drug release with a scaffold that could provide structural support and additional signals to promote tissue healing. Motivated as such, an injectable amphiphilic synthetic hydrogel is introduced that can effectively solubilize hydrophobic drugs while serving as a scaffold for tissue healing. This self-assembled hydrogel containing solubilized antiobiotics can also be coated as thin films on orthopaedic implants for anti-infectious arthroplasty operations.

The dissertation of Suwei Zhu is approved.

Andrea M. Kasko

Yunfeng Lu

Tatiana Segura, Committee Chair

University of California, Los Angeles

2015

Dedication

I dedicate this dissertation to my family.

Mom

Dad

Without all your love and support this dissertation would not have been possible.

TABLE OF CONTENTS

LIST OF FIGURES AND TABLES

ACKNOWLEDGEMENTS

The PhD dissertation is hardly the work of one individual alone. It would not have been possible without the support and guidance of so many individuals. First I would like to thank my mom. Mom, you have always provided me with the best moral support; and even though we cannot see each other most of the time in the past five plus four years, while I am in the United States and was in college, there has not been a single day where I have not thought of you, hoped for your well-being and aspired that one day soon I would be able to support for the family and to be by your side again. Han, you have been by my side since almost the beginning of my graduate school. You were the first friend I made at UCLA – in the lawn area in Weyburn Terrace before fall 2010. I have learned and grown so, so much from the stress and happiness in new environments, and you have been there for me, as I have for you.

I also want to thank Tatiana, an amazing professor, PhD mentor and role model for me. The rigorous academic training and professional advices you have been giving me in the past five years have really impacted how I do science and how I strive to do it well. While academic advisorship examples are too many to list, I find it equally enriching to learn the attitude towards life and work from you. You have always been encouraging and holding a positive attitude, under whose influence I gradually began to know how I could better express myself in life and in work. I am so lucky to have worked with you these last five years.

I also want to thank my friends and colleagues throughout these years. Leo and Quinn, I appreciate your advice on graduate school and PhD life for me; especially the coffee chats in Kerckhoff, the catching up in AICHE conference and the tour in Berkeley by Leo. Sean and Talar, I was really fortunate to have worked with you for some time in lab. You both were great lab mentors of different styles; and to date I still think the comradeship between you two is one

of the best I have seen and wished for. Shiva and Jon, you both have taught me different research techniques in lab, understood me from a senior grad student's perspective and helped me with my job search. One of the most fun things I will definitely miss is the laughs and "fights" between you two. Cynthia and Sandy, we have been through the ups and downs of grad school together for the longest amount of time; and I am really happy to have the friendship with you where we learn as we grow together. Don, Lina, Allyson and Juanjuan, I thank you for sharing with me not only knowledge but also life experience from PhD to post-doc experiences. You have/had great work in lab, possess good scientific minds and are very personable, all of which are admirable traits that have inspired me. Thank you to Giovanny, Nikki, Norman, Shayne, Victor, Elias, Jianjun and Anandika. You guys have been great labmates and have all become dear lab family members to me. I also cannot forget all the undergraduate and high school students I have worked with or known – Shannon, Angela, Alan, Eric -- for helping me grow in many different ways as a mentor.

I also would like to thank Prof. Robin Garrell, Laurie and Jia Ming for selecting me and guiding me in the Materials Creation Training Program (MCTP). I really believe this experience was a turning point in my career in graduate school, where I was given many, many opportunities to explore different aspects of academic training. Not only have I learnt a lot of chemistry and material applications, I also have made several good friends in other departments, with whom I still keep contact even after their graduation. Besides, I was given the chances to attend the prestigious Gordon Research Conferences in my 2nd year in graduate school and to gain experience from the internship at Novartis. Here I also want to acknowledge my amazing mentors at Novartis, Cornelia Forster and Dr. Christopher Brain. I was really fortunate to have worked with you and have got to know many of the great minds at Novartis through the

internship experience. Thank you both for giving me the freedom to propose and explore different ideas and the opportunities to share my work with others at Novartis. This internship was one of my favorite parts in graduate school.

To Dr. Lu, Dr. Liao and Dr. Kasko, thank you for serving on my committee. Dr. Lu, thank you for teaching me how to convey scientific ideas through writing research articles. I have listened to your polymer class, known of you from your exemplary students Juanjuan and Yang, and most importantly worked with you on writing research paper. The constructive criticisms you gave on my work and the conversation about how writing a paper is like creating a movie (just as how the title of a paper is like the name of a movie in attracting reader/audience's attention) are all enriching elements of my PhD study. Dr. Liao, thank you for being such an inspiring professor and a great chair for our department. I was really happy when I heard your lab became our neighbors on the 7th floor. The people in your lab are helpful and pleasant to interact with. The plate readers, gel-imaging machines and PCR thermocyclers are equipment that my research has often associated with. Thank you for letting me use your equipment. Additionally, you have fostered a great collaborative environment on the 7th floor with a shared cold room, autoclave, and pizza gatherings! Dr. Kasko, thank you for serving on my committee and as my co-advisor in my MCTP fellowship. You have given me insightful advice and comments on my research in polymer chemistry during my prospectus. Additionally, I would like to acknowledge Dr. Monbouquette, Dr. Chen, Dr. Hicks and Dr. Tang. Dr. Monbouquette, thank you for letting me be your TA for 104D and trusting me with your graduate students about my teaching notes. Dr. Chen, thank you for letting me use your equipment from time to time. You and your students are also very pleasant to interact with. Dr. Hicks, thank you for being a great professor/friend where you would sometimes challenge me with chemistry questions to

remind me of the fundamentals of Chemical Engineering. Dr. Tang, thank you for letting me use your HPLC and rotavap machines from time to time.

I would also like to acknowledge the collaborating professors, Dr. Carmichael, Dr. Bernthal and Dr. Miller. Thank you all for allowing me to explore the potential of my research in specific animal models that were developed in your lab. The people that I have worked with from your groups were very helpful, including Alexandra, Amanda, Jared and Sheriff.

I would like to thank Dr. Allyson Soon for helpful discussions in Chapter 2; graduate student Enbo Zhu in Prof. Yu Huang's lab for providing the techniques regarding solid-phase peptide synthesizer and HPLC for experiments related to Chapter 4; undergraduate researcher Angela Wong and high school researcher Eric Lin for their hard work on projects in Chapter 5 and Chapter 6; Dr. Talar Tokatlian, Dr. Sean Anderson for their mentorship on some experiments in Chapter 6; Dr. Juanjuan Du and Dr. Donald R. Griffin for their suggestions in the techniques in the synthesis in Chapter 7.

I also appreciate funding agencies for the work presented here, including the National Institutes of Health (NIH) grants no. R01NS079691 and no. R01HL110592, American Heart Association grant no. 11GRNT7630021AHA, and NSF IGERT: Materials Creation Training Program (MCTP) – DGE-0654431.

I would also like to thank Dr. William Lowry's research group and the California NanoSystems Institute (CNSI) for letting us use their cryostat and microtome instruments, the Electron Imaging Center for NanoMachines supported by NIH (1S10RR23057 to ZHZ) and the CNSI for the use of instruments. Additionaly, I would like to thank Genentech for generously providing the Segura Lab with recombinant human $VEGF_{165}$.

VITA

Education

B.S., Life Sciences (emphasis in biological sciences), Economics, Peking University, China 2010

Honors and Awards

2011-2013	NSF-IGERT Materials Creation Training Program (MCTP) Fellowship, UCLA
2013	1st place poster competition, Tech Forum of School of Engineering, UCLA
2013	Poster & presentation winner, UCLA-USC-Caltech Nanotechnology & Nanomedicine Symposium
2012	STAR Outstanding Abstract Award, Society for Biomaterials Symposium
2010	MCTP Bridge Program Fellowship, UCLA
2009	UM-PKU Chemistry Program Fellowship, University of Michigan
2008-2009	Chun-Tsung Scholarship and Research Grant, Peking University
2006-2007	Kwang-Hua Scholarship, Peking University

Research Experience

2010-2015 Graduate student researcher; Principal Investigator Tatiana Segura
Chemical & Biomolecular Engineering Department, UCLA
Research areas: Controlled protein delivery, ligand-receptor signaling pathways, engineering self-assembled polymers, and experience with skin wound healing models in normal and diabetic mice.

Fall 2012 Graduate student intern; Managers Cornelia Forster and Christopher Brain
Global Discovery Chemistry, Novartis Institutes for Biomedical Research
Research area: Engineering hydrogel systems for sustained release applications.

2008-2010 Undergraduate research assistant; Principle Investigator Ying Luo
Department of Biomedical Engineering, Peking University
Research area: Engineering controlled formation of hydrogel microspheres for endothelial cell cultivation.

Summer 2009 Undergraduate research assistant; Principle Investigator Kenichi Kuroda
School of Dentistry, University of Michigan
Research area: Anti-microbial polymer films for dental implant coating

Peer-Reviewed Publications

1. **Zhu, S.**, Nih, L., Carmichael, S.T., Lu, Y. and Segura, T., "Enzyme-responsive delivery of multiple proteins with spatiotemporal control", *Advanced Materials* (2015), in press.

2. **Zhu, S.**, Segura, T., "Hydrogel-based nanocomposites of therapeutic proteins for tissue repair", *Current Opinion in Chemical Engineering* (2014) 4:128–136.

Patent application

1. Segura, T., **Zhu, S.**, Wen, J. Lu, Y., "Enzyme Responsive Nanocapsules for Protein Delivery", #WO2013033717 A1, filed in 2012, published in 2013.

Podium presentations (* represents presenting author)

1. **Zhu, S.***, Lu, Y., Segura, T., "Sustained & Cell-demanded Release of Vascular Endothelial Growth Factor from Nanocapsules for Angiogenesis", UCLA-USC-Caltech Nanotechnology & Nanomedicine Symposium, Los Angeles, 2013
2. **Zhu, S.***, Lu, Y., Segura, T., "Synchronized Delivery of Vascular Endothelial Growth Factor With Protease Cues Sustains Activation Toward Vessel Formation", American Institutes of Chemical Engineers Annual Meeting 2013, San Francisco, CA.
3. **Zhu, S.***, Segura, T., "Cell-responsive and Sustained Release of Growth Factor from Protease-sensitive Nanocapsules", Society for Biomaterials Annual Symp. 2012, New Orleans, LA.
4. **Zhu, S.***, Luo, Y., "Investigating Hyaluronic-acid Hydrogel Microspheres as Three-dimensional Bioscaffold", China's National Conference on Biomaterials 2010, Chengdu, China
5. Niska, J.*, **Zhu, S.**, et al. "Controlled Release of Vancomycin and Tigecycline from an Orthopaedic Implant Coating Prevents *Staphylococcus aureus* Infection in an Open Fracture Animal Model", Western Orthopaedic Association Annual Meeting, 2014.
6. Stavrakis, A.*, **Zhu, S.**, et al. "*A Novel Antibiotic Coating In Preventing Periprosthetic Infection*", Western Orthopaedic Association Annual Meeting, 2015.

Poster Presentations (* represents presenting author)

1-3 **Zhu, S.***, Lu, Y., Segura, T., "Sustained & Cell-demanded Release of Vascular Endothelial Growth Factor from Nanocapsules for Angiogenesis", (1) UCLA-USC-Caltech Nanotechnology & Nanomedicine Symposium, 2013; (2) Tech Forum of Engineering School, UCLA 2013; (3) Gordon Research Conferences – Bioinspired Materials, 2012.
4. **Zhu, S.***, Palermo, E., Sovadino, I., Kuroda, K., "Layer-by-layer Deposited Antimicrobial Polymeric Surface", Summer Undergrad. Research Regional Symposium, 2009.

Teaching and Mentoring Experience (F=fall, W=winter, S=spring, Su=summer quarter)

S11, F13, S14	CBE 104D "Molecular Biotechnology Laboratory: From Gene to Product"
Su11-W15	Graduate research mentor, Segura Laboratory, UCLA

CHAPTER 1:

OVERVIEW OF DISSERTATION AND SPECIFIC AIMS

1.1 MOTIVATION AND OBJECTIVES

Since the discovery of insulin in the 1920s, protein-based therapeutics have been investigated for suitable routes of delivery and extended biological half-life [1]. Recently advanced techniques have been developed to enhance the efficiency of protein or peptide drugs for use in preventing and treating human injury and a number of life-threatening diseases. Growth factors (GFs) in particular are attractive candidates because of their unique roles in signaling cells and regenerating tissues. There are currently over 6,000 clinical trials regarding the use of growth factors (Figure **1**).

When using GFs as candidate drugs, controlled and therapeutic delivery of these proteins is of pivotal importance for medicinal and economical reasons. Particularly in the case of multiple protein delivery, the order, location and duration of the release of each protein need to be carefully designed for the most therapeutic benefit.

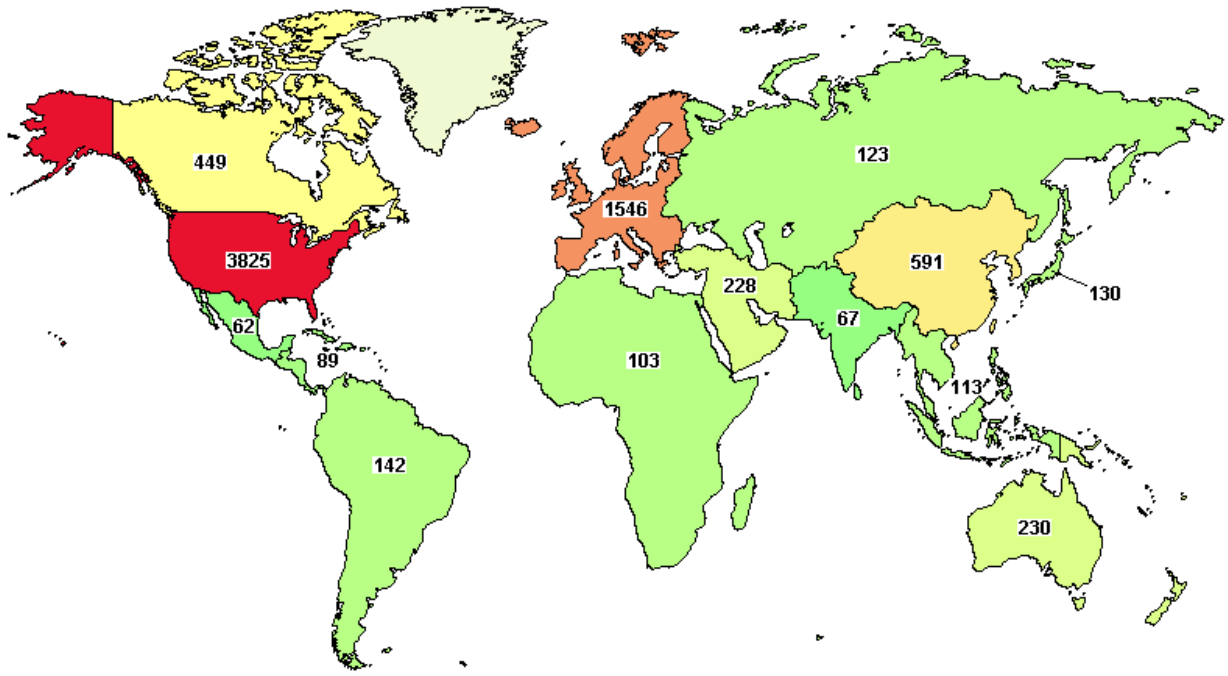

Figure 1 Clinical trials of growth factors worldwide as of May 2015. (Source: http://ClinicalTrials.gov).

Current multi-protein delivery strategies mainly rely on hydrolysable scaffolds and thin films of protein-containing polymers, which cannot be programmed to respond to biological signals. For example, existing approaches to achieve either sustained release or sequential release of proteins rely on polymer hydrolysis or passive leaching. The Langer Laboratory at MIT pioneered the most successful example of this type of delivery, with proteins entrapped within poly lactic-co-glycolic acid (PLGA) scaffolds that are released as the polymer hydrolyses [2]. The Mooney group at Harvard University expanded this approach to allow sequential delivery of two proteins through differential entrapment methods[3]. Recent development includes the hybrid polymer matrices with different degrading rates, barrier polymer films [4] for sequential delivery or orthogonal binding pairs to allow for multiple protein release, resulting in poor temporal control.

However, these developments for ordered delivery of multiple proteins have certain limitations. First, the release is driven by hydrolysis; therefore it is not responsive to the biological milieu and may not be adaptive to the pathological development of tissues. Second, in existing approaches, the incorporation of proteins into polymer matrices generally involves intense mixing and/or use of organic solvents; and only certain polymers are used (i.e. PLGA, PLA). Such harsh chemical processes can easily denature the proteins, precluding their use as a general delivery vehicle. Last, in previous attempts to achieve enzyme-responsive delivery of proteins from one scaffold, existing approaches are generally limited by the types and the number of available orthogonal-binding functional groups in the composition of the scaffold.

In light of these developments and limitations, the ***first objective*** of this dissertation is to develop a platform technique for general enzyme-responsive delivery of multiple proteins. Since the spatiotemporal levels of proteases are highly regulated by the pathophysiological state in diseased tissues, we believe that by realizing enzyme-responsive delivery in either sustained or sequential mode, the spatiotemporally defined delivery of multiple proteins can be achieved.

Angiogenesis is the physiological process of the formation of new blood vessels from pre-existing ones. Blood vessels form vasculature network that reaches every part of a human body, with a depth from skin surface as small as 1 mm. When wounding occurs, blood vessels are shattered; thus, the regeneration of blood vessels, angiogenesis, is an important process of wound healing. Vascular endothelial growth factor (VEGF) directly mediates the proliferation, migration and sprouting of endothelial cells; therefore it is the mediator for inducing revascularization in ischemic tissue. Despite several clinical trials of recombinant protein or gene transfer of VEGF [5,6], the delivery has not been successfully translated into approved therapies.

Although sustained VEGF delivery has been shown to outperform bolus delivery of the same growth factor for the promotion of angiogenesis and improved therapeutic outcome in vivo [5,6], the mechanism by which this improvement occurs is poorly understood.

In light of this circumstance, the ***second objective*** of this dissertation is to understand how, if true, the cells sense differently between bolus VEGF and sustained released VEGF, in order to find the missing link between sustained ligand delivery and beneficial cellular response.

Along similar lines of wound healing, hydrogels have played a significant role in wound care for over 20 years. Among all, injectable hydrogels have a major advantage of ensuring an even coverage of deeper or uneven wounds. The natural extracellular matrix (ECM) is primarily a self-assembled network, allowing cells *in vivo* to navigate and modulate the environment. In tissue engineering, cell culture in three dimensions (3-D) has been made possible with scaffolds of hydrogels, and delivery of cells, biomacromolecules and small molecule drugs in such matrices is a promising therapy in regenerative medicine. A large emphasis has been placed on covalently crosslinked hydrogels where matrices can undergo proteolytic degradation as tissue endogenous proteases accumulate to allow cellular migration and spreading with a variety of applications including bone [7,8], vascular tissue [9] and cartilage [10]. However, a change in mechanical properties with time of these hydrogels as they degrade makes it challenging to decouple biochemical cues from mechanical cues in understanding and guiding cellular behaviors. Further, the rapid gelation time of covalent crosslinking or the requirement for external triggers to induce gelation has limited the injectability of hydrogels and facileness for delivery of therapeutics in minimally invasive approaches.

Physically associated hydrogels have broadened the spectrum of biomaterials from rigid scaffolds to interactive networks. The spontaneous and reversible organizations of molecular units by non-covalent, "weak" interactions give rise to physically associated hydrogels of many kinds: ionically chelated [11], crystallite assisted [12], hydrogen bonded [13], amphiphilic driven [14], peptide/protein interacted [15], and even DNA-based hydrogels [16]. Dynamic bondings and molecular interactions provides access to shear-thinnable and injectable network [17].

Small molecule drugs make up over 90% of current medicine. The active ingredients of these drugs often render the compounds hydrophobic. For example, the anti-microbial agent, Tetracycline, can be used in preventing infection during skin wound healing [18]. Without being sufficiently solubilized, drug candidates may undergo crystallization and result in acute toxicity.[19] On the other hand, local interactions between small molecules and tissues rely on the proximate bioavailability of these drugs to induce cells in the three-dimensional milieu. Penicillin, for example, was shown more effective when applied locally than via systemic intramuscular administration in the treatment of corneal microbial infections, due to the localized concentration of the drug reached at the infection site. [20] Although numerous block copolymers have been devised for drug loading and delivery in the form of micelles (using amphiphilic block copoloymer such as Pluronics [21]) or nano/microparticles (made from PLGA polymer), these particulate sizes of delivery vehicle only covers the surface of wound cavity. Incorporating these particles into bulk hydrogel may allow for cell infiltration in a structurally supported biocompatible environment, but it is an inconvenient two-step process.

In order to combine hydrophobic drug release with an injectable scaffold that could provide structural support and additional signals to promote tissue healing, we propose the ***third objective*** of this dissertation to be optimizing branched, amphiphilic block copolymer, 4 arm

poly(ethylene glycol-polypropylene sulfide), (PEG_{113}-*b*-$PPS_x)_4$, for the delivery of hydrophobic molecules both as a wound cavity dressing material and as a coating materials for medical implants.

1.2 SPECIFIC AIMS

1.2.1 SPECIFIC AIM 1 (CHAPTER 5)

This aim developed protease-sensitive protein nanocapsules with engineered peptide chirality in the shell for sustained delivery of one protein and sequential delivery of two proteins in vitro and in vivo. Specifically vascular endothelial growth factor 165 and platelet derived growth factor BB were optimized for promoting vascularization in dermal wound healing models and an ischemic stroke model in mice.

Hypothesis 1: Protein nanocapsules with shells that are crosslinked by D-chiral peptides will slow down the protease-mediated degradation of nanocapsules compared to L-chiral nanocapsules, thus delaying the release of proteins. By mixing protein nanocapsules of different surface chirality, the enzyme responsive sustained and sequential delivery of proteins can be achieved.

1.2.2 SPECIFIC AIM 2 (CHAPTER 6)

This aim investigated sustained released VEGF in comparison to bolus delivered VEGF for conveying differential receptor responses to endothelial cells and how the sustained VEGF delivery can lead to enhanced angiogenesis in murine dermal wounds.

Hypothesis 2: Sustained released VEGF, either by pipetting in small quantities of naked VEGF over time or through the use of our bioengineered VEGF nanocapsules, is capable of

maintaining receptor activation over time. This extended receptor activation is associated with the sprouting of endothelial cells in vitro and angiogenesis in vivo.

1.2.3 Specific aim 3 (Chapter 7 and 8)

This aim studies the shear-thinning properties and the capability to solubilize hydrophobic compounds of 4-arm branched $(PEG\text{-}PPS_x)_4$. Therefore the potential of this self-assembled hydrogel is assessed as a depot for drug release in the forms of a wound dressing filler material and thin films for orthopaedic implant coatings. Hydrophobic propylene sulfide can be oxidized to hydrophilic propylene sulfone.

Hypothesis 3: By increasing the x from 2.5 to 16, $(PEG\text{-}PPS_x)_4$ becomes more hydrophobic and it forms stiffer hydrogel when solvated in aqueous solution. It can also solubilize and retain hydrophobic drugs within the hydrogel in vitro and in vivo.

Hypothesis 4: Drug-impregnating $(PEG\text{-}PPS_x)_4$ can be chemically grafted and physically self-assembles on titanium surfaces, which releases the antimicrobial drugs via both passive elution and active oxidation-accelerated mode.

1.3 Dissertation outline

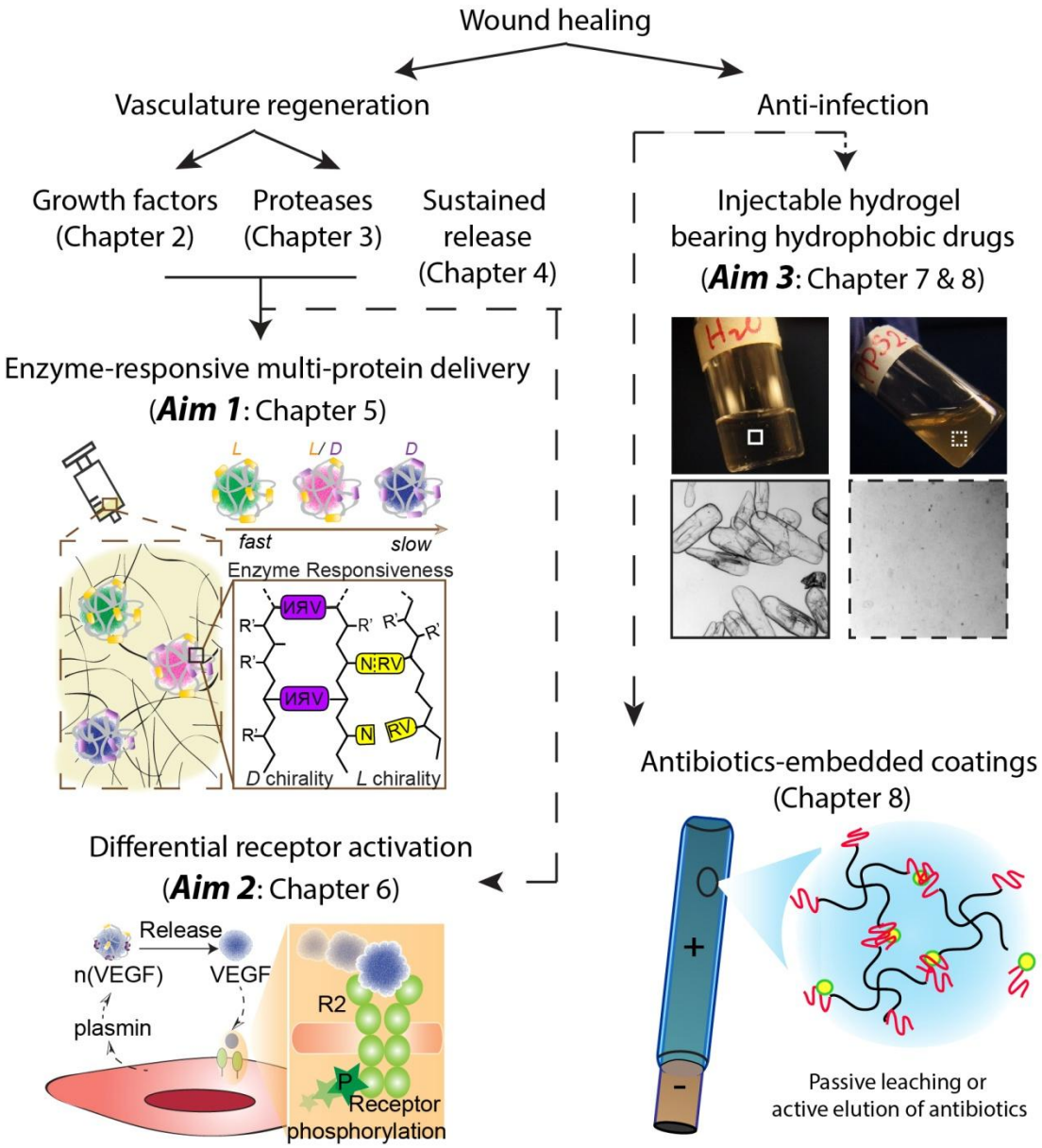

Figure 2 Outline of dissertation.

CHAPTER 2:

GROWTH FACTOR THERAPEUTICS AND THEIR USE IN TISSUE ENGINEERING

2.1 HISTORY, CURRENTLY IN-TRIAL AND APPROVED THERAPEUTICS

Since the discovery of insulin in the 1920s, protein-based therapeutics have been investigated for suitable routes of delivery and extended biological half-life [1]. Particularly growth factors (GFs) are attractive candidates because of their unique roles in signaling cells and regenerating tissues [22-24].

Current GF-based therapies in clinical trials are listed below (Table 1).

Table 1 Representative clinical trials for GF-based therapies for tissue repair as of 2014.

Source: http://www.clinicaltrials.gov

Condition	Application	GF type	GF carrier	Route	Phase	Sponsor
Periodontitis (inflammation of tooth bone or ligaments)	Alveolar bone increase rate	bFGF[a]-2	3% solution of hydroxypropylcellulose	Injection during flap operation	3	Kakan
Melanoma(IV)	Suppressing plasma FGF	Interferon alpha-2b	PEG[b]-ylated	weekly SC[c]	2	Eastern Cooperative Oncology Group
Heart failure (ischemic cardiomyopathy)	Autologous cardiac-derived stem cell	bFGF controlled release	Gelatin hydrogel sheet	Intra-myocardial injection	1	Naofumi Takehara
		Ad-HGF[d]		Trans-endocardial injection	1/2	Jiangsu Province Hospital
		IGF[e]-1 (mecasermin)	0.9 % NaCl solution	Intracoronary injection	1/2	University College Cork
		hVEGF[f]-165	Mini-thoracotomy	intramyocardial injection	2	Instituto de Cardiologia do

						Rio Grande do Sul
Neuropathic diabetic foot ulcer	Wound closure	bFGF (Trafermin)	Spray	Topical	3	Olympus Biotech
		EGF[g]			3	Daewoong Pharmaceutical
Venous leg ulcer		5-amino acid deleted rhHGF (CHRONSEAL®)		Topical	1/2	Kringle Pharma
Burn wound		EGF	Silver sulfadiazine cream	Topical	2/3	Chulalongkorn University
	Complete healing of 3rd degree thermal electrical burn	rhPDGF[h] (R-Pdf/Gbb)	0.01% gel	Topical	2	American Scitech International, Johnson & Johnson
Cartilage injury repair	knee	Human FGF18 (AS902330)		Weekly intra-articular injection	2	Merck KGaA
lateral epicondylitis (soreness or pain on the outside of the upper arm near the elbow)	Tennis elbow	rhPDGF	sodium acetate buffer	injection	2	BioMimetic Therapeutics
Tendon injury	Rotator cuff	rhPDGF	Fibrin matrix	Local during surgery	3	Hospital for Special Surgery, New York
Skin lesion	Rash side effect from Erlotinib	EGF	ointment	Topical	2	Dong-A University Hospital
Oral Mucositis	Preventive during chemotherapy	EGF	With povidone iodine, chlorhexidine, & nystatin	Topical twice daily	2	Seoul National University Hospital
Fulminant hepatic failure	Unable to receive liver transplantation	rhHGF			1/2	Kyoto University
Hepatitis C-related cirrhosis	Hepatocellular Carcinoma Prevention	Interferon alfa-2b	pegylated		3	Schering-Plough
22q13 Deletion Syndrome; RETT Syndrome	Children	IGF-1		SC injection	2	Mount Sinai School of Medicine; Children's Hospital Boston
Idiopathic Short Stature		r-hGF (Saizen®)		SC	3	Merck KGaA
Prevent autoimmunity	Promote thymic T cell	KGF[i] (Palifermin (Kepivance®))	Bolus	IV[j] injection	1/2	Cambridge University Hospitals NHS Foundation Trust
Lung	Airway endothelium; Asthma treatment	KGF	Bolus “collapsed”	IV injection	2	University Hospital Southampton

						NHS Foundation Trust
Brain	Improve neurological function	NGF[k]		Intranasal	2	Jinling Hospital, China
Eye	Neurotrophic keratopathy	KGF		Eye drop	1/2	Dompé s.p.a.
Stroke	Preventive	E-selectin		Nasal	1	NINDS[l]
Bone	Stimulate ossification	BMP[m]-2	Collagen type 1	Local injection	1	Northern Orthopaedic Division, Denmark

Abbreviations: a. fibroblast growth factor, b. polyethylene glycol, c. subcutaneous, d. hepatocyte growth factor, e. insulin-like growth factor, f. vascular endothelial growth factor, g. epidermal growth factor, h. platelet-derived growth factor, i. keratinocyte growth factor, j. intravenous injection, k. nerve growth factor, l. national institute of neurological disorders and stroke, m. bone morphogenetic protein.

U.S. Food and Drug Administration (US FDA) has approved several growth factor related products for promoting wound healing. Dermagraft®, a human fibroblast-derived dermal substitute, was approved in 2001 for use in the wound closure of diabetic foot ulcers. It is composed of human fibroblasts, an extracellular matrix, and a bioabsorbable polyglactin mesh scaffold that secrete interleukins, IL-6 and IL-8, and other growth factors at wound bed. Repeated applications of Dermagraft® provide the wound with a clean, healthy dermal layer. Regranex® is the first growth factor based product approved by FDA, which contains 100 μg/g of rhPDGF-BB in an aqueous based gel. The use of Regranex® is to promote healing of full thickness, lower extremity, neuropathic diabetic ulcers that have adequate blood supply.

2.2 Structural-Function Analysis

Alternate splicing variants

The central dogma of biology explains that DNA is the genetic material which codes for RNA, which subsequently codes for proteins. A single gene can give rise to several forms of

proteins through alternative mRNA splicing, and these distinct isoforms carry out different biological functions.

Human vascular endothelial growth factor (VEGF), as an example, is a secreted mitogen that acts on endothelial cells and affects vascular biology. It has six isoforms as a result of the difference in the presence or absence of sequences encoded by exons 6 and 7 (Figure 3). The importance of the splice variants lies in their ability to interact with cell-surface components and the extracellular matrix.

Alternatively, platelet-derived growth factor (PDGF) is another major mitogen for connective tissue cells and other cell types. It is a dimeric molecule consisting of either homodimeric or heterodimeric forms of A- and B-polypeptide chains (Figure **4**). The consequent cellular effects are different depending on which protein tyrosine kinase receptor is activated. Similarly, splice variants exist, i.e. a cell-retention signal piece is present in the B-chain and in the long splice version the the A-chain [25].

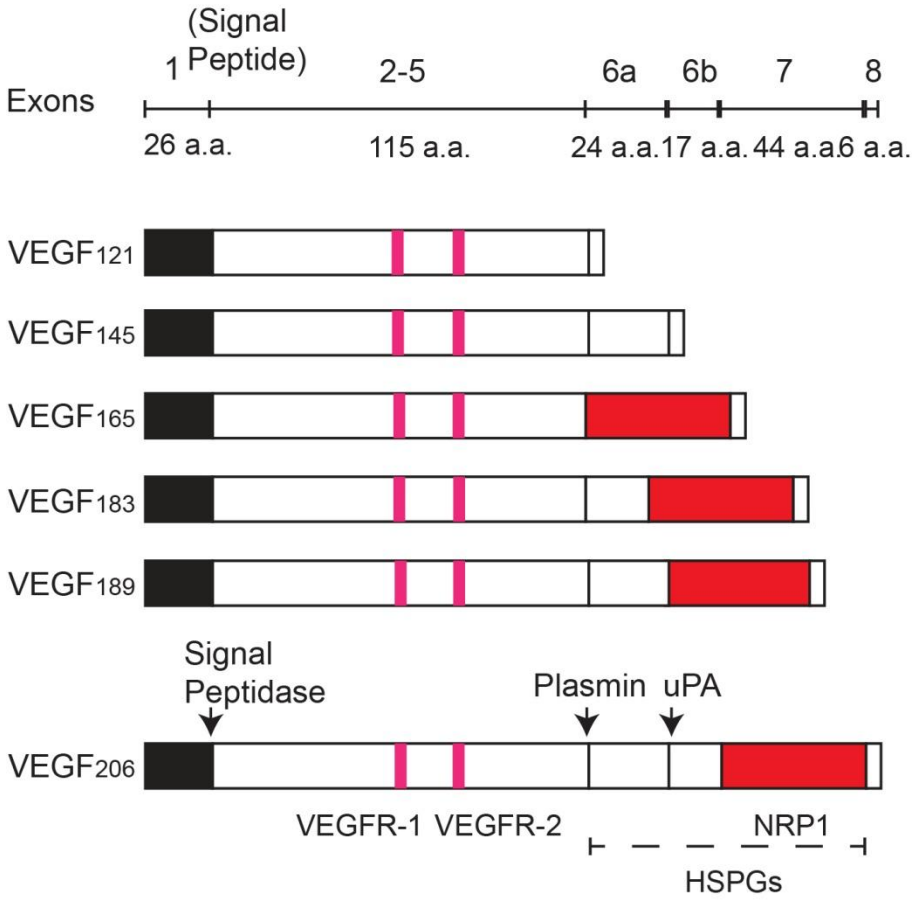

Figure 3 The splice variants of human VEGF (modified and redrawn from C.J. Robinson and S.E. Stringer 2001 [26]). Sites of interaction with VEGF receptors (VEGFRs), coreceptor neuropilin-1 (NRP1) and heparin sulphate proteoglycans (HSPGs) are indicated on the VEG_{206} isoform, as are certain enzyme cleavage sites.

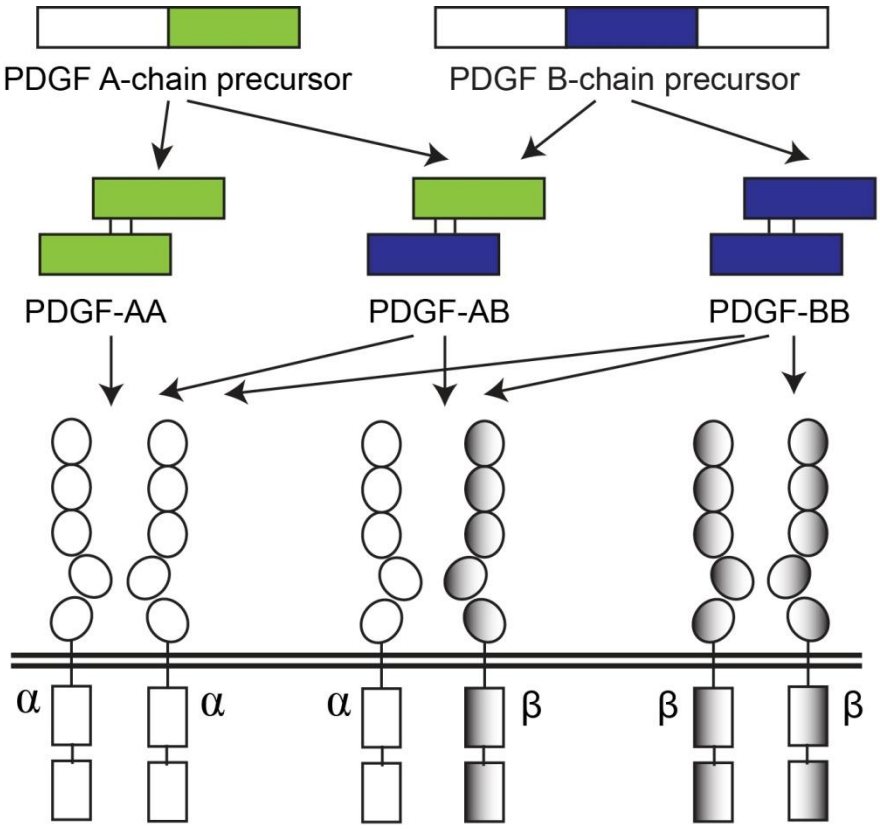

Figure 4 Processing and action of PDGF isoforms (modified and redrawn from C-H Heldin and B. Westermark 1999 [27]). A- and B-chains of PDGF are produced from precursor molecules, and they form disulfide-bonded dimers, which bind to and dimerize α- and ß-receptors with different specificities.

Other important structural factors of growth factors include their surface charge, hydrophobicity and size (molecular weight). **Table 2** summarized the reported isoelectric points and the molecular weights of several common growth factors. These physical properties of growth factors will lay the foundation for research in growth factor delivery via protein nanocapsules (Chapter 5).

Table 2 Structural features of major families of growth factors related to wound healing.

Acronym	**Isoelectric point**	**Molecular weight**	**Mode of actions**	**Refs**

VEGF	8.5	20,000 - 45,000	Autocrine and paracrine.	[28]
PDGF	8.5-10.5	24,000 – 31,000	Secreted outside cells; Endocrine or paracrine/autocrine.	[29,30]
Angiopoietin	5.6 – 8.3	56,000 – 70,000 (monomer)	Autocrine/paracrine	[31]
Transforming growth factor, TGF-ß	8.5 – 9.5	25,000 - 44,000	Paracrine/autocrine	[32,33]
bFGF	8 - 10	16,000 – 18,500	Cell-membrane bound, or matrix bound	[34,35]
aFGF	5 - 7	15,000 – 18,000	Paracrine/autocrine	[36]
Epidermal growth factor, EGF	4.60	6,100	Autocrine, paracrine, juxtacrine and/or endocrine	[37,38]

2.3 PHYSIOLOGICAL AND PATHOLOGICAL AVAILABILITY OF GROWTH FACTORS

Through reverse transcription polymerase chain reaction analysis, Corral et al have observed a 6- to 7-fold increase in the mRNA expression of VEGF in both normal and ischemic rabbit ear dermal ulcer wounds, which was seen at day 1 and persisted for 10 days after wounding [39]. Specifically, ischemic wounds upregulated VEGF mRNA expression 3- to 5-fold over nonischemic skin. Although the endogenous level of VEGF was upregulated after skin wounding, single-dose treatment of rabbit ear wounds with either exogenous VEGF121 or VEGF165 at 30 µg per wound improved granulation tissue formation. In ischemic wounds, VEGF121 and VEGF165 improved the formation of granulation tissue by 100% and 150% at day 10, respectively; in nonischemic wounds, they improved the formation by 50% and 70%, respectively [39].

Although improved angiogenesis and formation of granulation tissue is seen with exogenous VEGF, it requires prolonged exposure to wound cells. Therefore repeated dosing or sustained slow release vehicles is commonly seen in VEGF delivery systems. Moreover, excess VEGF may lead to complications, as evidence suggests that the increased serum level of VEGF is responsible for the anasarca and edema[40]. For the purpose of this dissertation, VEGF165 isomer is chosen since it is readily available and seems to the most biologically active in vivo – no less than other isoforms [41].

Through western blot analysis, Soma et al have identified PDGF-AA homodimer as the predominant isoform in human platelets and acute human wound fluid; in contrast, no PDGF B-chain was detected from 6 to 18 hours post surgery [30]. It was indicated that 15 – 20 ng/mL of PDGF A-chain is present in as early as the 6-hour time point. Moreover, Beer et al have observed reduced expression of PDGF and PDGF receptors during impaired wound healing [42]. Although both the PDGF ligands and their receptors were expressed in normal and wounded skin, no significant induction of these genes was found to the author's surprise. Additionally, in healing-impaired, genetically diabetic db/db mice, there was a significant reduction in PDGF A, PDGF B and their respective receptor expression in non-wounded and wounded skin.

These results started to shed light on the beneficial effects of exogenous PDGF-BB in the treatments of wound-healing disorders.

2.4 DIFFERENT STRATEGIES OF GROWTH FACTOR PRESENTATIONS

Understanding how the physical presentation and cooperative/synergistic association of these proteins, as well as how the topology and adhesiveness of the underlying matrices can impact cellular fates, may hold the key to favorable therapeutic outcomes. Initial approaches

have utilized polymeric scaffolds to vary the temporal availability of growth factors [3], recombinant engineering to create hybrid modalities [43] and synergistic association [44]. Critical issues in protein therapy include protein stability, bioavailability, multivalency, delivery, and presentation. Current advances in protein-based nanomaterials have been proposed to overcome these limitations.

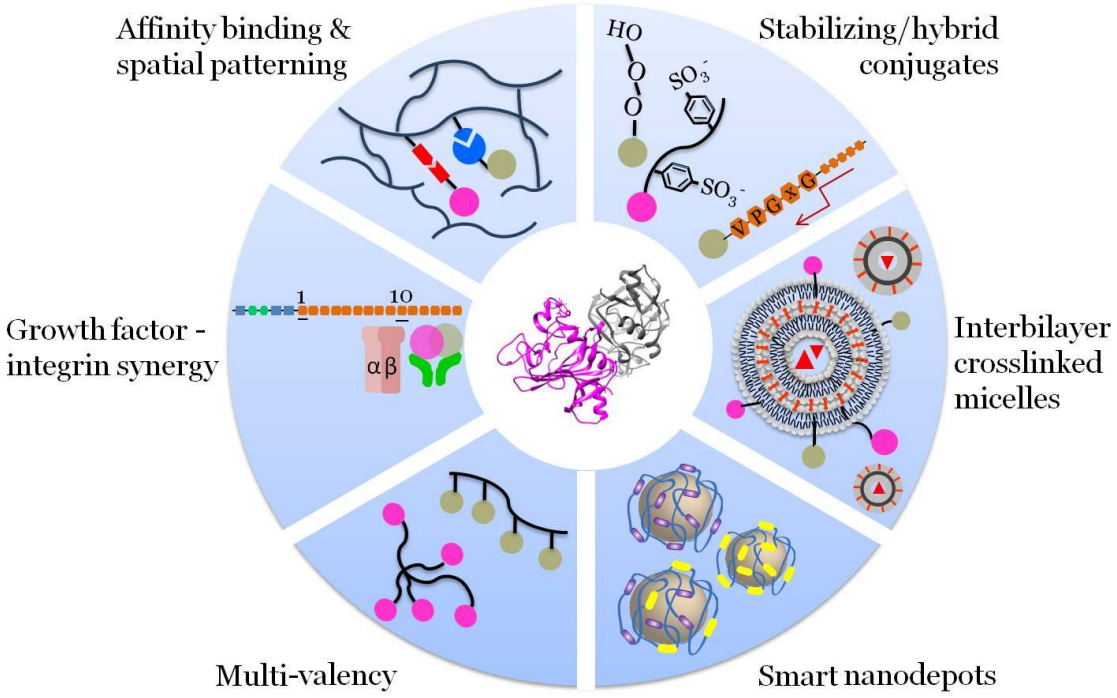

Figure 5 Recent advances in nanotechnology to address the leading challenges in the applications of protein-based therapeutics. Segments are divided according to the order of appearances of the corresponding paragraphs in this paper and are clockwise oriented in this figure starting from the upright position. See text for detailed description and references.

2.4.1 Approaches to increase long-term activity

Widely used in polymer conjugation, the attachment of poly(ethylene glycol) to proteins, termed PEGylation, improves the stability and lowers the immunogenicity of modified proteins, yet preserving the bioactivity for the long-term is still challenging with most random PEGylation

approaches. Strategies to introduce polymerization sites at specific sites within a protein have been reported. Specific N-terminal amine modification based onits different p*K*a from the lysines on the side chains of protein surfaces was used for *in situ* atom transfer radical polymerization (ATRP) of PEG-like conjugates [45]. In an alternative approach, posttranslational protein splicing was used to insert an intein, the cleavage of which would provide a thioester moiety for the initiation of ATRP on the C-terminus of proteins to also polymerize a PEG-like polymer [46]. Intravenous injection of these conjugated proteins showed a 15- to 40-fold increase in their blood exposure than the unmodified proteins, and demonstrated tumor accumulation via the enhanced permeability and retention effect [46]. Beyond the scope of PEGylation, site-selective modifications of proteins have been demonstrated with enzymatic transformation, i.e. protein prenylation, and chemospecific chemical modifications at the end terminus with pyridoxal 5'-phosphate [47]. Polymers mimicking the polysaccharide heparin when conjugated to basic fibroblast growth factor can preserve the bioactivity of this heparin-binding protein to stimulate proliferation of fibroblasts under a variety of stressors [48]. Zwitterionic polymers have also been introduced to conjugate proteins to increase their stabilities and it results in an improved binding affinity due to protein-substrate hydrophobic interactions [49]. Besides polymeric conjugation, techniques such as fusion protein chimeras with thermally sensitive peptides and non-covalent encapsulations of proteins into nanocomposites also preserve the activity of proteins [50,51].

2.4.2 Approaches to control bioavailability

Retaining protein agents in hydrogel depots offers a locally concentrated reservoir for the long term delivery of therapeutics, ideally at a rate that coordinates with the pathological state of tissues.

Motivated by promoting long term availability of bioactive signals and therapeutics, direct tethering of peptide or protein molecules has been applied on engineered surfaces [52], three-dimensional hydrogel scaffolds [53] and nanoparticles [54]. Dynamic microenvironment of RGD adhesive peptides affects myogenic differentiation of myoblasts when photoactivatable peptides are functionalized on 2-D surfaces [52]. Tethering anti-inflammatory proteins on the surfaces of particulate nanocomposites prevents rapid clearance after intra-articular delivery to modulate osteoarthritis. An alternative to the direct tethering is to immobilize protein-binding molecules for target proteins to adhere via intrinsic affinities. Block copolymer-heparin conjugates were shown to complex into micelle structure for the retention and delivery of growth factors [55]. Single-stranded nucleic acids with high affinities to proteins, called aptamers, have also been incorporated into polymeric backbone to retain and prolong the release of proteins [56].

Thermally responsive conjugates on the proteins allow for the *in situ* formation of protein-depot composites upon temperature change, i.e. subcutaneous injection. For example, elastin-like peptides (ELPs) have been engineered to generate recombinantly fused protein-ELP chimeria nanoparticles [57] and injectable depots [43]. ELPs are composed of a tandemly repeated sequence, $(Val\text{-}Pro\text{-}Gly\text{-}X\text{-}Gly)_n$, derived from the precursor and soluble form of elastin, which undergo a phase transition from an extended soluble structure to a collapsed insoluble one above its transition temperature. Elastin also has an intrinsic biological activity in inducing the proliferation of fibroblasts. As such, reserving growth factors in a smart injectable depot not only enables sustained release of protein therapeutics but also allows for seamless filling of tissue cavities.

Polymeric nano/micro spheres have been used in the development of a number of products in the market based on polylactide (PLA) and its copolymer with glycolide (PLGA).

The clinical and commercial success of the first parenteral sustained-release formulation, Lupron Depot® utilizing PLA, propelled extensive studies and the resulted booming patents on the delivery of proteins using polymeric delivery systems. However, hydrolytically mediated extended release takes little consideration of the cellular microenvironment (i.e. pH or protease levels). In addition, the acidic environment from PLGA degradants and the hydrophobicity of the polymer may render proteins to deactivate. As such, other delivery systems have advanced to get around those limitations.

Liposomes are a widely used lipid bilayer platform to encapsulate drugs and vaccines with a number of clinically proven formulations. Assembled by the entropic driving force, this vesicle material raises concerns regarding its chemical and mechanical stability. A recent development by the Irvine group has covalently crosslinked the lipid headgroups across the opposing faces of adjacent bilayers with a pH-sensitive small compound, dithiolthreitol, within the vesicle walls, forming interbilayer-crosslinked multilamellar vesicles (ICMVs) [58]. The utility of these submicrometre-particle reagents was exemplified by entrapping protein antigens in the vesicle core and lipid-based immunostimulatory molecules in the vesicle wall, generating subunit vaccines which elicited strong T-cell and antibody response, i.e. ~1000 times and ~10 times greater humoral response than soluble antigen and non-crosslinked multilamellar vesicle immunizations in mice [59].

Another core-shell design to protect protein agents from environmental attacks and denaturations is to encase them in thin shell nanocapsules weaved with polymeric nano-sized matrices. Our laboratory has demonstrated the release of a single or multi-factorial proteins from these nanocapsules due to their degradable shell compositions that allow for the incorporation of a variety of environmental cues [51]. This platform has been successfully applied to encapsulate

functional enzymes [60-65], growth factors [51] and even siRNA [66] with a number of advanced features, i.e. an enhanced and extended bioactivity, a specific cytoplasmic or extracellular delivery, a sustained release efficacy and flexible application routes of subcutaneous injection or embedded within scaffolds. Protein cargos can be either pre-modified or non-covalently entrapped within an *in situ* interfacial polymerized shell matrix. Different modalities have been included as release triggers to attain a cell-regulated long term delivery, such as intracellular or extracellular proteases, redox environments and photo-activations. Remarkably, release rates can be facilely tuned resulting in a differential delivery of intact cargos from these nano-reservoirs; and for the first time complementary protein complexes have been precisely assembled within these robust yet permeable thin shell matrices to greatly improve therapeutic efficiency, which opened up endless possibilities for the creation of novel molecular machineries.

2.4.3 ENGINEERING MULTIVALENCY OR INCREASED PROTEIN DENSITY

Nano-scale clustering of ligands can potentiate their binding abilities with receptors resulting in a signaling alteration and practical utilities, i.e. reducing dosage concentrations thus bringing down the cost. A biomolecular engineering strategy to present a precise valency of ligands is to fuse with bioactive molecules a component of the distinct coil-coil oligomerization sequences derived from different tissues, i.e. cartilage oligomeric matrix protein (COMP) for pentameric constructs [67]. Extracellular matrix molecule fibronectin contains the 7^{th} to the 10^{th} type III fragment ($FNIII_{7-10}$) for the recognition by integrin $\alpha_5\beta_1$. Covalent immobilizations of clustered $FNIII_{7-10}$ on the surface of titanium implants showed an enhanced signaling efficiency by forcing integrin colocalizations and greatly improved the integration of the implants with surrounding tissues [68]. The recruitment of integrins can also synergize with the signaling of

growth factor. The 12th to 14th fragment of fibronectin ($FNIII_{12-14}$) indiscriminately binds to several growth factors. A proximal co-presentation of $FNIII_{7-10}$ and $FNIII_{12-14}$ in the same polypeptide chain showed potent, synergistic effects in signaling and morphogenesis, but not when the two fragments were on different polypeptide chain [44]. As an alternative oligomerization strategy, dendritic polymers have been used to facilitate multivalent bindings resulting in an enhanced avidity between the ligand and the target [69]. Another strategy utilizes linear polymer for the multivalency of ligands, i.e. an angiogenic factor, Sonic hedgehog, or stem cell signaling ligand, ephrin-B2, which exibited much more potency than the soluble form of a same concentration, exceeding the current standard approach of antibody-assisted clusterings [70,71]. Lately our laboratory has designed nanoparticles comprised solely of heparin molecules to mediate the covalent immobilization of of bioactive VEGF at different densities, which showed a potential in steering the migratory or proliferative pathways of endothelial cells in the angiogenesis process [72].

2.4.4 DELIVERY APPROACHES

The therapeutic outcomes of peptide/protein agents are largely affected by routes of administrations. Systemic approaches offer a fast distribution of agents with minimal invasiveness, but may suffer from barrier issues. These difficulties can be in part solved by including modifiers in the protein formulations. Enhancers such as protein transduction domains or cell-penetrating peptides facilitate the cell permeation, whereas adjutants such as chitosan or thiomers can lower the surface resistivity to promote paracellular transports. On the other end of the spectrum, local delivery has been applied in multiple situations with advantages such as minimizing non-target errors and creating a high local concentration and gradient. Research of

both direct topical applications and surgical implantations has emerged actively to target various tissue types and organs. For delivery of growth factors via hydrogel scaffold, readers can refer to Chapter 4.

2.4.5 Protein presentation impacts cell activation and tissue repair

As mentioned the ECM can bind growth factors with a high affinity resulting in their immobilization; this binding not only enhances the stability of growth factors but also modulates the fate and phenotype determination of nearby cells [73,74]. Elegant experiments temporally controlling the bioavailability and dose of vascular endothelial growth factor have demonstrated the delicate balance between appropriate dosing and time of release with therapeutic outcome in muscle as well as bone regenerations strategies [75,76]. In our laboratory we have demonstrated that the presentation of VEGF, bound, soluble, clustered or slowly released can each have different signaling responses to endothelial cells. For example, high density clusters of VEGF were developed using nanoparticles comprised solely of heparin [72]. High density VEGF clusters result in different responses in endothelial cell branching and VEGF-receptor 2 phosphorylation than less clustered and soluble VEGF. In addition, we have found that both covalently bound VEGF and electrostatically bound VEGF have differential signaling responses to endothelial cells [77,78] than soluble VEGF. In general, bound VEGF promoted migration (p38 activation), receptor clustering and integrin recruitment compared to soluble VEGF that promoted proliferation (p42/44 activation).

The spatial control of growth factors in 3-D hydrogel matrices presents tremendous chances in cell culture via its biomimetic gradient of concentrations and micrometer-resolved heterogeneity. Developed by the Shoichet group, agarose hydrogels with coumarin-caged thiols

have been exploited for the creations of FGF-2 patterning [79], VEGF gradient [80] and spatially controlled simultaneous multiple growth factor patterning in 3-D [81]. Facilitated by multiphoton confocal laser, the intensity of the immobilized functionalities is correlated to the number of scans, while orthogonal physical binding pairs can be selected for mild immobilization conditions. The Chen and West groups utilized surface patterning to spatially control the presentation of VEGF in PEG hydrogel and observed accelerated endothelial tubulogenesis in micron-scale immobilized VEGF patterns [82]. It is worth noting that micro-patterning of the topology alone of hydrogel substrates, therefore restricting cell shapes, has shown to be necessary and sufficient to replace soluble factor signaling in mediating the commitment of stem cells to different lineages [83]. By solely manipulating the topology of hydrogel substrates, a gene-expression level towards myocardial lineage of mesenchymal stem cells was observed [84]. It remains to be investigated how these effects on gene expressions would ultimately impact the physical processes of tissue morphogenesis or regeneration. Lately, the tortuosity and geometry of microfluidic devices are also utilized to yield GF gradients that can modulate the morphogenesis of embedded cells [85]. To the authors' opinion, the *in vitro* replication of *in vivo* chemoattractant gradients is of particular interest because it provides an opportunity to affect signaling cascade and phenotypic changes of cells to simulate physiological environment.

The temporal control on the delivery of growth factors has traditionally comprised of tunable sustained dosages of singly factors and sequential releases of multiple factors. Other than chemical modifications or carrier developments discussed in the sessions of "Protein with a smart conjugate" and "Protein with a robust shell", sustained release strategies have heavily relied on affinity-based approach in the material design. Orthogonal physical binding pairs exploited for the tunable retention of growth factors in depots include biotin-streptavidin,

barnase-barstar, Src homology 3 binding with proline-rich peptide [86]. In addition, the binding domains for various types of growth factors have been found on extracellular matrix molecules such as heparin, collagen, fibronectin and vitronectin. The simultaneous or sequential delivery of multiple GFs for aiding tissue constructs should be selected based on the synergistic and combinatorial effects of the proteins of interest. For example VEGF and Ang-2 are pro-angiogenesis factor that cooperatively promote endothelial sprouting and pericyte detachment from pre-existing vessels, whereas pro-maturation factors PDGF and Ang-1 when added subsequently following VEGF/Ang-2 promote vessel maturation and vascular remodeling [87].

2.4.6 Other protein nanomaterials

While studies of appropriate vehicles have blossomed with novel designs mentioned above and clinically proven synthetic materials, research in untapped areas of protein delivery have shown exciting advances (**Table 3**). These protein nanomaterials are not currently used in the applications of tissue repair but may provide unique characteristics in tissue regeneration.

Table 3 Non-conventional nanocomposite designs and delivery approaches.

Considerations	Type	Details	Refs
High loading concentration	Cosolutes	·Introducing trehalose to induce nanoclustering of naked proteins (up to 400 mg/mL) in dispersion ·Viscosity is well below SC injection limit and shows normal pharmacokinetics	88,89
Protein "lego"	Self-assembly	·12-subunit 16-nm cage assemblies was obtained with atomic level accuracy by designing the two oligo building blocks and their interface linking component	90,91
Protein-producing device	Cell-free system	·Transcriptional and translational components are put in an artificial boundary for the photoactivated synthesis of proteins	92
Carrier, vector-free	Shear-induced	·Compression and shear forces result in transient holes in cell membranes for diffusion delivery of diverse biomolecules into cell cytosol ·High throughput rate and cell-type independent	93
Enzyme-assisted photolithography	MEMS[a]	·Micron-scale patterning of peptide ligands or antigen for cell patterning and sorting	94
Source-host separation	Microfluidic	·Parallel channels hosting GF cocktails and endothelial cell covered artificial vessels to study angiogenic sprouting	95

		morphogenesis	
Direct cellular uptake & good serum stability	Lipid-core nanoparticle	·Supramolecular self-assembled peptide-modified Au-NP stabilizes proteins on the exterior of a lipid-core capsule	96

Abbreviation: a. micro-electro-mechanical system.

CHAPTER 3:
PROTEASE BIOLOGY AND PROTEASES AT DISEASE SITES

3.1 PLASMIN

The activation of plasminogen plays an important role in tissue remodeling events. By targeted plasminogen gene disruption, Romer et al [97] reported the healing of skin wounds was severely impaired in mice; particularly, the migration of keratinocytes, thus the reepithelialization process, was impeded. This dissertation also includes immunohistochemistry staining of plasmin(-ogen) and urokinase plasminogen activator (uPA) in the epithelial tongue of skin wounds in mice (Figure 8).

Although plasminogen is shown to be necessary and required for normal reepithelialization, it was not clear if the mechanism of action was due to the contribution of plasmin to degrade other matrix components or due to the plasmin-mediated activation of other key matrix proteinases [98] or of growth factors [99], or due to the combination of both. Irrespective of the mechanism of action, the lack of plasminogen in skin wound does not compromise the cell migration in general – infiltration of inflammatory cells, formation of granulation tissue and neovascularization are still evident.

There are mainly two plasminogen activators (PAs), urokinase-type (uPA) and tissue-type (tPA). In the healing of tympanic membrane perforations, the migration of keratinocytes

was delayed and misoriented, causing delayed healing in single gene-deficient uPA(-/-) mice but not tPA(-/-) mice [100].

The activation/inhibition of plasmin and its relation with the other extracellular matrix components is shown in Figure **6**.

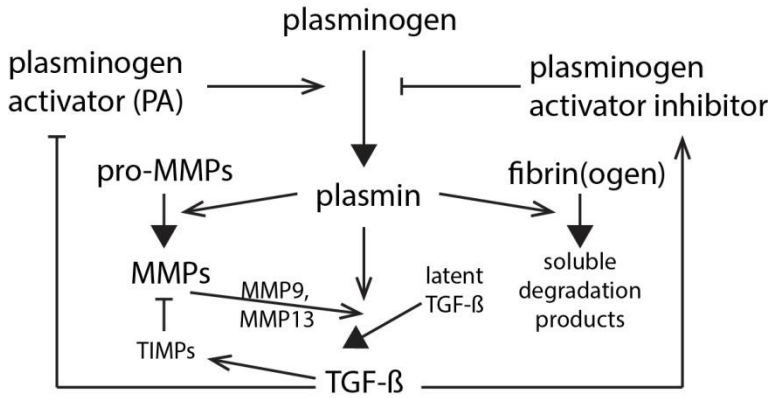

Figure 6 Schematic diagram of the function of plasmin/plasminogen activator system , and its relations with matrix metalloproteinases (MMPs) and some growth factors (Ref [101]).

3.2 MATRIX METALLOPROTEINASE (MMP)

As summarized by Zhang et al [102], the activity of matrix metalloproteinase is regulated at several levels, including the transcription level, the activation (conversion from pro-MMP to active MMP) level, and the tissue level by tissue inhibitors of metalloproteinases (TIMPs). Once activated and left uninhibited, MMPs can either degrade extracellular matrix (ECM) inducing classical tissue remodeling or regulate numerous biological activities through the modulation of various cell signaling mechanisms.

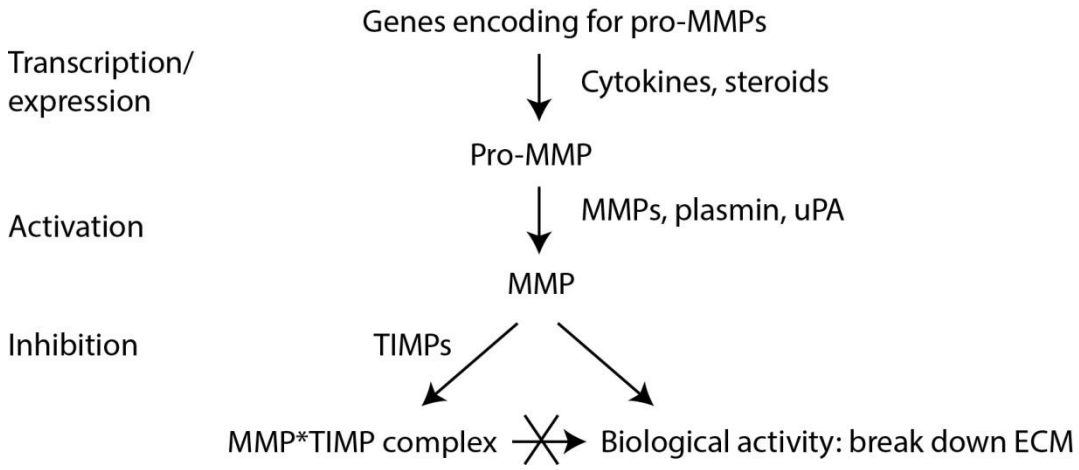

Figure 7 Schematic diagram of the metalloproteinase (MMP) system. The activity of MMPs is regulated at three levels: 1. The transcriptional level where certain cytokins and steroid induce the transcription and expression of MMPs; 2. The activation step where pro-MMPs are cleaved to become mature, biologically active MMPs, which are capable of breaking down specific extracellular matrix (ECM); and 3. The tissue level inhibition by tissue inhibitors of metalloproteinases (TIMPs).

3.3 SPATIOTEMPORAL EXPRESSION OF PROTEASES IN WOUNDS

By analyzing the wound fluids collected from chronic venous leg ulcers compared to acute surgical mastectomy wounds, Wysocki et al found that the levels of active uPA in chronic wounds were five-fold and two-fold higher than sera and mastectomy wounds, respectively [103]. Similarly, the level of active plasminogen activator inhibitor in chronic wounds was four-fold and two-fold higher than sera and mastectomy wounds. As chronic wounds progress towards healing, uPA converted from the active form to bound uPA-plasminogen activator inhibitor-1 complex.

In human diabetic chronic wound fluid, there is elevated MMP-2 and reduced MMP-9 expression levels compared to acute wound fluid [104]. However, the data for diabetic mice differs. While wound closure, epidermal tongue area and granulation tissue area are all less profound in

wounds in diabetic mice than in normal mice, the differences of the expression levels of (pro-) MMP-2 and (pro-)MMP-9 between diabetic mice and normal mice during the early stages (first 10 days) of dermal wound healing[104]. In wound tissue, there is more pro-MMP-2 expression in normal mice than in diabetic mice, although the active MMP-2 amount is similar. In wound fluid at day 3, there is significantly more pro-MMP-2 in diabetic mice than in normal mice; but reversely at day 7. For MMP-9, there is significantly more pro-MMP-9 in diabetic wound tissue than in normal wound tissue; and similar trend in wound fluid.

3.4 PLASMIN AND MMP AT SKIN WOUNDS

This dissertation looks at dermal wound healing models in both normal (Balb/c) mice and diabetic (db/db) mice. The immunohistochemical staining of plasmin(-ogen), uPA and (pro-)MMP-2 is shown below.

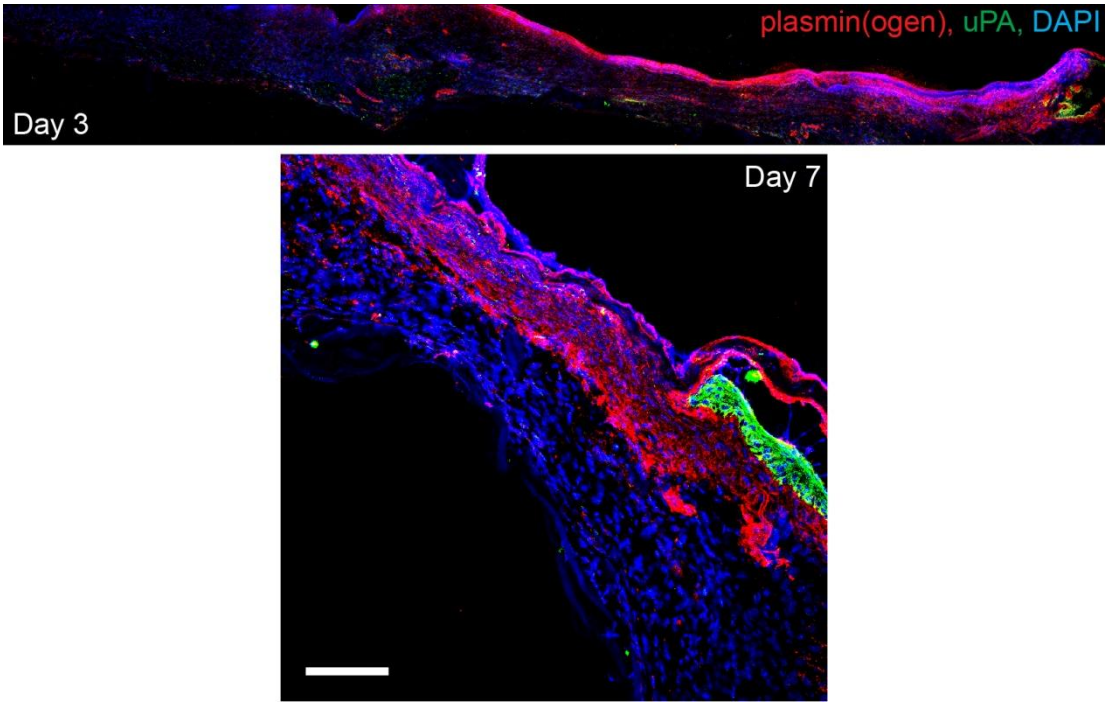

Figure 8 Immunohistological staining of endogenous plasmin(-ogen) and urokinase plasminogen activator (uPA) in excisional skin wounds on balb/c mice at day 3 and day 7 post surgery. scale bar is 20 µm.

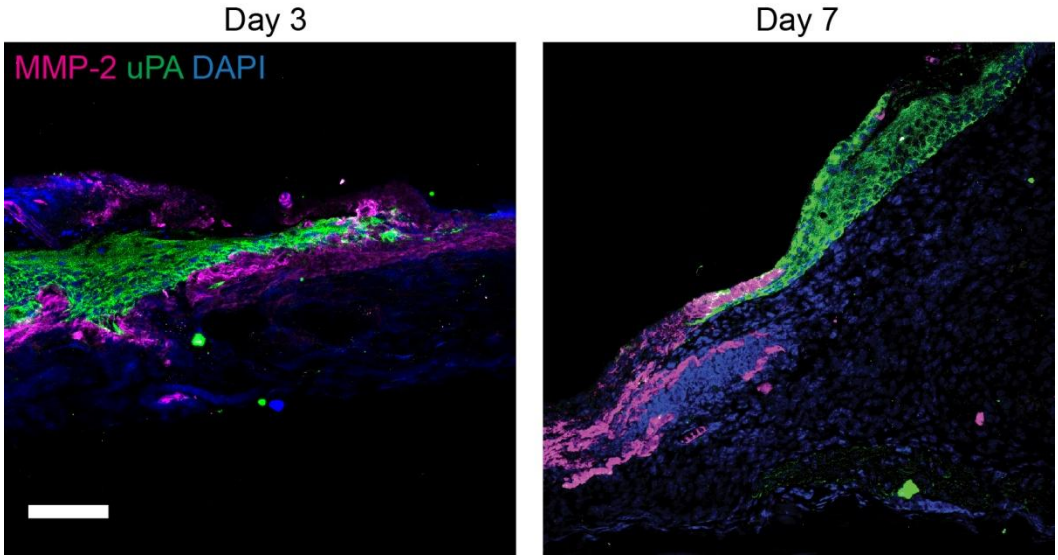

Figure 9 Immunohistological staining of endogenous (pro-)MMP-2 and urokinase plasminogen activator (uPA) in excisional skin wounds on balb/c mice at day 3 and day 7 post surgery. scale bar is 20 µm.

3.5 PLASMIN AND MMP AT STROKE

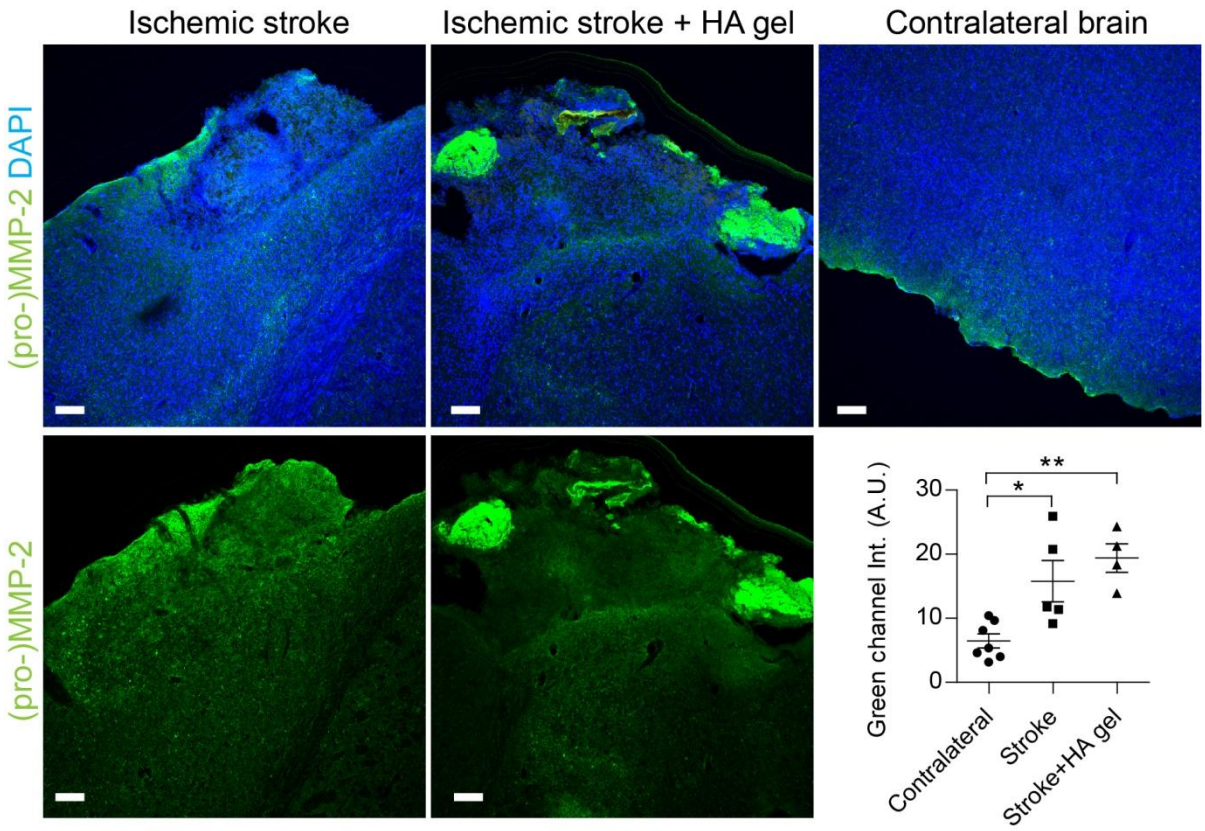

Figure 10 Immunohistological staining of endogenous (pro-)MMP-2 in mouse ischemic stroke brain (10 days post stroke). Representative images of no treatment (ischemic stroke), treatment with hyaluronic acid hydrogel crosslinked by a peptide sequence sensitive to MMP-2 (ischemic strok + HA gel) and the contralateral brain (control) were shown. Scale bar is 100 µm.

CHAPTER 4:

PROTEIN DELIVERY FROM HYDROGEL FOR REVASCULARIZATION

4.1 SUSTAINED RELEASE FORMULATIONS

Therapeutic angiogenesis *in vivo*, a crucial process towards wound healing, requires continuous presence of VEGF, which is subject to a narrow therapeutic window.[105,106] However the frequent re-dosing of high concentrations of VEGF (tens of μg) to wound beds has been the standard practice due to inevitable passive leaching of naked proteins from conventional scaffolds and matrices.[107,108]

Biomaterials for tissue repair create a permissive environment to promote tissue formation in vivo or to study cell differentiation, morphogenesis and cell fate decisions in vitro. The delivery of proteins is an ideal approach to promote and guide these processes, however, delivery of proteins poses challenges due to their low stability in serum and the need to control their temporal spatial bioavailability to match the need of the tissue or differentiation state of the cell. In the natural extracellular matrix (ECM), stability as well as bioavailability of proteins can be controlled by the extracellular matrix environment. For example, heparan sulphate, a component of the ECM, can bind growth factors with a high affinity resulting in their immobilization; this binding not only enhances the stability of growth factors but also modulates

the fate and phenotype determination of nearby cells [73,74]. Elegant experiments temporally controlling the bioavailability and dose of vascular endothelial growth factor have demonstrated the delicate balance between appropriate dosing and time of release with therapeutic outcome in muscle as well as bone regenerations strategies [75,76].

Growth factor nanocomposites are generally applied within hydrogel scaffolds comprised of natural extracellular matrices such as matrigel, collagen and fibrin, or synthetic mimics like alginate, PLGA/PLA, hyaluronic acid, self-assembling peptides. Exemplary current research of the local delivery of growth factors is summarized in Table 4.

Table 4 Growth factors in hydrogel-based therapy for tissue repair.

Tissue	Animal model	Details	Refs
Bone	8mm calvarial defects in rats	·Dual delivery of rhPDGF-BB[a] (transient) and BMP2[b]-expressing BMSCs[c] (long term) in collagen gel ·Suppressive modulation of PDGF-BB on osteogenic differentiation and receptor expression of BMSCs ·Enhanced bone formation & mineral density in vivo	109
	8mm mid-fermoral defect in rats	·BMP2-containing alginate gel within nanofiber mesh tube, in comparison to collagen sponge	110
Brain	Stroke in mice	·Epi-cortical delivery of EPO[d], PEGylated EGF[e] or in PLGA[f] particles in hyaluronic-methylcellulose gel to stimulate endogenous NSPC[g] and promote tissue repair	111-113
Heart	Cardiac ischemia-reperfusion in rats	·PLGA microparticles for sustained VEGF[h] delivery ·After 1 month, increase in angiogenesis and arteriogenesis and greater LV[i] wall thickness	114
Skin	Mouse deep burn- wound model	·Engineered human vasculature in hyaluronic acid hydrogel implanted to cover wound for integration with host vasculature and regression later during remodeling	115
Spinal cord	Subacute spinal cord injury in rats	·NT-3[j], PDGF in fibrin scaffold delivering mouse embryoid bodies of ESNPCs[k] ·Inclusion of heparin did not make a difference in increasing number of ESNPCs but ESNPC-derived NeuN[l]-positive neurons	116
Other	Bladder lesion 2.2mm in diameter in rats	·IGF-1[m] fused with a substrate sequence tag derived from α_2PI_{1-8}[n] is covalently incorporated in fibrin for sustained release at lesion site stimulated considerable smooth muscle cells and host tissue response	117

Abbreviations: a. recombinant human platelet derived growth factor (BB homodimer), b. bone morphogenetic factor 2, c. bone marrow mesenchymal stromal cells, d. erythropoeitin, e. epidermal growth factor, f. poly(lactic-co-glycolic acid**)**, g. neural stem/progenitor cell, h. vascular endothelial growth factor, i. left ventricle, j. neurotrophin 3, k. embryonic stem cell-derived neural progenitor cell, l. neuronal nuclei, m. insulin-like growth factor 1, n. α_2-plasmin inhibitor.

4.2 SEQUENTIAL DELIVERY OF GROWTH FACTORS

During tissue repair, the orderly presentation of signal proteins in coordination with proteolytic enzymes generally directs the hierarchical remodeling of diseased tissues.[118] For example, angiogenic growth factors in association with tissue-specific protease cascades direct vascular sprouts and subsequent stabilization of blood vessels.[119,120] In order to deliver multiple signal molecules in a desired sequence, researchers have attempted to develop delivery vehicles with spatiotemporal control by trapping proteins within degradable polymers such as poly(lactide-co-glycolic acid), poly(ε-caprolactone), and hydrogels. Representative examples include the composite films made by the layer-by-layer assembly of proteins and polymers,[4] as well as the composite scaffolds made by electrospinning[121] or by fusing polymer particles that contain desired proteins using organic vapor or high-pressure CO_2.[3,113] For the composite films, the sequential release of the proteins is achieved through a hydrolysable barrier that separates layers of first protein from the subsequent ones; after releasing the first protein, the hydrolysis of the barrier allows for the release of the subsequent proteins. For the composite scaffolds, the sequential release is achieved based on different hydrolysis rates of the polymer moieties within the composites. Although these delivery vehicles enable the sequential elution of multiple proteins, the release process is constitutive which cannot be programmed to respond to any particular biological event. Furthermore, the synthesis of such composites requires harsh chemical processes involving the use of intense mixing and/or organic solvents, which can easily denature growth factors.

4.3 PROTEASE-BASED DELIVERY STRATEGY

Protease-based protein delivery systems were previously studied by others to either directly conjugate proteins to matrices via a protease-sensitive peptide linker or to attach proteins within a bulk hydrogel that is crosslinked by protease-sensitive peptides.[122] However, both approaches expose proteins to the reactive chemical environment, which challenges the stability and bioactivity of proteins.[123,124] Additionally these approaches are highly dependent on the number and the type of the functional groups on backbone scaffolds for modifications with different peptide linkers, which limits the applicability of multiple proteins with temporal release control and the variety for the selection of buffers or matrices.

CHAPTER 5:
ENZYME-RESPONSIVE PROTEIN NANOCAPSULES AS SMART, INJECTABLE DELIVERY VEHICLES

5.1 INTRODUCTION OF GENERAL PROTEIN NANOCAPSULES

Researchers at UCLA have developed the original single-protein nanocapsule technology back in 2009. Yan and Du et al. have designed the 1st generation of single-protein nanocapsules for intracellular protein delivery [125]. At that time, each individual protein molecule was encapsulated within a permeable, polyacrylamide-based thin shell that was *covalently anchored* to the protein core for the primary purpose to increase the stability of proteins in physiological environment. The polymer skin was either crosslinked by non-degradable methylenebisacrylamide or *acid-degradable* glycerol dimethacrylate (sensitive to intracellular late endosomal low pH of ~5.5) for pH-specific release of proteins. A huge library of proteins including enzymes, serum proteins and apoptosis biologics agents can be incorporated as protein cores to form nanocapsules for various applications; even different types of biomolecules such as siRNA[66] or adenovirus [126] have been successfully encapsulated this way.

A major innovation on the protein nanocapsule technology came where multiple protein molecules were stoichiometrically constructed and form multi-core protein nanocapsules [65]. Through conjugation to single strand DNA (ssDNA), three or four enzyme molecules were precisely positioned via the self-assembly of ssDNA into a branched Holliday structure. Subsequent acrylation on one or some of the enzyme molecules allows the anchored growth of a

polymer skin around the multi-protein core. This advancement greatly broadens the application of protein nanocapsules by enabling the mimicry of multi-component, higher structures of tissues, which potentially may lead to the development of artificial mini-organs.

Further advancement came along as researchers re-engineered the shell of nanocapsules to incorporate targeting capabilities and responsiveness to biological milieu. First, polyethylene glycol-based nanocapsules were developed in lieu of polyacrylamide based materials [127]. Second, click chemistry was utilized to incorporate tumor-specific targeting ligands on the surface of nanocapsules for the intracellular delivery and accumulation of tumor suppressor protein p53 [128]. Third, a protease-labile peptide sequence was chosen as the enzyme-responsive crosslinker for the construction of polymer shells of protein nanocapsules [123]. These shells were in a non-covalent interaction with the capsule core, which protected the pristine activity of encapsulated protein. This last advancement opens the door for extracellular delivery of growth factors and other cytokines in the regenerative medicine.

5.2 Engineering the protease-sensitivity to achieve sequential multi-protein delivery

Work in this dissertation has focused on the development of a platform for extracellular, sequential protein delivery strategy based on a mild encapsulation process, in which individual whole proteins are wrapped within an in situ formed thin polymer shell.[125] Since the spatial and temporal patterns of protease expressions are closely related to pathophysiological states,[129] incorporating protease-specific and cleavable peptides within the polymer shells allows for disease-state–specific delivery of signal molecules. Here, we investigated the peptide substrates made from *L* or *D* chiral form of amino acids. The D-chiral enantiomer has lower degradation kinetics compared to the L-chiral peptide [130,131]; thus, n(VEGF) synthesized with an increasing

D-chiral peptide content will have slower degradation rate and therefore slower release rate. Thus by controlling the *L* to *D* ratios of peptide crosslinkers within the shells, the delivery of multiple proteins with spatiotemporal control in response to the proteolytic enzymes in diseased sites could be achieved.

Figure 11 illustrates our design using plasmin-sensitive peptides as labile crosslinkers. Driven by non-covalent interactions, monomers with neutral ***1***, positive ***2*** or negative ***3*** charges, as well as peptide crosslinkers, are spontaneously enriched around protein molecules. Free-radical polymerization gradually grows a nanogel shell around each protein, leading to the formation of protease-responsive nanocapsules denoted as n(Protein)$_{x\%}$, where Protein denotes the protein core and *x%* denotes the molar percentage of *L* peptide in the total *L+D* peptide crosslinkers used for the nanogel shell (Figure 11a). Increasing the ratio of *L* crosslinker (*x%*, fast degrading rate) leads to nanocapsules with a faster release kinetic, while decreasing *L* percentage results in slower releasable nanocapsules (Figure 11b). Upon protease degradation the released protein can exert its normal biological function upon nanocapsule degradation and the nanogel polymeric fragments, charged polyacrylamide segments with cleaved peptides, are expected to be compatible in the biological milieu as has been previously observed for similar polymers.[132] Furthermore, such nanocapsules can be homogenously dispersed within an injectable hydrogel, providing an injectable delivery platform for enhanced wound healing and tissue repair (Figure 11c).

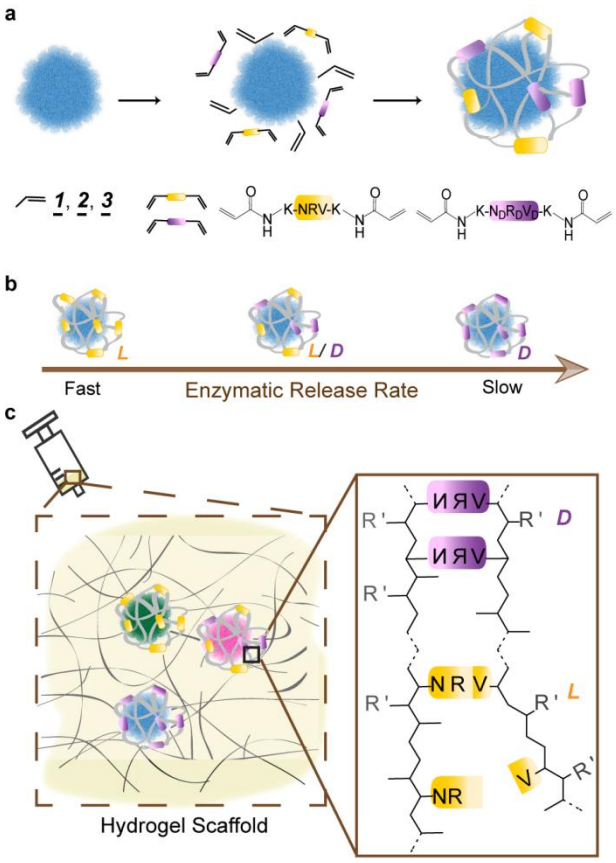

Figure 11 Illustration of chirality-controlled, enzyme-responsive protein nanocapsules with temporal control. (a) The synthesis of the nanocapsules by enriching monomers and crosslinkers around an individual protein molecule and by subsequent *in situ* polymerization. The monomers can be acrylamide (*1*, neutral), N-(3-aminopropyl)methacrylamide (*2*, positively charged), or 2-acrylamino-2-methyl-1-propanesulfonic acid (*3*, negatively charged). The crosslinkers include the mixtures with designed molar ratios of *L* (yellow) and *D* (purple) enantiomers of the peptide Asn-Arg-Val, being the substrate of plasmin. (b) The rate of enzymatic degradations of individual nanocapsule is tuned by varying the ratio of *L* to *D* peptide crosslinkers used: faster with more *L* peptide, slower with more *D* peptide. (c) Nanocapsules of different proteins and of varying degradation rates can be mixed in matrices (or buffer) of choice for injectable delivery of multiple proteins with precise temporal control in protease-specific disease models.

5.3 Engineering the protease-selectivity to achieve specificity in protein delivery

In light of the differential protease expression profiles in wounds, we intended to choose MMP-2 or MMP-9 sensitive peptide sequences as the crosslinkers for the formation of nanocapsules. The sequences were identified from literature publications as detailed below.

5.4 Materials and Methods

All chemicals were purchased from Sigma-Aldrich unless otherwise noted, and were used as received. Concentrated pure VEGF-A was a generous gift from Genentech. The peptide sequence Lys-Asn-Arg-Val-Lys of both L- and D- forms were purchased from China Tech Peptide Co. Ltd. and GenScript. N-(3-aminopropyl) methacrylamide hydrochloride (APPMA) was purchased from Polysciences. Plasmin and rat anti-mouse CD31 antibody were purchased from BD Biosciences. Carbon-film 300-mesh copper grid for TEM was purchased from Zhongjingkeyi Technology Co. Mono-sulfo-NHS-nanogold (1.4nm) and HQ silver enhancer for EM were purchased from Nanoprobes. Human VEGF MAb, biotinylated PAb and streptavidin-HRP were purchased from R&D Systems. TMB substrate was purchased from Cell Signaling Technology. Aprotinin was purchased from MP Biomedicals. Human fibrinogen 1 plasminogen-depleted was purchased from Enzyme Research Laboratories. Human dermal fibroblasts were a gift from Prof. Luisa Iruela-Arispe's lab and they were cultured in Dulbecco's modified Eagle medium (DMEM) supplemented with 10% (vol/vol) fetal bovine serum (FBS) and 1% (vol/vol) penicillin-streptomycin, obtained from Invitrogen.

5.4.1 SYNTHESIS AND MODIFICATION OF PEPTIDE

Solid phase peptide synthesis: The following sequences of peptides were synthesized using the solid phase peptide synthesizer in Dr. Yu Huang's lab with the help of a graduate student, Enbo Zhu: NH_2-G**RSLSR↓LTA**K-amide (↓ indicates the cleavage site by MMP-2 as previously reported [133], herein denoted as RLT peptide) and Acetyl-**KGPRS↓LSGK**-amide (↓ indicates the cleavage site by MMP-9 as previously reported [134], herein denoted as SLS peptide). All amino acids were Fmoc protected; and lysine was also protected with a Boc group. The solid phase used was an Fmoc-Rink amide MBHA resin (Anaspec).

After the synthesis, the peptide-resin was transferred to a vessel and drained under Ar to remove excess DMF. Three times of alternating washes between ethanol and DCM were performed on the peptide-resin. After drying under Ar for 1 hour, a cleavage cocktail to dissociate the peptide from the resin was prepared. It contained 250 mg phenol, 4.75 mL TFA, 125 µL triisopropylsilane (TIPS) and 125 µL water. The cleavage cocktail (5 mL in total) was added 1 mL at a time to the peptide-resin, and the reaction was stirred at room temperature under Ar for 2 hours. Finally the reaction liquid was precipitated in ice-cold ether and collected via centrifugation at 3500 rpm at 4°C for 5 minutes. The mass and the purity of the peptide were tested via liquid chromatography-mass spectrometry. Alternatively, SLS-peptide was acetylated on the N-terminus via the following step. Before the ethanol/DCM washes, the acetylation agent was added to SLS-peptide-resin to react with stirring at room temperature for 1 hour. The acetylation agent contained 350 µL acetic anhydride, 350 µL diisopropylethylamine (DIEA) and 6.3 mL DMF. To confirm full acetylation (resin turns from purple to white color), the reacted P9-peptide-resin was incubated with 0.1 w/v% ninhydrin in 200-proof ethanol at 90°C for 10 minutes.

Plasmin-sensitive peptide [135], K**NR↓V**K (herein denoted as NRV), was purchased from GenScript. The d-chiral form of this sequence $K_DN_DR_DV_DK_D$ was also purchased.

Acrylation of peptide to form crosslinker: N-acryloxysuccinimide (NHS-Ac) was used to convert the amine groups on the N-terminus of P2-peptide and the lysine groups of all the peptides to an acryl group; thus, peptides would be bisacrylated. The peptide was dissolved in MES buffer at 5 mg/mL. NHS-Ac (20 molar eq.) was directly added to the peptide/MES solution. The reaction was stirred at room temperature for overnight, and the bisacrylated peptide was purified via an HPLC prep column (C18, 3 mL/min, 5% - 95% ACN from 5 – 35 min). The purity and the mass of final peptide crosslinkers were tested via LCMS.

Kinetic constant measurements: The kinetic parameters of peptide hydrolysis catalyzed by plasmin were measured using a fluorometric assay previously described[136]. Briefly, both L and D chiral forms of peptide KNRVK were individually treated with plasmin at 40 nM in buffer solution (50 mM tricine, 50 mM NaCl, 10 mM CaCl2 and 0.05% Brij-35, pH 7.5). The enzymatic reaction was stopped at various time points by centrifugation (NMWL 10,000) to remove plasmin. The reaction filtrate was incubated with fluorescamine at 2.5 mM and detected for the fluorescence (Ex/Em 387/480) on a spectrofluorometer. Propylamine was used as the standard compound to generate a calibration curve of fluorescence vs. amine concentrations. Initial velocity rates were obtained from plots of fluorescence vs time where no more than 40% of hydrolysis took place, and the kinetic parameters were determined by fitting rate vs substrate concentration data for the Lineweaver-Burk analysis.

5.4.2 DIFFERENT PROTEIN NANOCAPSULE FORMATION (VEGF, PDGF, ANG-1, B-GAL)

Synthesis of Protein Nanocapsules: The nanocapsules were synthesized using in situ free-radical polymerization. As an example, VEGF was diluted in a buffer solution of 10 mM sodium bicarbonate (pH = 8.55) at a final reaction concentration of 100 μg/mL. Acrylamide (AAM) and N-(3-aminopropyl)methacrylamide (APM) and crosslinkers (bisacrylated *L*/*D*-KNRVK, or methylene bisacrylamide) were subsequently added to the mixture (molar ratio of VEGF:AAM:APM:crosslinker = 1:3000:3000:600). To synthesize n(PDGF), PDGF was diluted in phosphate buffer saline (PBS) (pH = 7.2-7.4) at a final reaction concentration of 100 μg/mL. Acrylamide, 2-acrylamino-2-methyl-1-propanesulfonic acid (AAMPS) and crosslinkers (bisacrylated *L*/*D*-KNVRK) were subsequently added to the mixture (molar ratio of PDGF:AAM:AAMPS:crosslinker = 1:1500:4500:600). Then, freshly prepared ammonium persulfate (APS) (molar ratio of Protein:APS = 1:745) and tetramethylethylenediamine (TEMED) (molar ratio of Protein:TEMED = 1:45000) were added at to initiate *in situ* polymerization to form the nanocapsules. The reaction was carried out under inert gas for 1.5 hours at 4 °C. The mixture was purified by dialysis against 10 mM phosphate buffer (pH ~7.0).

The formation of nanocapsules that encapsulate PDGF-BB, Angiopoietin-1 or b-galactosidase was carried out in a similar way. The detailed calculations can be seen in 5.7 Protocols.

5.4.3 SIZE CHARACTERIZATIONS

Electron microscope: n(GF) suspension was transferred to a copper grid and stained with 2% (vol/vol) phosphotungstic acid for 1 min. Samples were imaged with T12 cryo-electron microscope and images were quantified with ImageJ to measure the size of nanocapsules. Mono-

sulfo-NHS-nanogold (Nanoprobes, Yaphank, NY) was used to modify VEGF according to manufacturer's instructions, and gold labeled VEGF was further fabricated to form n(VEGF-AuNP). TEM images were taken with one additional treatment step using HQ Silver Enhancer (Nanoprobes, Yaphank, NY) according to manufacturer's instructions.

Dynamic light scattering (DLS): DLS measurements were taken with ZetaSizer (Malvern Instruments) at 173° backscatter angle. Dialyzed nanocapsules of at least 20 µL were measured in the precision cell made of quartz SUPRASIL® (Hellma).

5.4.4 Enzyme release assay

ELISA: $n(VEGF)_{x\%}$ (of a VEGF content 50 ng) with x = 100, 50, 25 and 0 were individually treated with plasmin (0.25 µg, activity of 6.6 units/mg) for 20 min. Subsequent proteolytic activity of plasmin was inhibited with aprotinin. Samples were further diluted to 3 ng/mL in 1% BSA for ELISA with a standard curve following manufacturer's instructions.

5.4.5 Activity assay

5.4.5.1 Receptor activation

Human dermal fibroblasts (HDFs) were used to assay the phosphorylation levels of PDGF receptor-ß (pPR-ß). Cells were cultured in completed DMEM media (described in Materials) 37°C with 5% CO_2 until confluency and passaged onto 12-well plates at 100,000 cells per well. Attached cells were starved in serum-free media for 6 hours and treated with phosphatase inhibitor sodium vanadate (at 0.1 mM) for 5 min before being exposed to $n(PDGF)_{x\%}$ with x = 100 or 0, un-encapsulated PDGF or PBS at 50 ng/mL in PBS for different

amounts of time. Treated cells were rinsed with ice-cold PBS with 0.2 mM sodium vanadate and collected in mRIPA lysis buffer (50 mM Tris, pH 7.4, 1% Nonidet P-40, 0.25% sodium deoxychlorate, 1mM EDTA, 150 mM sodium chloride, 1 mM sodium vanadate, 10 mM β-glycerophosphate) with fresh aprotinin (20 µg/mL), leupeptin (20 µg/mL) and PMSF (1 mM). The supernatants of cell lysates (at least 5 µg protein mass each) were loaded onto NuPAGE 4~12% gradient bis-Tris gel for electrophoresis (100 min at 150 V) and transferred to nitrocellulose membranes (2 h at 400 mA at 4°C).The membranes were incubated in blocking buffer (5% milk in 0.1% Tween-20 in TBS) for 1 hour at room temperature before overnight incubation with primary antibodies. Phosphorylated proteins were detected by immunoblotting using anti-phospho-PDGRR-ß (Cell Signaling Technology) at 1:1000 dilution in blocking buffer followed by secondary antibodies coupled with horseradish peroxidase (Invitrogen) at 1:5000 for 2 hours at room temperature and visualized (with ECL detection reagents, GE Healthcare, Piscataway, NJ) using a Typhoon scanner (GE, Amersham Biosciences, Piscataway, NJ). Protein-loading control was assessed by Western blot using anti-ß-actin (Cell Signaling Technology). Typhoon images of three biological samples were analyzed. The phosphorylation signal of PDGFR-ß was normalized to the intensity of ß-actin bands using ImageJ software. The normalized activation signal (pPR-ß/ß-actin) of the 5-min treatment time point with un-encapsulated PDGF of each set was defined as 100%, and normalized activation signals of 15-min and 30-min time points were compared with the 5-min time point.

5.4.5.2 Activity in the long term

The thermal stability of n(VEGF) in comparison to VEGF was studied by incubating 300 ug/mL of samples at 37°C for 10 days and assayed with human umbilical endothelial cells (HUVECs, Lonza) followed by western blot analysis

5.4.5.3 Chick chorioallantoic membrane (CAM) assay

This assay was modified from previous publications [72]. Briefly, fertilized white leghorn eggs (California Hatchery) were incubated in a humidified chamber for 2 days at 38°C. The eggs were opened and the embryo was transferred into a petri dish for continued growth within the humidified chamber for 6 days at 38°C. The fibrin matrices were prepared as previously mentioned in the sprouting assay, with the exception of Cytodex bead incorporation. Meanwhile, hyaluronic acid hydrogel was prepared according to previous report [137]. The matrices containing VEGF specimens of interest were grafted onto regions of the CAM located at a distance from the embryo and major vessels. After 2 days of further incubation in the incubator, embryos and grafts were imaged under a dissecting microscope. A 30-gauge needle with a micro-syringe (500 uL) was used to manually inject 400 µl FITC-dextran (MW 2,000,000) into the vein at a rate of about 200 µl per minute. The FITC dextran solution was allowed to circulate for 5 minutes. The embryos were then incubated at 4°C for 5 minutes and the regions of interest were dissected off the CAM and fixed in 4% paraformaldehyde for fluorescent imaging under Zeiss microscope.

5.4.6 TISSUE ELISA FOR IN VIVO RELEASE

Eight to 12-week old female Balb/c mice (Charles River Laboratories #CRL028, Wilmington, MA) were used. The surgical part of this method was approved by the Animal Research Committee (ARC) of University of California Los Angeles and all animal care was

performed in accordance with guidelines. The animals were housed as five per cage prior to surgery and alone post procedure in a temperature controlled animal facility with a 12-hour light/dark cycle. The mice were acclimated to their environment for at least 1 week prior to the procedure. Mice were individually anesthetized with 4% isoflurane and maintained at 1.5-2.5% isoflurane during surgery. Artificial tear ointment was applied to the eyes of mice, and nails were clipped. Buprenorphine (fours dosages of 60 uL each of 0.015 mg/mL per 20 g of mouse weight administered before, 8 hours, 20 hours and 28 hours after surgery) was injected subcutaneously. The dorsal surface was shaved with an electric clipper followed by a short application of Nair (1 minute), a depilatory agent, to remove any remaining hair. The skin was sterilized with 3 serial washes of betadine (one time) and 70% ethanol (two times). Mice were placed on a sterile pad atop warming heat pads for surgery. Two excisional full-thickness skin wound (4 mm in diameter) were created on the back of each animal. *In situ* polymerized fibrin matrices (of fibrinogen at 10 mg/mL, thrombin at 2 U/mL, factor XIII at 4 U/mL, calcium at 5 mM) containing 1) $n(VEGF)_{100\%}$ (100 ng) and $n(PDGF)_{25\%}$ (100 ng) or 2) no additional growth factors, were injected to the wounds. One piece of Tegaderm was adhered to cover the entire back of a mouse except the center area where the wounds were was covered with double layers of Tegaderm through which the non-sticky surface was in contact with wounds. At three and six days after surgery, the wound and its surrounding tissues of circular shape was collected using an 8-mm biopsy punch, weighed and homogenized in lysis buffer (T-PER extraction buffer with Protease inhibitor mini-tablet). The protein extraction process was continued for another 24 hours at 4 °C, followed by 2 hour centrifugation at 14,000 rpm at 4 °C. The clear supernatant (excluding fat layer) was transferred for two ELISAs detecting VEGF and PDGF separately.

5.4.7 STROKE MODEL

Hyaluronic acid (HA, 60,000 Da, Genzyme, Cambridge, MA) was functionalized with an acrylate group using a two-step synthesis[138]. Briefly, HA was first functionalized with hydrazide via carbodiimide chemistry, and later further functionalized with acrylate groups (14.9% degree of modification) via NHS-Ac. HA was chosen for its biocompatibility, controllable gelling kinetics and angiogenic potentials shown previously[139]. HA (3.5 w/v%) hydrogels to be used in the stroke model was with 500 μM RGD adhesion peptide in their clustered form[140] with 1) no additional growth factors, 2) naked VEGF of 200 ng, or 3) $n(VEGF)_{100\%}$ of 100 ng and $n(VEGF)_{25\%}$ of 100ng, and crosslinked (thiol : acrylate = 0.45 : 1) with a bis thio-containing peptide Ac-GCREGPQGIWGQERCG-NH_2 (matrix metalloproteinase degradable) in 0.3 M HEPES buffer. Animal procedures were performed in accordance with the US National Institutes of Health Animal Protection Guidelines and the University of California Los Angeles Chancellor's Animal Research Committee. Focal and permanent cortical stroke was induced by a middle cerebral artery occlusion (MCAo) on young adult C57BL/6 male mice (8-12 weeks) obtained from Jackson Laboratories. Briefly, under isoflurane anesthesia (2–2.5% in a 70% N2O/30% O2 mixture), a small craniotomy was produced over the left parietal cortex. One anterior branch of the distal middle cerebral artery was then exposed, electrocoagulated and cut to be permanently occluded. Bilateral jugular veins were clamped for 15 min. Body temperature was maintained at 36.9 ± 0.4 °C with a heating pad throughout the operation. Five days following stroke surgery (due to post-stroke ipsilateral VEGF up-regulation and peak peri-infarct microvascular density[141]), gel precursor was loaded into a Hamilton syringe (Hamilton, Reno, NV) connected to a pump for the injection of 6 μL gelling solution into the stroke cavity using a 30-gauge needle at stereotaxic coordinates 0.26 mm anterior/posterior (AP), 3 mm medial/lateral

(ML), and 1 mm dorsal/ventral (DV) with an infusion speed of 1μL/min. The needle was withdrawn from the mouse brain immediately after the injection was complete. Ten days following the hydrogel transplantation, mice were sacrificed via transcardial perfusion of 0.1 M PBS followed by 40 mL of 4 (w/v) % PFA. The brains were isolated and post-fixed in 4% PFA for overnight followed by submersion in 30 (w/v) % sucrose solution for 24 hours. Tangential cortical sections of 20 μm-thickness were sliced using a cryostat and directly mounted on gelatin-subbed glass slides for immunohistological staining of Glucose Transporter 1 (Glut-1-, Abcam, Cambridge, MA, USA) and Platelet-derived Growth Factor Receptor β (PDGF-Rβ, R&D system R&D Systems, Minneapolis, MN) to label vascular endothelial cells and pericytes respectively. Primary antibodies were 1:100 diluted for incubation of overnight period at 4 °C, while alexa fluor-labeled secondary antibodies at 1:400 dilution was 1 hour at room temperature followed by nuclei stain using DAPI (1:500, Invitrogen) for 10 minutes. Images were taken with a Nikon C2 confocal microscope on 3 coronal brain levels at +0.80 mm, -0.80 mm and -1.20 mm according to bregma, which consistently contained the infarct area. Vascular area was quantified in 3 to 8 randomly chosen regions of interest (of 0.3 mm^2) in the infarct and peri-infarct areas. The positive area for Glut-1 and PDGFR-β was measured using pixel threshold on 8-bit converted images (ImageJ v1.43, Bethesda, Maryland, USA) and expressed as the area fraction of positive signal per region of interest (ROI). Values were then averaged across all ROI and sections, and expressed as the average positive area per animal.

5.4.8 CHRONIC WOUND HEALING MODEL

This protocol was approved by the Animal Research Committee (ARC) of University of California Los Angeles and all animal care was in accordance with guidelines. Eight to ten-week

old female db/db mice (Jackson Laboratory #000642, strain: BKS.Cg-*Dock7*^{m} + / + *Lepr*^{db} /J) were used. Pre-surgical procedures including anesthesia, buprenorphine injection, depilation and sterilization were identical to *tissue ELISA* procedures unless otherwise noticed. Four excisional full-thickness skin wound (6 mm in diameter) were created on the back of each animal. After *in situ* polymerization of fibrin matrices (of fibrinogen at 10 mg/mL, thrombin at 2 U/mL, factor XIII at 4 U/mL, calcium at 5 mM) containing test subjects of interest to the wounds, one piece of Tegaderm was adhered to cover the entire back of a mouse except the center area where the wounds were was covered with double layers of Tegaderm through which the non-sticky surface was in contact with wounds. At the time of sacrifice, half of the wounds were paraffin embedded for slicing into 5-μm thickness, while the other half was submerged in Tissue-tek CRYO-OCT for fresh cryo embedding and sliced into 20-μm thickness. H&E staining was performed on paraffin-embedded sections of tissues, and antibody staining was performed with cryo-embedded sections. For staining on cryo sections, the slides were first fixed in 4% PFA for 5 minutes followed by PBS rinse, blocking in 10% normal goat serum for 1 hour at room temperature, and primary antibody incubations: rabbit anti-NG2 (1:200) and rat anti-CD31 (1:100) at 4 °C for overnight. After three times of washing in PBS-tween, slides were incubated with Alexa-phore-conjugated secondary antibodies (1:200) along with DAPI (1:500) for 2 hours at room temperature. Sections were subsequently washed three times in PBS-tween and one final time in PBS before mounted with Anti-fade mounting media (Life Technologies). Three sections per wound (150 μm apart) and at least three regions in the granulation tissue per section were stained, imaged and analyzed to generate an averaged number. At least four wounds (n = 4) per condition were analyzed in the same way to generate the mean and standard error deviation for the plots. Images were taken with a Nikon C2 confocal microscope, and the positive area for

CD31 or NG-2 was measured using pixel threshold on 8-bit converted images (ImageJ software) and expressed as the area fraction of positive signal.

5.5 Results and Discussion

5.5.1 Peptide hydrolysis kinetics catalyzed by enzymes

First, the difference in the hydrolysis of L and D chiral peptides of the same sequence was studied in the presence of plasmin. Table 5 summarizes the distinct proteolytic kinetics between the two forms. Specifically, there was a ~10 fold smaller kcat for *D* enantiomer than the *L* enantiomer.

Table 5 Kinetic hydrolysis constant of *L* and *D* peptides of KNRVK catalyzed by plasmin.

	***L* peptide**	***D* peptide**
k_{cat} **(s^{-1})**	11.25	1.59
K_m **(μM)**	46.36	95.97
k_{cat}/K_m **(s^{-1}/M)**	2.43×10^5	1.66×10^4

Second, the specificity of plasmin, MMP-2 and MMP-9 to catalyze the proteolysis of peptides KNRVK, RLT and SLS, respectively, was assayed to confirm their selectivity as has previously been reported in literature.

5.5.2 Morphology of protein nanocapsules

As an example, nanocapsules with full-length vascular endothelial growth factor-A 165 as the core, designated as $n(VEGF)_{100\%,}$ were synthesized using ***1*** and ***2*** as the co-monomer and 100% plasmin-labile *L*-peptide as the crosslinker (as illustrated in Figure 11). Nanocapsules synthesized with different ratios of enantiomeric peptides, including $n(VEGF)_{100\%}$, $n(VEGF)_{50\%}$ and $n(VEGF)_{25\%}$, exhibit similar hydrodynamic diameters, indicating an unbiased polymerization

activity between the *L* and *D* peptide crosslinkers (Figure 12). Transmission electron microscope (TEM) images of purified n(VEGF)$_{100\%}$ showed an average diameter of 22 ± 3 nm (Figure 12). Furthermore, nanocapsules with full-length platelet derived growth factor-BB (PDGF) or full-length angiopoietin-1 (Ang-1) as the core were also synthesized; they were denoted as n(PDGF)$_{100\%}$ and n(Ang-1)$_{100\%}$, respectively (Figure 12). Specifically monomers ***1*** and ***3*** were used as the co-monomer for the synthesis of n(PDGF). The choice of the charged monomer for the synthesis of the nanocapsule shell is based on the overall surface charge of the core protein in the reaction buffer; thus, it is determined by the isoelectric point of the proteins. For example, VEGF has an isoelectric point of 8.5 [142]; therefore, it is overall negatively charged at pH 8.6 phosphate buffer. As a result, acrylamide (***1***, neutral) and amino-propyl methacrylamide (***2***, pKa = 9.6; thus, positively charged at pH 8.6) were selected as the co-monomer for the surface adsorption onto VEGF prior to polymerization.

Similarly, the shell of nanocapsules can be formed with other crosslinkers, which provides the nanocapsules with different specificities. As an example, a non-degradable compound, methylene bis acrylamide, was used as the crosslinker to form none-n(VEGF). As another example, the bisacrylated, MMP-2 sensitive peptide could be used as the crosslinker to form nanocapsules with ß-galactosidase as the core protein (Figure 12).

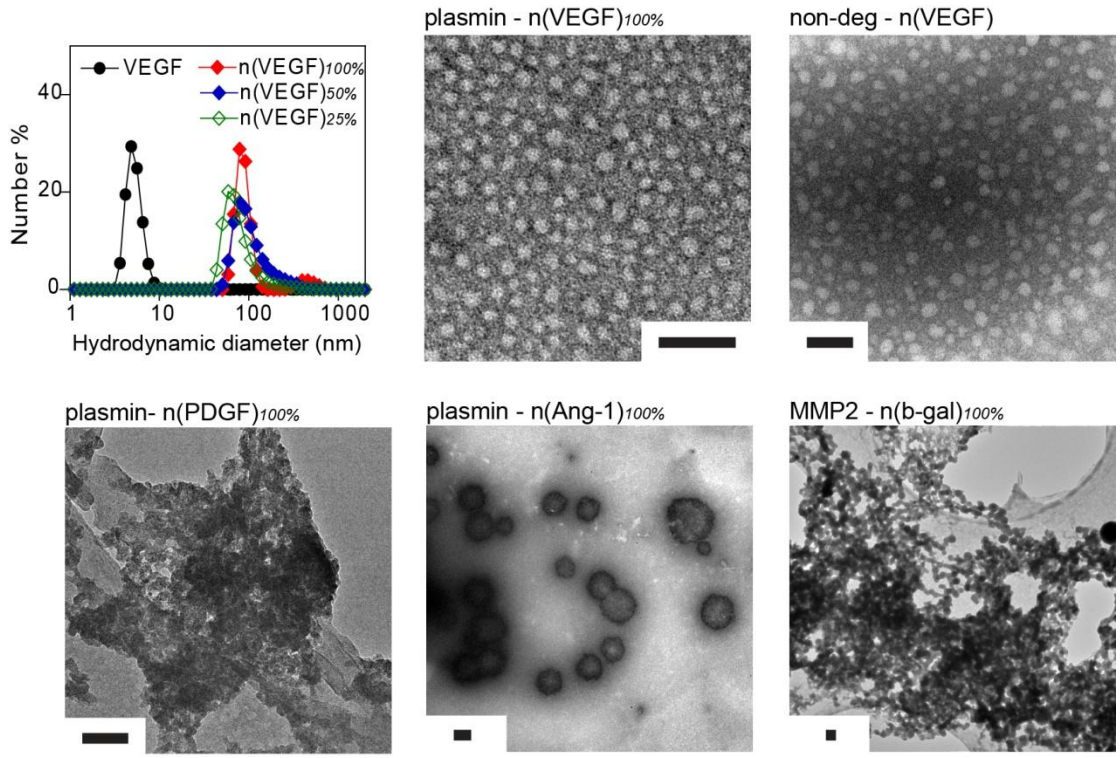

Figure 12 The sizes and morphologies of various types of protein nanocapsules. With VEGF as the core and plasmin specificity for the shell, nanocapsules that were crosslinked by the bisacryl l-chiral peptide or l/d mixed chiral peptide shared similar hydrodynamic sizes. With VEGF as the core, nanocapsules with either plasmin specificity or that are non-degradable by any protease showed particulate morphology under TEM. With plasmin specificity for the shell, PDGF and Ang-1 were also encapsulated to form n(PDGF) and n(Ang-1). With ß-gal as the core and MMP-2 specificity for the shell, nanocapsules for ß-gal were formed as well. Scale bars are 100 nm for each image.

By labeling VEGF with a gold-nanoparticle, each nanocapsule is found to contain one to two VEGF molecules (Figure 13**)**.

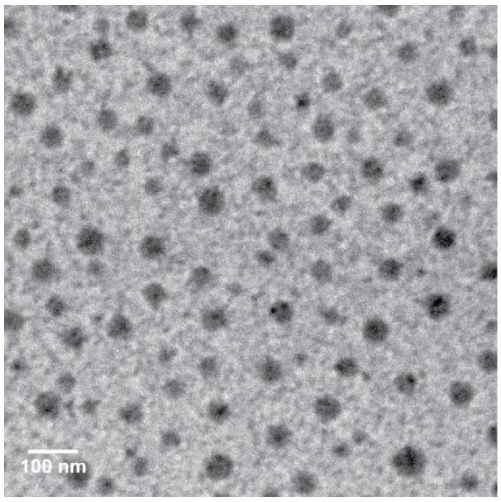

Figure 13 A TEM image of nanocapsules with gold nanoparticle (AuNP, 4 nm)-labeled VEGF as the core. AuNP is stained with silver enhancer kit to exhibit as dark black dots within the grey spheres of n(VEGF-AuNP)$_{100\%}$. (Scale bar 100 nm)

5.5.3 ENZYME-SPECIFIC DEGRADATION OF NANOCAPSULES TO RELEASE ACTIVE PROTEINS

First the incubation of plasmin-specific n(VEGF) in plasmin but not collagen IV (Col-IV) for 5 min resulted in significant release of VEGF (Figure 14a). At later time points (20 and 30 min), the tryptic impurity of collagenase IV could release some VEGF from nanocapsules.

Second, by balancing between L- and D-chiral peptide crosslinkers, the degradation of the shell of nanocapsules is modulated in response to a specific protease; thus, this platform features a programmable, enzyme-responsive release rate. Figure 14b compares the amount of VEGF released from n(VEGF)$_{100\%}$, n(VEGF)$_{50\%}$, n(VEGF)$_{25\%}$ and n(VEGF)$_{0\%}$ after the incubation with plasmin for 20 minutes. While a 6-fold increase of VEGF was observed with n(VEGF)$_{100\%}$ after plasmin incubation, only 1-fold increase in the quantity of VEGF with n(VEGF)$_{0\%}$, confirming decreasing the *L*-peptide content within the shells leads to decreasing *in vitro* release rates.

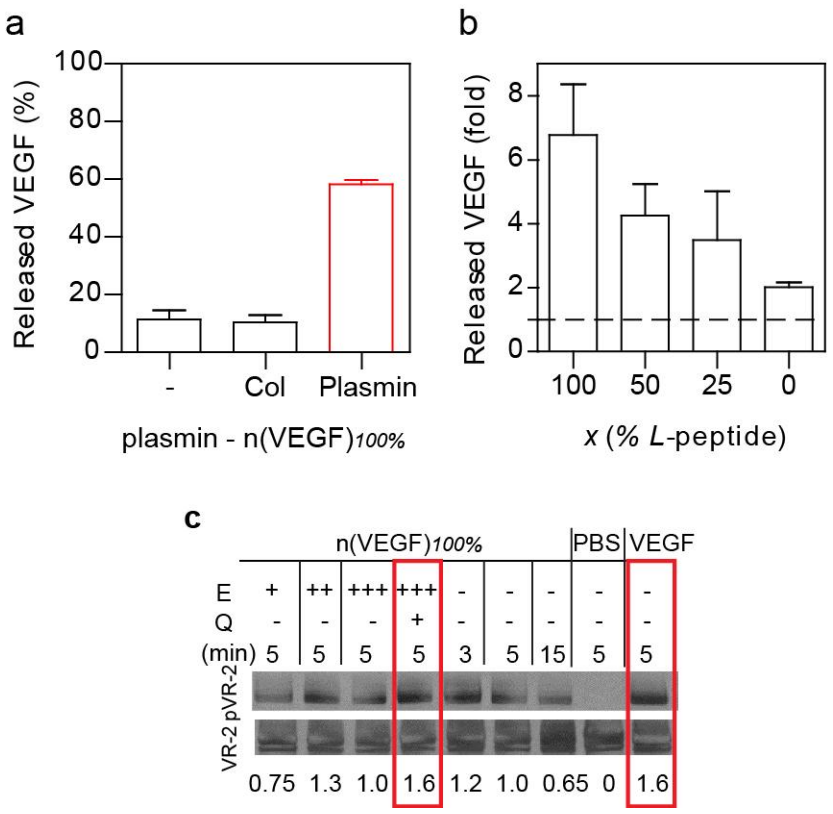

Figure 14 *In vitro* degradation of nanocapsules and the activity of released protein. a. Plasmin-specific n(VEGF) could release VEGF in the presence of plasmin, but not collagenase IV. b. Incubating $n(VEGF)_{100\%}$, $n(VEGF)_{50\%}$, $n(VEGF)_{25\%}$ or $n(VEGF)_{0\%}$ with plasmin for 20 minutes in ELISA measures the *in vitro* enzymatic release rates of nanocapsules. c. Western blotting analysis of the activity of encapsulated VEGF remains identical to free VEGF in inducing receptor phosphorylation. The encapsulated VEGF was first released from $n(VEGF)_{100\%}$ at 50 ng/mL via incubation with an enzyme (E), trypsin, at increasing mass ratios of trypsin:$n(VEGF)_{100\%}$ = 0.05:1 (labeled as E +), 0.1:1 (labeled as E ++), and 0.2:1 (labeled as E+++). To prevent the released VEGF from being degraded, an inhibitor, aprotinin, was subsequently used to quench (Q) the excessive proteolytic activity of trypsin. Released VEGF, as well as $n(VEGF)_{100\%}$ without enzyme pretreatment and free VEGF (50 ng/mL) were incubated with serum-starved human vein endothelial cells for specified amounts of time (min). The activity was indicated by the normalized intensity amounts with the phosphorylation of VEGF receptor-2 normalized by actin.

The activity of encapsulated proteins is protected and can be released by isolated enzymes or cell-secreted proteases. First, the degradation of the shell of nanocapsules is triggered by trypsin, followed by a treatment of a protease inhibitor to quench subsequent proteolytic degradation, and the released VEGF was able to induce the phosphorylation of cell-surface receptors to the same extent as free protein did (Figure 14c). This data suggests that 100% of the encapsulated proteins can be retrieved with appropriate amounts of enzymes and that the encapsulated proteins retained 100% of its activity.

The thermal stability of n(VEGF) was determined by its ability to activate tyrosine phosphorylation of VEGF receptor (VEGFR-2) using n(VEGF) that had been incubated at 37°C. While native VEGF after 10 days of incubation at 37°C could activate VEGFR-2 at 50% of the phosphorylation achieved with fresh VEGF, n(VEGF) stored at similar conditions induced VEGFR-2 phosphorylation to the same level as fresh VEGF did (Fig. 2e). In addition nanocapsules that contain 75% L-chiral peptide and 25% D-chiral peptide resulted in higher levels of phosphorylation at 10 and 14-days compared to 100% L-chiral peptide n(VEGF) capsules.

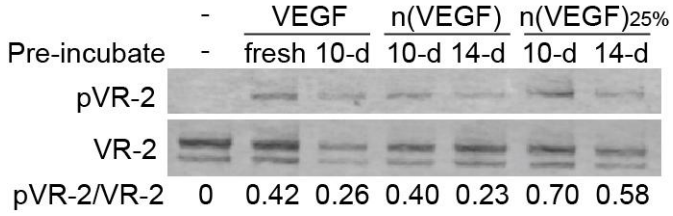

Figure 15 The thermal stability of proteins after encapsulation. Western blot analysis of the ability to induce receptor phosphorylation of n(VEGF) and VEGF that were previously stored at 37°C for 10 days (10-d) and 14 days (14-d) in comparison to fresh VEGF (as a positive control).

The stability of protein molecules determines the availability of delivered VEGF, which was improved by encapsulating the protein inside in situ formed nanocapsules. While naked proteins are highly sensitive to thermal deactivation and proteolytic degradation as shown by others [143,144] and our receptor activation assay, VEGF nanocapsules protected the protein against thermal denaturation even after 2 weeks of incubation at an elevated temperature and were able to stimulate receptor phosphorylation to a similar level as fresh VEGF. Furthermore, by substituting the l-peptide crosslinker used in the nanogel for d-peptide crosslinker, we observed an improved stability of VEGF nanocapsule. While other methods have extended the half-life of protein biologics including PEGylation and mixture of stabilizing factors (i.e. heparin) [145], they either covalently altered the structure of proteins or had to resort to alternate splicing variants.

5.5.4 Cell-mediated release and activation by encapsulated proteins in vitro and ex vivo.

Additionally, cells can mediate the release of proteins from nanocapsules with the proteolytic and fibrinolytic proenzymes[146] secreted by cells. We incubated $n(PDGF)_{100\%}$, $n(PDGF)_{0\%}$ and free PDGF with human dermal fibroblasts and observed some degree of receptor phosphorylation induced by nanocapsules (Figure 16), which indicated that some degree of encapsulated protein was released from $n(PDGF)_{100\%}$ in the timeframe tested.

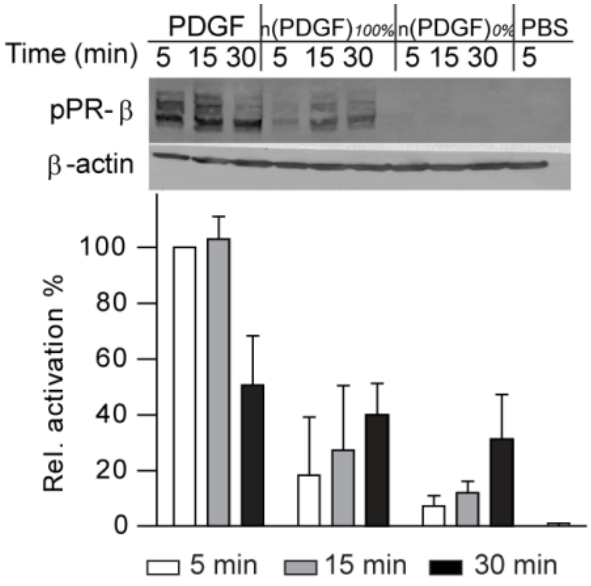

Figure 16 Western blotting analysis for cell-mediated degradation of nanocapsules. $n(PDGF)_{100}$, $n(PDGF)_0$, or PDGF (50 ng/mL) were incubated with serum-starved human dermal fibroblasts for specified amounts of time, and the phosphorylation of PDGF receptor-β induced by released ligands was quantified by normalization with actin bands (N = 3 independent blots).

Further analysis of the cell-mediated release of proteins from nanocapsules can be seen in Chapter 6.

To confirm that the angiogenic activity of n(VEGF) in vitro is translatable to in vivo applications, we adopted an ex vivo chick chorioallantoic membrane (CAM) assay to look at the activity of n(VEGF). By incorporating n(VEGF) into either fibrin or hyaluronic acid hydrogels for the implantation on developed CAM, capillaries were formed after two days in a radial orientation toward the implants, suggesting that nanocapsules can be degraded in vivo to induce angiogenesis (Figure 17). A similar angiogenesis response was seen with delivering VEGF from the implants, whereas blank implants did not induce it.

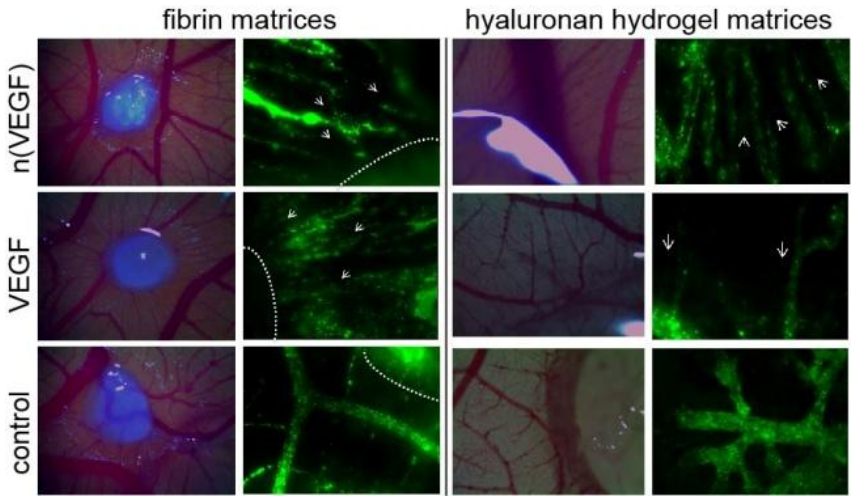

Figure 17 Chicken Chorioallantoic Membrane (CAM) assay where n(VEGF) or VEGF was incorporated within fibrin or hyaluronic acid hydrogel for grafting. Phase images of the macroscopic structures of grafts 2 days post implantation is shown, where fibrin grafts were opaque white color, and hyaluronan hydrogel grafts were clear gel with reflection. Corresponding fluorescent images after vessel perfusion with FITC-dextran were included, where the implants were outlined in dotted white line and the capillaries sprouting towards the implant was marked with white arrows.

5.5.5 WOUND-ENVIRONMENT-PROTEASE-MEDIATED SEQUENTIAL PROTEIN RELEASE.

Figure 18 shows that the release profile of n(VEGF)$_{100\%}$ and n(PDGF)$_{25\%}$ co-delivered to skin wounds from the same scaffold. As expected, VEGF was detected between 0 and 3 days and PDGF was detected between 3 and 6 days demonstrating the sequential release (Figure 18). Specifically, n(VEGF)$_{100\%}$ led to an excess of 200 pg VEGF per mg of tissue than endogenously present VEGF at day 0, but no significant difference on day 3 or day 6, suggesting that n(VEGF)$_{100\%}$ was mostly released by day 3 since urokinase plasminogen activator is initially activated in wounds and subsequently deactivated as wound heals and decreases in size.[103] However with the incorporation of D chiral peptide, the excess of PDGF detected with n(PDGF)$_{25\%}$ on day 3 and 6 further demonstrated in vivo delayed release enabled by chiral

protein nanocapsules. Such time scales are relevant for angiogenesis in mouse skin wounds where the angiogenic peak occurs at 3-5 days.

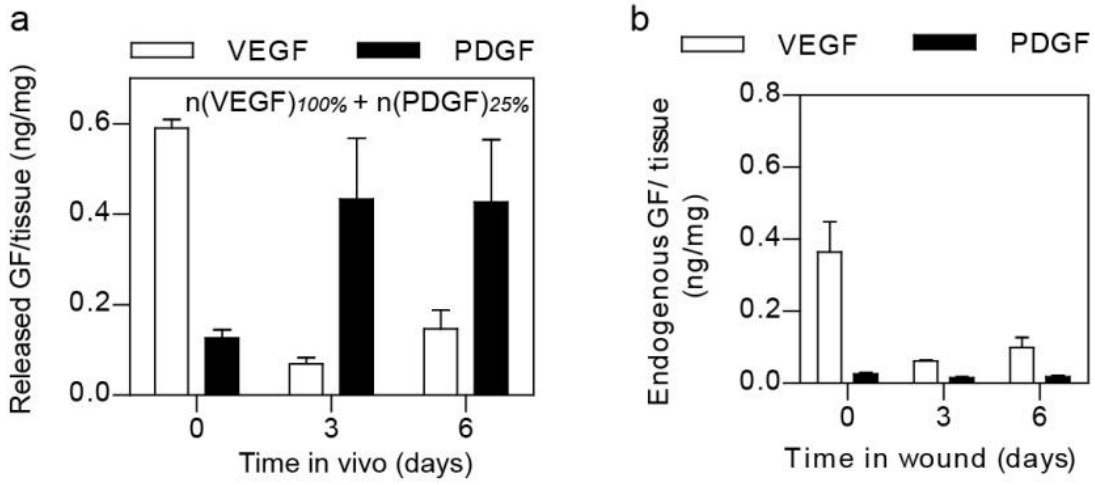

Figure 18 Tissue-ELISA analysis of wound-mediated differential release of proteins from nanocapsules with different chirality. a. The amount of VEGF and PDGF from skin wounds that were dressed with $n(VEGF)_{100\%}$ and $n(PDGF)_{25\%}$ at day 0, 3, and 6 post surgery. b. Endogenous levels of growth factors produced by skin wounds dressed with *in situ* polymerized fibrin gels analyzed.

5.5.6 Vascularization at stroke promoted by sustained delivery of VEGF

Here, we tested the ability of $n(VEGF)_{100\%}$/$n(VEGF)_{25\%}$ mixture (100 ng each, 200 ng combined) to promote vascularization in a challenging environment: the avascular stroke cavity. VEGF is one of the candidate molecules used in post-stroke neural repair therapies to enhance angiogenesis and functional recovery. However, the delivery of VEGF to ischemic brains is often complicated by the induction of disordered vasculature.[147,148] Immunohistological analysis of glucose transporter 1 (highly expressed in the brain endothelium) and PDGF receptor-ß (highly expressed in pericytes) showed that the bolus delivery of VEGF within a hyaluronic acid (HA) hydrogel did not improve the level of vascularization compared to HA hydrogel alone. In

contrast, the n(VEGF)$_{100\%}$/n(VEGF)$_{25\%}$ mixture led to statistically significant increases in vascularization and pericyte coverage in both the infarct (inside the stroke cavity) as well as peri-infarct (surrounding the stroke) regions (Figure 19). This result confirms that the nanocapsules are responsive to brain wound environments to allow for active VEGF release at a rate and level sufficient for enhanced vascularization.

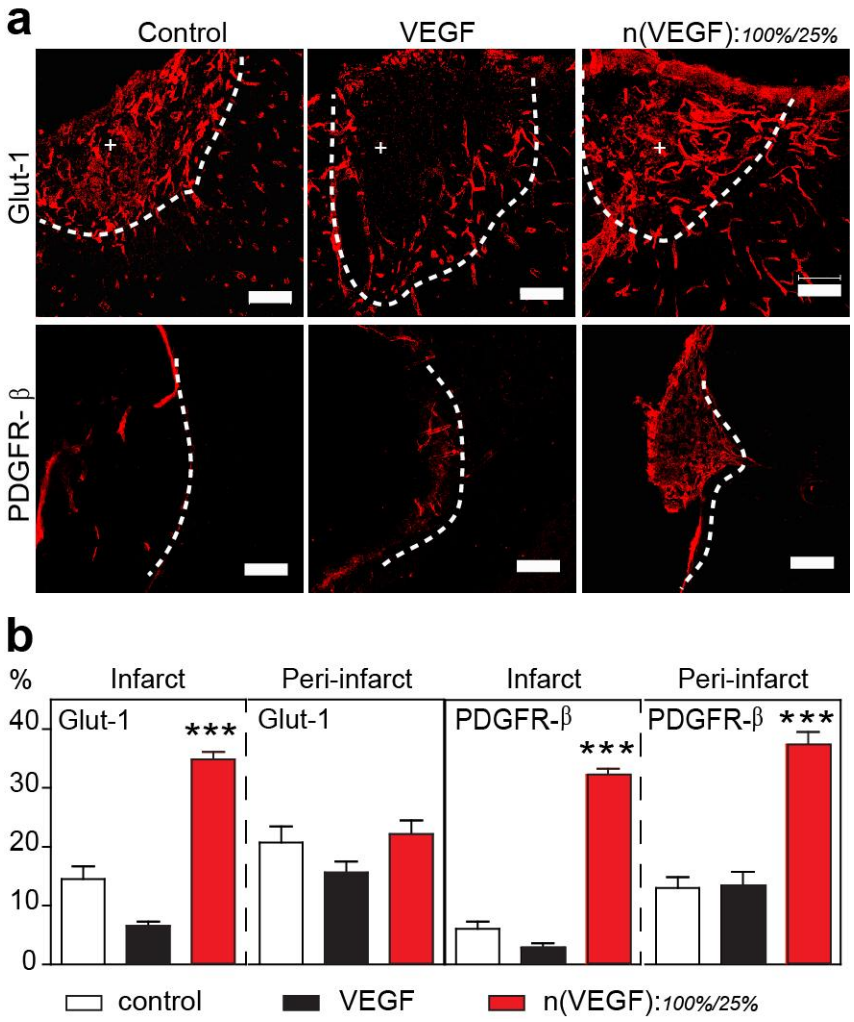

Figure 19 Temporal control of VEGF delivery in mouse stroke model. (a) Representative confocal images of blood vessels (Glut-1+) and their maturity markers (PDGFRβ+) in the infarct (indicated by +) and peri-infarct areas of stroke (separated by the dashed line). The stroke was treated with *in situ* crosslinked, adhesion peptide-modified hyaluronic acid hydrogels containing no VEGF (control),

unencapsulated VEGF (200 ng), or $n(VEGF)_{100\%}$: $n(VEGF)_{25\%}$ at 100 ng : 100 ng. (b) Analysis of Glut-1 and PDGFR-β markers for the vascularization in the infarct and peri-infarct areas of stroke. (AVONA with Tukey's post test, mean ± SEM, N = 3~4, * $p<0.05$, ** $p<0.01$, *** $p<0.001$.) (Scale bar, 100 μm).

5.5.7 Vascularization in chronic skin wound promoted by sequential delivery of VEGF followed by PDGF

To further analyze the ability of using enantiomeric nanocapsules to achieve sequential release of growth factors, we sought to demonstrate with the well-documented synergistic effects of VEGF and PDGF[3] in inducing pericyte coverage of nascent blood vessels in a diabetic skin wound healing model.[149] Because impaired wound closure in diabetic patients is correlated with impaired angiogenesis and angiogenesis is correlated with the ability to sustain granulation tissue, we compared the formation of granulation tissue and related angiogenesis process. The nanocapsule mixture of $n(VEGF)_{100\%}/n(VEGF)_{25\%}/n(PDGF)_{25\%}/n(PDGF)_{10\%}$ comprises a sequential delivery strategy of VEGF followed by PDGF, whereas $n(VEGF)_{25\%}/n(VEGF)_{10\%}/n(PDGF)_{100\%}/n(PDGF)_{25\%}$ forms the reverse sequence of PDGF release followed by VEGF. Among the two sequential, parallel and bolus delivery strategies, only the sequentially released VEGF then PDGF (condition iv in Figure 20 and Figure 21) led to enhanced formation of granulation tissue and increased vessel density with pericyte coverage. This observation further confirms that these chirally different nanocapsules can be engineered to release proteins in multi-phases in a wound environment. In contrast, nanocapsules that released both VEGF and PDGF in parallel (condition iii in Figure 20) did not show enhanced angiogenesis or mature blood vessels. Interestingly, we observed a non-significant difference in the CD31 expression between wounds treated with the reverse sequential strategy (PDGF first

then VEGF, condition v) and the orthogonal sequential delivery (VEGF first then PDGF condition iv), on which a recent report could possibly shed some light where the angiogenesis process in mouse bone healing was promoted by increasing PDGF secretion from preosteoclasts or treatment with exogenous PDGF[150]. Nevertheless the reverse sequential strategy failed to promote pericyte coverage in our study. This last example further exemplifies the ability to control protein release rates with our nanocapsules at disease sites.

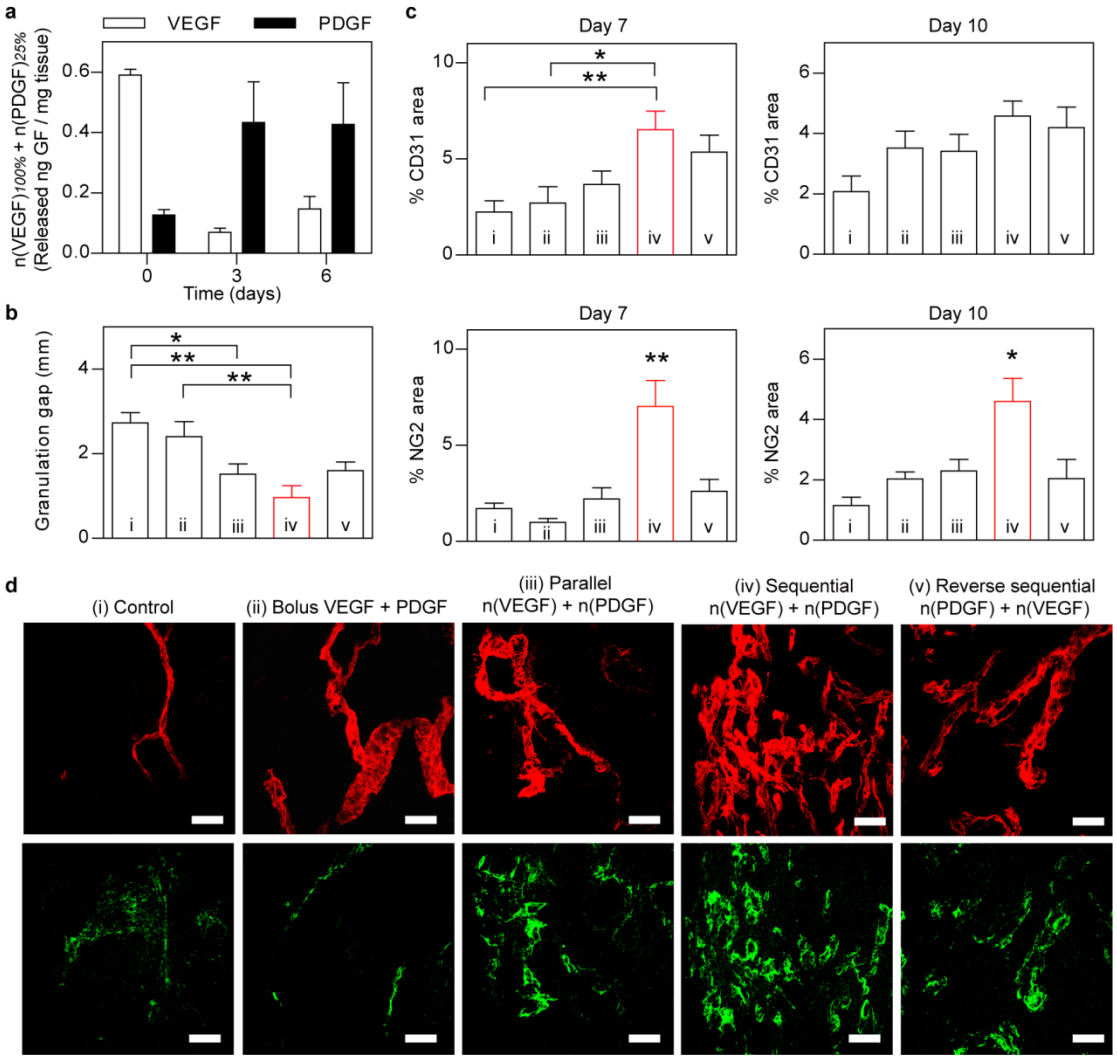

Figure 20 *In vivo* co-delivery of VEGF and PDGF with temporal control in diabetic mouse skin wounds. (a) Tissue-ELISA analysis of wound-mediated release of proteins from $n(VEGF)_{100\%}$ and $n(PDGF)_{25\%}$ at day 0, 3, and 6 post surgery. (b) Quantification of the gap of granulation tissues in diabetic skin wounds at

day 7. Wound was dressed with fibrin matrices that contained (i) no growth factors (control), (ii) un-encapsulated VEGF (200 ng) and PDGF (200 ng), (iii) mixture of $n(VEGF)_{100\%}/n(VEGF)_{25\%}/n(PDGF)_{100\%}/n(PDGF)_{25\%}$ at 100 ng/100 ng/100 ng/100 ng (parallel), (iv) mixture of $n(VEGF)_{100\%}/n(VEGF)_{25\%}/n(PDGF)_{25\%}/n(PDGF)_{10\%}$ at 100 ng/100 ng/100 ng/100 ng (sequential), and (v) mixture of $n(VEGF)_{25\%}/n(VEGF)_{10\%}/n(PDGF)_{100\%}/n(PDGF)_{25\%}$ at 100 ng/100 ng/100 ng/100 ng (reverse sequential). (c) Immunohistochemical analysis of vessel endothelium (CD31+) and pericyte coverage (NG2+) at day 7 and day 10. (d) Representative confocal images of CD31 (upper row) and NG2 (lower row) in the granulation tissue of diabetic skin wounds at day 7. (AVONA with Tukey's post test, mean ± SEM, N = 4~6, * $p<0.05$, ** $p<0.01$.) Scale bar = 50 μm (d).

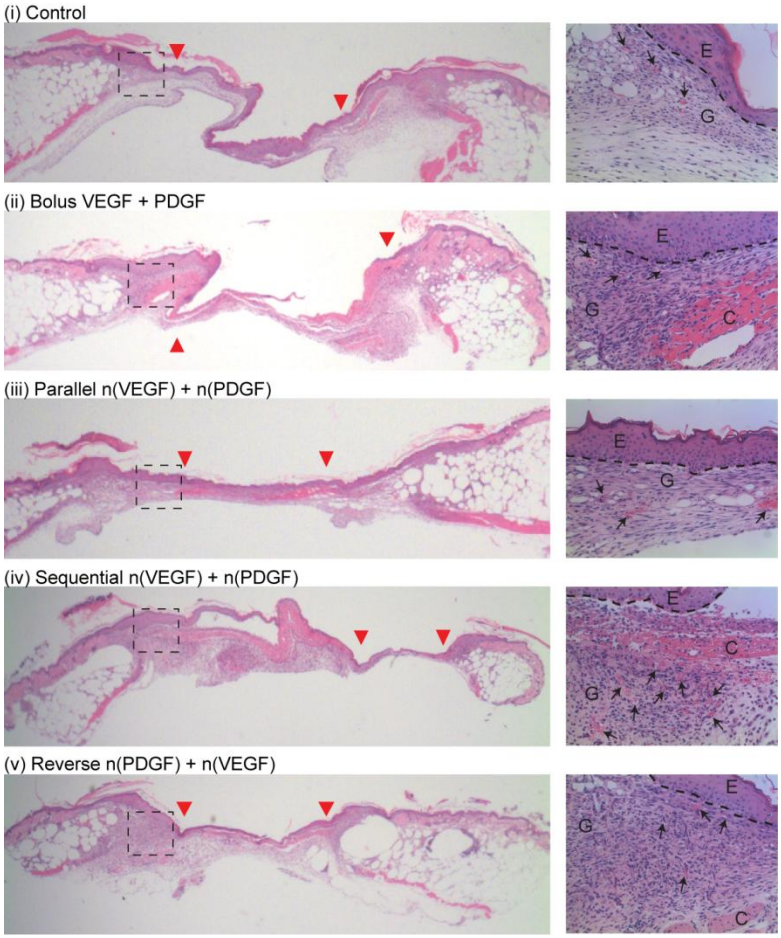

Figure 21 H&E images of day-7 db/db mouse skin wounds (6 mm biopsy punched) with dressing. Wound was dressed with fibrin matrices that contained (i) no growth factors (control), (ii) un-

encapsulated VEGF (200 ng) and PDGF (200 ng), (iii) mixture of $n(VEGF)_{100\%}/n(VEGF)_{25\%}/n(PDGF)_{100\%}/n(PDGF)_{25\%}$ at 100 ng/100 ng/100 ng/100 ng (parallel), (iv) mixture of $n(VEGF)_{100\%}/n(VEGF)_{25\%}/n(PDGF)_{25\%}/n(PDGF)_{10\%}$ at 100 ng/100 ng/100 ng/100 ng (sequential), and (v) mixture of $n(VEGF)_{25\%}/n(VEGF)_{10\%}/n(PDGF)_{100\%}/n(PDGF)_{25\%}$ at 100 ng/100 ng/100 ng/100 ng (reverse sequential). The edge of the gap of granulation tissue was marked with red triangles. Higher magnification images with a focus on the granulation tissue were shown on the right, with epidermis (E), granulation tissue (G), collagen (C) and blood vessels (arrows) labeled accordingly.

5.6 CONCLUSIONS

In conclusion, a general platform is demonstrated for multi-protein delivery with spatiotemporal definitions. This level of specificity in the control is initiated by endogenous protease cues in the wound environment, and enabled by enantiomerically engineered protein nanocapsules. Peptide chirality is for the first time utilized to modulate the enzymatic release of proteins and, enabled by the nanocapsule technology, to achieve spatiotemporal control of multiple proteins in cell-instructed microenvironments. These nanocapsules are facilely formed, robust and applicable to proteins in general, providing highly effective protein therapeutic vehicles for disease-specific tissue engineering and regenerative medicine.

CHAPTER 6:

SUSTAINED RELEASED VEGF INDUCE DIFFERENTIAL RECEPTOR ACTIVATION

6.1 INTRODUCTION

Since the discovery of insulin in the 1920s, protein-based therapeutics have been investigated for suitable routes of delivery and extended biological half-life [1]. Particularly growth factors (GFs) are attractive candidates because of their unique roles in signaling cells and regenerating tissues [22-24]. The challenges of controlled dosing and reducing the frequency for administration have driven designs to extend the physical presence of proteins by sustained delivery formulations [151-154]. However, little has been studied on the receptor activation and potentially signaling alterations of cells that are exposed to continued physical presence of growth factors.

Vascular endothelial growth factor (VEGF) is a widely studied growth factor to induce revascularization of ischemic tissues. However, despite several clinical trials of recombinant protein or gene transfer of VEGF [5,6], the delivery has not been successfully translated into approved therapies. It is now increasingly clear that the mode of delivery is critical for VEGF-induced angiogenesis with the dose and timing being critical for successful revascularization and therapeutic benefit [105,106,155]. Thus, bioengineering approaches to tune the delivery of VEGF to

achieve sustained release have been extensively investigated. These approaches have shown enhanced revascularization and therapeutic benefit; however, the mechanism by which sustained release of VEGF outperforms bolus delivered VEGF is poorly understood.

Although improved bioavailability (maintaining the VEGF dose at a therapeutic level) and stability (decreased degradation) have been cited as the proposed mechanism for the improvement, I propose that the improvement is also due to the manner in which receptor activation occurs. In other words, the sustained delivery of small doses of VEGF will induce differential signaling responses to endothelial cells compared to the bolus delivery of VEGF.

Previously the aqueous-based synthesis of a polymer shell that non-covalently encapsulates proteins was reported.[51] Release of the cargo is achieved by introducing extracellular protease degradable peptide crosslinkers to the polymer shell, achieving cell-demanded release of the protein. Herein, we utilize these protein nanocapsules to study the molecular and cellular differences of sustained VEGF delivery versus bolus delivery. In addition, we demonstrate that our nanocapsule delivery approach for VEGF can be tuned to deliver VEGF at a rate that promotes angiogenesis within granulation tissue that results improved tissue healing.

6.2 Materials and Methods

All chemicals were purchased from Sigma Aldrich unless otherwise noted.

6.2.1 Endothelial cell-mediated release of VEGF

HUVECs (p5-7) were used for incubation with 50 ng/mL of n(VEGF) or un-encapsulated VEGF, followed by western blotting analysis with details previously described [72]. Briefly,

HUVECs were starved in serum-free media for 6 hours before exposure to n(VEGF) or VEGF for different amounts of time. Treated cells were lysed in mRIPA lysis buffer (supplemented with fresh aprotinin, leupeptin and PMSF) and collected for supernantants. After performing Dc protein quantification assay (Biorad), 5 µg protein mass of cell lysates were run in NuPAGE 4~12% gradient bis-Tris gel for electrophoresis (100 min at 150 V) and transferred to nitrocellulose membranes (2 h at 400 mA at 4°C). Western blotting analysis was performed according to manufacturer's instructions with primary antibodies (1:1000, Cell Signaling Technology) and horseradish peroxidase (1:5000, Invitrogen) for visualization (with ECL detection reagents, GE Healthcare, Piscataway, NJ) using a Typhoon scanner (GE, Amersham Biosciences, Piscataway, NJ). Protein-loading control was assessed with corresponding antibodies (Cell Signaling Technology). Images of three biological samples were analyzed in ImageJ. PathScan phospho-VEGFR-2 (Tyr 1175) Sandwich ELISA antibody pair was also used in the analysis of cell lysates according to manufacturer's instructions.

6.2.2 SPROUTING ASSAY

Early passages (p2-4) of HUVECs were harvested and incubated with 2500 autoclaved Cytodex beads at a density of 1 million cells in 1.5 mL of media for 4 hours with gentle shaking every 20 min to allow for coating of cells on the surface of beads. Bead/cells were transferred to a 25-cm^2 cell culture flask and cultured overnight in 5 ml of EGM-2 media (Lonza). Fibrin matrices with bead/cells incorporated were formed with fibrinogen (at a final concentration of 2 mg/mL), aprotinin (37.3 µg/mL), penicillin/streptomycin (0.1% v/v), bead/cell (500 beads/mL), thrombin (20 U/mL), $CaCl_2$ (2 mM Ca^{2+}) and VEGF samples in Lab-Tek chambered cover glass for clear imaging facileness. Four conditions were tested (i) VEGF added to fibrinogen mixture

during gelation process at 200 ng/mL, (ii) no VEGF added, (iii) plasmin-sensitive n(VEGF) added to fibrinogen mixture during gelation at 200 ng/mL, and (iv) non-degradable n(VEGF) added to fibrinogen mixture during gelation at 200 ng/mL. Human dermal fibroblasts, previously cultured in DMEM media supplemented with 10% FBS and penicillin/streptomycin (0.1% v/v), were harvested and resuspended in VEGF-withdrawn EBM-2 media at a density of 40,000 cells/mL. 20,000 fibroblasts were added on top of fibrin matrices for every 250 cell-beads in a gel. The media were refreshed every two days where VEGF-withdrawn media was supplemented with different amounts of or no VEGF as indicated in the Results. Nanocapsules of VEGF were added in the fibrin matrices from day 0. Bright field images were acquired with Zeiss microscope. Three different gels of each condition were studied, and each gel was analyzed by averaging the measurements from five different beads within the same gel.

6.2.3 MOUSE EXCISIONAL WOUND CLOSURE AND VASCULARIZATION ANALYSIS

This protocol was approved by the Animal Research Committee (ARC) of University of California Los Angeles and all animal care was in accordance with guidelines. This is an established protocol of splinted wound healing model previously published by others [156]. Briefly, ten to 12-week old female Balb/c mice (Charles River Laboratories) were acclimated to the environment for at least 1 week upon delivery prior to the procedure. Mice were individually anesthetized with 4% isoflurane and maintained at 1.5-2% isoflurane during surgery. Buprenorphine (fours dosages of 60 uL each of 0.015 mg/mL per 20 g of mouse weight administered before, 8 hours, 20 hours and 28 hours after surgery) was injected subcutaneously. The dorsal surface was shaved with an electric clipper, depilated by Nair (1 minute) and sterilized with betadine and ethanol before surgery on an aseptic pad atop warming heat pads.

Using sterile biopsy punches (4 mm wide), two clean, well-defined wounds side-by-side were created slightly above the middle of the animal's back. Fibrin matrices (of fibrinogen at 10 mg/mL, thrombin at 2 Units/mL and $CaCl_2$ at 2.5 mM) of 25 µL were applied to wounds, each containing test agents of interest. In *in-situ* gelation approach, fibrin matrices (of fibrinogen at 10 mg/mL, thrombin at 2 U/mL, factor XIII at 4 U/mL, calcium at 5 mM and test agents of interest) of 30 µL were injected on wounds. Aseptic silicon ring splints formed prior to surgery had a 6-mm wide window that was double-sided with Tegaderm. Mastisol liquid adhesive was added on the splints which were placed on a wound. Eight interrupted sutures around each splint were made as a secondary means to hold down splints. Animals were monitored until awakening and housed individually in cages. Wounds were imaged every other day and analyzed using ImageJ. Remaining wound area was compared to the initial wound area (day 0). Statistical comparisons were made from four different replicates. Animals are euthanized on designated time points and wound tissues were fixed with 1% paraformaldehyde (PFA) for 16-18 hours at 4°C and paraffin embedded for slicing into 5-µm thickness. Three slides (50~100 µm apart) and each with three fields of view were imaged using a Zeiss fluorescent microscope with fixed exposure times after standard immunohistochemistry (IHC) staining procedures. Specifically, rat anti-mouse CD31 antibody (1:100, BD Pharmingen) was used with goat anti-rat Alexa 568 (1:200, Invitrogen) and 4', 6-diamidino-2-phenylindole, DAPI, nuclear stain (1:500). No primary antibody controls were included to confirm the absence of fluorescent antibody binding. Nine images of each wound were quantified for CD31 positive signals and averaged to generate one data point, and at least four wounds per condition were quantified for statistical analysis.

6.3 Results and Discussion

6.3.1 Prolonged receptor activation

Fresh native VEGF and plasmin-degradable n(VEGF) were compared side by side in the exposure to endothelial cells (ECs) and consequently the receptor activation. In a two-hour time course, the phosphorylation of VEGFR-2 (pVR-2) was strongly induced by native VEGF at 5 minutes but decreased rapidly thereafter. In contrast, n(VEGF) sustained pVR-2 throughout the first 30 minutes and decreased slowly afterward (Figure 22a). When EC-exposed VEGF or n(VEGF) was recycled and repeatedly applied to new ECs, "recycled" n(VEGF) resulted in substantial and increasing receptor phosphorylation levels up to 90 minutes (three EC-exposure cycles), while recycled naked VEGF remained a low receptor activation throughout (Figure 22b). Together this data suggests that ECs can continuingly degrade nanocapsules, release VEGF, and activate VEGFR-2 resulting in prolonged receptor phosphorylation. This hypothesis was further confirmed using naked VEGF to mimic sustained release where VEGF is added at t = 0 minutes followed by subsequent additions at t = 5, 10, 25, 55 and 115 minutes. In this experiment, a similarly persistent profile of receptor activation was observed through 120 minutes (Figure 22c).

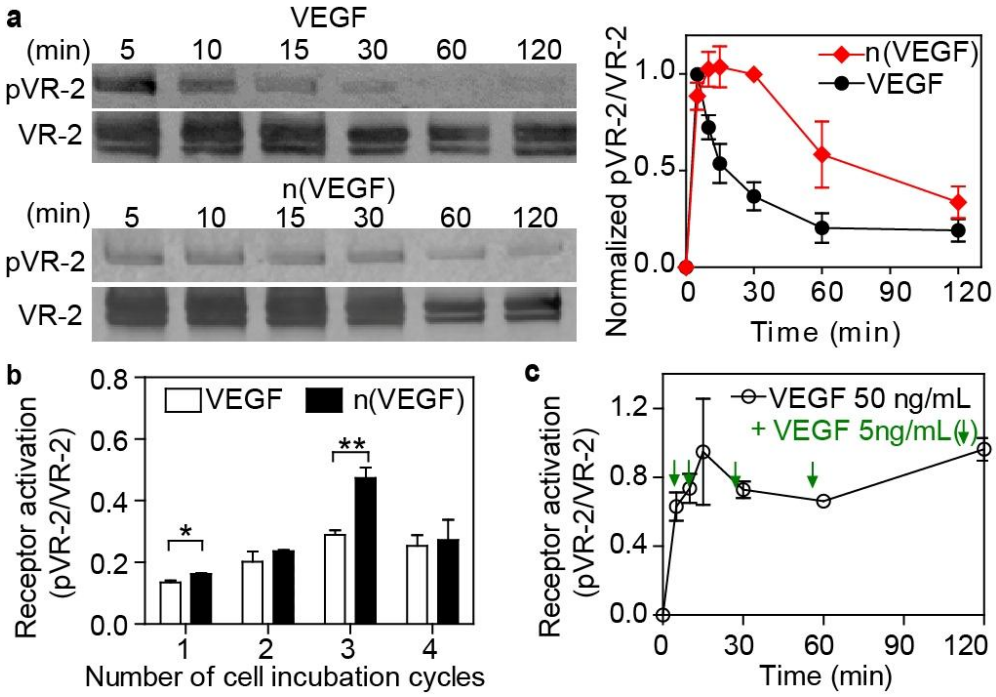

Figure 22 The dynamics of VEGF/VEGF receptor-2 interactions and its downstream signal pathways when VEGF is presented in a bolus manner or through cell-mediated slow release from n(VEGF). a. Western blot analysis and quantifications of VR-2 after incubation with VEGF or n(VEGF) at 50 ng/mL for 5, 10, 15, 30 60 and 120 min. (N=3) b. Phospho-ELISA readout of the (remaining) activities of VEGF or n(VEGF) (at 50 ng/mL) after consecutively reapplied to fresh HUVECs for four times and 30 minutes each. c. Phospho-ELISA readout of a prolonged phosphorylation of VR-2 over 2 hours induced by an initial bolus delivery of VEGF (50 ng/mL) followed by repetitive additions of VEGF (5 ng/mL) at 5, 10, 25, 55 and 115 minutes.

Our previous work with bound VEGF has already demonstrated that bound VEGF convey differential signaling responses to endothelial cells [77]. In those studies, we also showed that bolus VEGF delivery saturates all the available receptors at the surface of endothelial cells [78], which suggested to us that no new receptor activation could occur because there were no receptors at the cell surface to phosphorylate. Here, we validate that this observation of persistent receptor activation is also true with sustained released VEGF, which is realized either by

pipetting in small quantities of naked VEGF over time or through the use of our bioengineered n(VEGF) nanocapsules. This is in contrast to bolus delivery where phosphorylation peaks early in the time course (5 min) and subsides. This persistent receptor phosphorylation suggests of a changed ligand/receptor interaction and/or receptor availability at the cell surface, which either alone or together result in sustained receptor activation. Since similar sustained activation was observed by pipetting small quantities of VEGF, through n(VEGF) exposure and through n(VEGF) recycling, we conclude that n(VEGF) can be continuingly degraded by endothelial cells and that the release VEGF can activate nearby receptors.

6.3.2 DOWNSTREAM SIGNALING AND GENE EXPRESSION

Observing the change in the dynamics of receptor activation, we compared the effect of cell-demanded VEGF release from n(VEGF) to that of bolus delivered VEGF on activations of serine/threonine kinase AKT [157], mitogen activated protein kinases (p42/p44 MAPK) [158] and p38 (stress activated protein kinase-2) [159,160]. The activation of AKT and p38 was prolonged for n(VEGF) exposure, while the activation of MAPK was similar for both (Figure 23). Although all methods of VEGF delivery were capable of activating VEGFR-2 downstream signaling, in further analysis of known signaling pathways relating to the survival, proliferation and migration of endothelial cells, an extended activation profile was present with n(VEGF) for pathways relating to migration and survival.

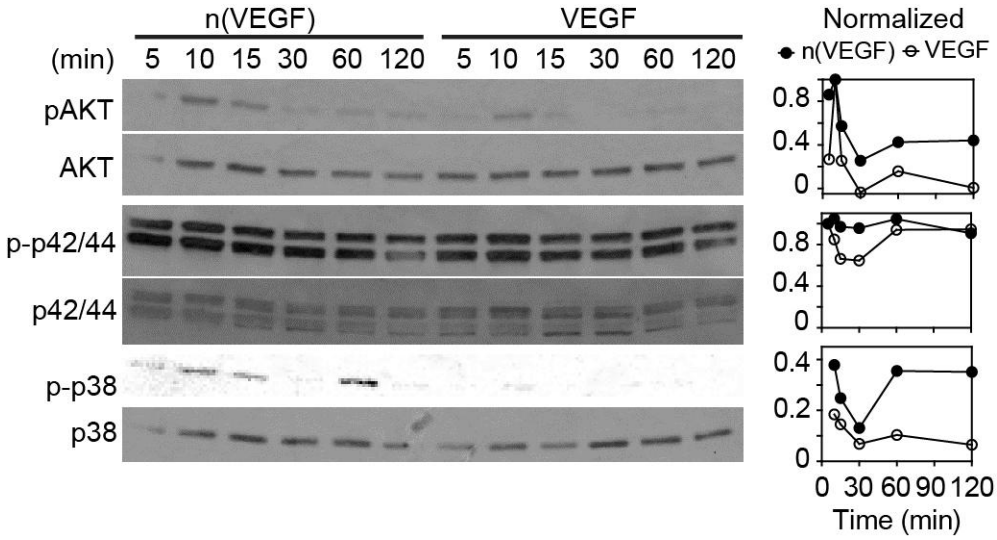

Figure 23 Western blot analysis of kinases: AKT, p42/p44 and p38 from HUVECs treated with VEGF or n(VEGF) at 50 ng/mL.

The expression levels of VEGF receptors (1, 2, and 3) were studied using quantitative polymerase chain reaction (qPCR). VEGFR-1 was up-regulated in ECs that were treated with n(VEGF) or multi-dose small amounts of VEGF, but not with bolus VEGF, indicating of a possible up-regulation in Notch signaling [161] when VEGF is slowly released (Figure 24). Our receptor activation and signaling cascade studies begin to point out the influence of slowly released VEGF in comparison to bolus administered VEGF, which may ultimately lead to a change in the expression levels of associated genes.

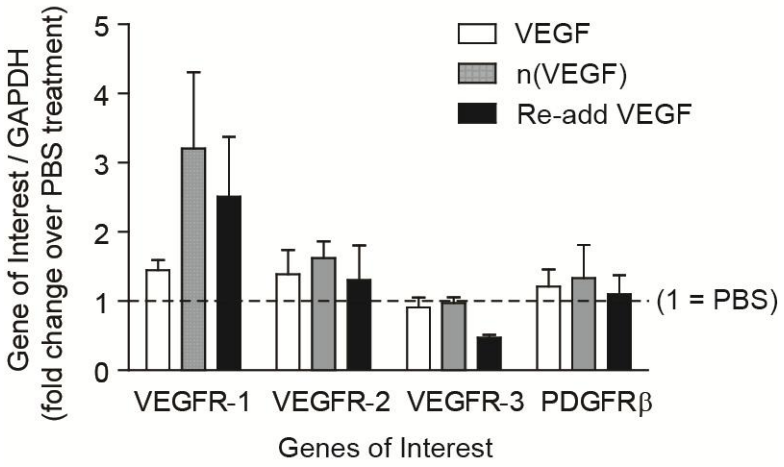

Figure 24 The rate and manner in which VEGF is delivered to endothelial cells (ECs) affects the mRNA expression levels of angiogenesis related genes. Serum-starved ECs were treated for 30 minutes with VEGF (50 ng/mL), n(VEGF) (50 ng/mL) or VEGF that was added at 10 ng/mL each time at t = 0, 5, 10, 15 and 25 minutes, followed by 2 hours of post incubation at 2% fetal bovine serum for 4 hours.

6.3.3 Dosing effect of VEGF on EC sprouting

To investigate if n(VEGF) was able to release VEGF in a protease mediated fashion that would promote sprouting of ECs over a time course of days, we utilized an *in vitro* sprouting bead assay [162]. One-time delivery at t = 0 day of naked VEGF at 200 ng/mL (bolus delivery) resulted in insignificant endothelial cell sprouting and tube formation for 7 days, whereas multiple replenishments with VEGF at 200 ng/mL at t = 0, 2, 4, 6 days resulted in a thick layer of cells but barely an sprout. In contrast, resupplying naked VEGF at 2.5 ng/mL every other day led to significant sprouting in 7 days (Figure 25). A one-time delivery at t=0 of n(VEGF) resulted in significant sprouting and tube formation for 7 days, indicating that n(VEGF) can be degraded to release VEGF at a rate that enables endothelial cell sprouting. Importantly, utilizing non degradable n(VEGF) (crosslinked with bisacrylamide or 100% D-chiral peptide) resulted in

no sprouting (Figure 26). These non-degradable nanocapsules were also characterized for their morphology and cell-mediated release profile (Figure 27).

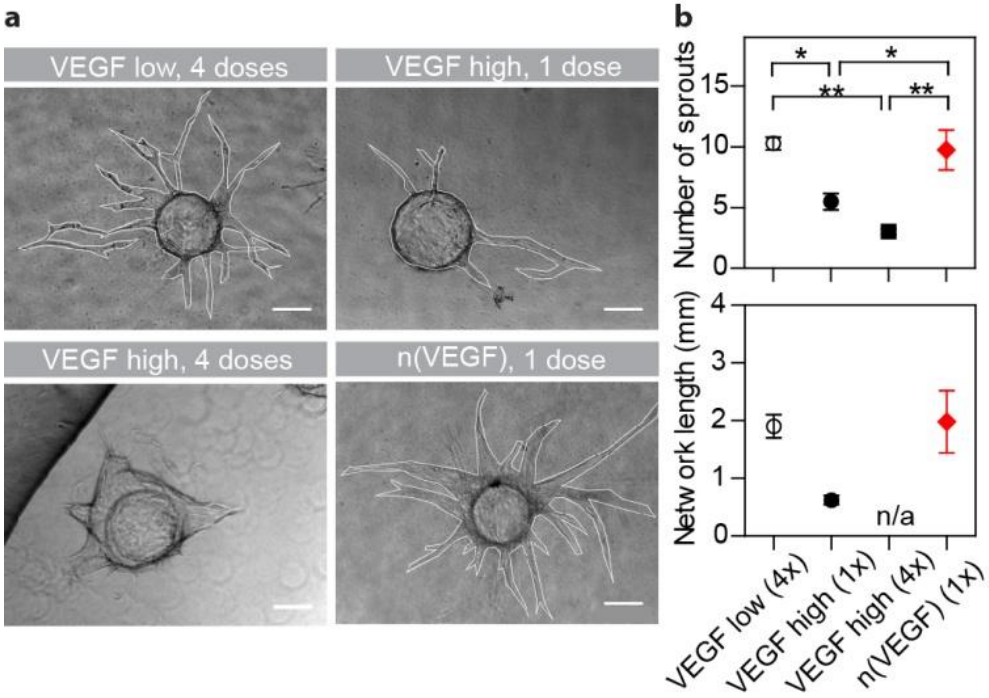

Figure 25 Single dose plasmin-degradable n(VEGF) supports endothelial sprouting and tubule formation. a. Microscopic images of endothelial cell (EC)-coated beads with EC sprouts (outlined) after 7 days incubation in fibrin matrices that were incorporated with either 2.5 ng/mL VEGF at day 0, 2, 4, 6 (VEGF low, 4 doses, 4x), 200 ng/mL VEGF at day 0 (VEGF high, 1 dose, 1x), 200 ng/mL VEGF at day 0, 2, 4, 6 (VEGF high, 4 doses, 4x), or 200 ng/mL n(VEGF) comprised of plasmin degradable crosslinker at 0 day (n(VEGF) 1 dose, 1x), Scale bar = 100 μm. b. Quantifications of 15 beads from 3 groups of gels were measured for each condition. *$p<0.05$, **$p<0.01$, one-way ANOVA with Tukey's multiple comparison test.

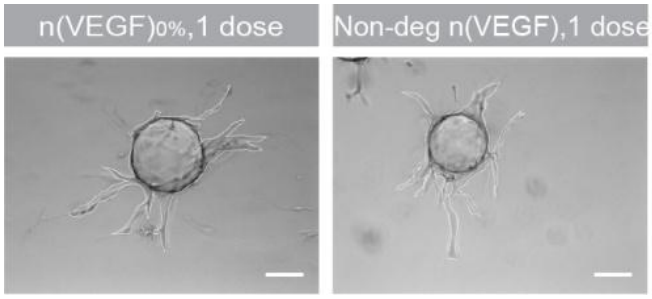

Figure 26 Plasmin-resisting nanocapsule and non-degradable nanocapsule of VEGF did not induce significant sprouting and tube formation of ECs. Microscopic images of EC sprouting assay in fibrin matrices that were cultivated in media containing either d-peptide crosslinked n(VEGF) (denoted as $n(VEGF)_{0\%}$) or bisacrylamide crosslinked n(VEGF) (denoted as non-degradable n(VEGF) at 200 ng/mL at day 0.

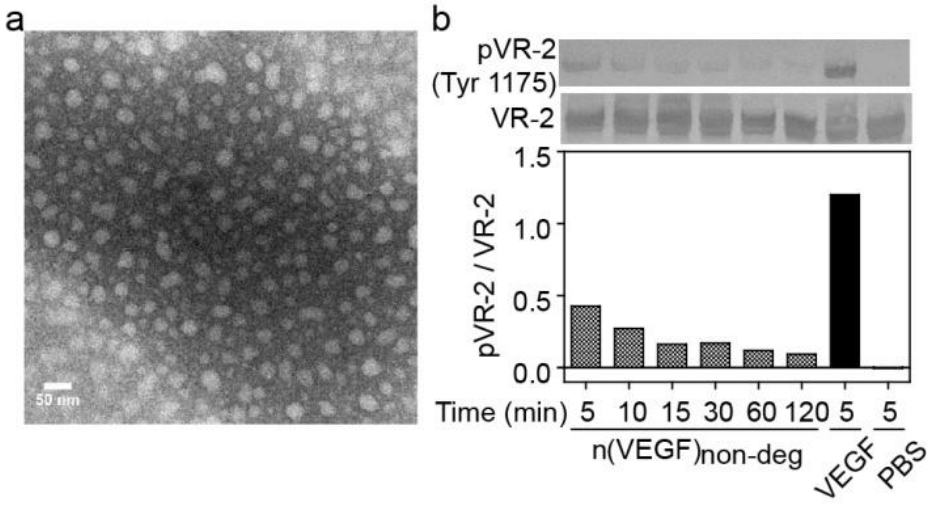

Figure 27 Characterization of non-degradable n(VEGF) made with N,N'-methylenebis(acrylamide) as the crosslinker for shell. **a**. A TEM image of non-degradable nanocapsules, scale bar is 50 nm. b. Western blot analysis of the phosphorylation of the tyrosine residue Y1175 of VEGF receptor-2 (pVR-2) after incubation with the non-degradable n(VEGF) (in comparison to positive control, VEGF, or blank control, PBS) at 50 ng/mL for 5, 10, 15, 30 60 and 120 minutes, showing of a minimal activation signal due to the non-degradability of nanocapsules.

In the event to recapitulate the angiogenesis process in vitro, previous reports have shown that replenished VEGF at a low dose of 2 to 5 ng/ml resulted in the optimal three-dimensional sprouting for endothelial cells in vitro [162]. Although the rapid diffusion of VEGF as well as the cell-laden, protease rich environment may be part of the reason for the necessary replenishments of fresh VEGF to support endothelial tubule formation it is not the entire explanation. Delivery of high doses of VEGF every two days does not result in robust sprouting and rather results in enhanced proliferation of endothelial cells at the bead surface, further demonstrating the importance of VEGF presentation (high or low dose, immediate or continued) on endothelial cell activation. Importantly, a single dose of n(VEGF) nanocapsules incorporated into the cell-laden matrice from day 0 was able to support similar sprouting as the resupply of low dose VEGF.

6.3.4 Sustained VEGF delivery and vascularization in the granulation tissue

Microenvironmental concentrations and a balanced distribution of exogenous VEGF are the critical factors in determining normal angiogenesis in vivo [105,106]. Therefore the delivery of VEGF in a cell-demanded and adaptive way would particularly be beneficial and it is achieved here by the modulation of protease levels at wound sites. To study if VEGF nanocapsules can deliver VEGF at a rate necessary for a therapeutic benefit, a splinted skin wound healing model was used where contraction, a primary mode of wound closure in mice, was prevented, and the healing through vascularized granulation tissue became a determinant factor, simulating the wound repair in humans[163].

VEGF nanocapsule retains in vivo angiogenic activity and promotes skin wound closure.

To investigate the therapeutic benefit of n(VEGF) delivery, a humanized full-thickness skin wound Balb/c mouse model was used. In this model, a splint was sutured on the periphery of the

wound in order to prevent skin contraction -- the primary mode of healing in mice. By doing so, the wound closure in human is better simulated because closure is promoted through vascularized granulation tissue (Figure 28a)[163]. A fibrin gel was directly applied to the wound bed either loaded with saline, naked VEGF (200 ng) or n(VEGF) (200 ng). The wounds were monitored over 11 days and by day 5, wounds implanted with n(VEGF) had significantly faster wound closure than naked VEGF or control (Figure 28b,c). By day 11, wounds addressed with n(VEGF) or VEGF were 40~60% open, whereas plain fibrin wounds were 80% open ($p = 0.0708$). However, the amount of endothelial marker CD31 at 11 days post wounding was statistically similar in the granulation tissue among treatment groups (Figure 28d and Figure 29).

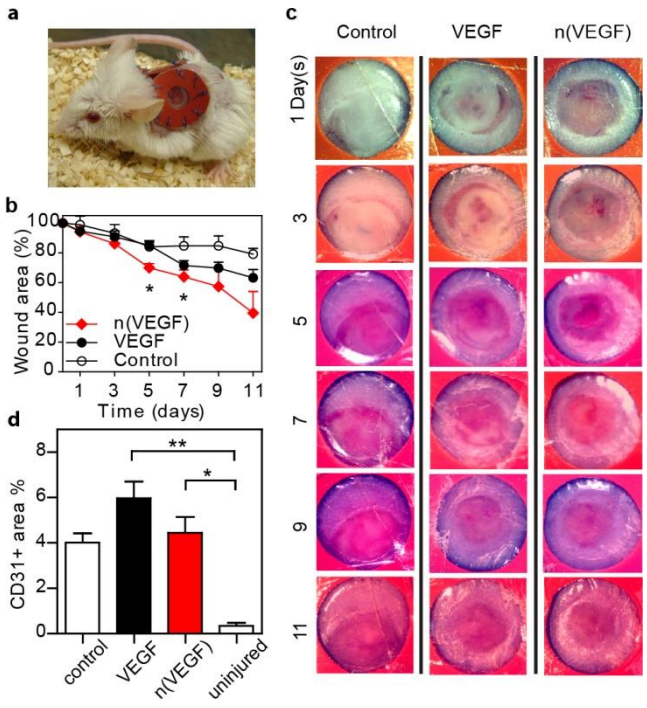

Figure 28 Wound repair in rodent splinted dermal excisional wound model. a. Splinted 4-mm wound model prevented loose skin from contraction and allows healing by the formation of granulation tissue. Silicon ring splints contained a window for visualization of wounds. b. Remainder wound area percentage quantified from 4 wounds per group and n(VEGF) dressing led to a significantly smaller wound than VEGF and control in day 5 and control in day 7 (*$p<0.05$). c. Images of remainder wounds dressed with

25 µL of fibrin matrix (control), fibrin matrix with 200 ng VEGF, or fibrin matrix with 200 ng n(VEGF). d. Statistical analysis on angiogenesis marker CD31+ on 11-day skin samples (n=4, one-way ANOVO with Tukey's post test, *p<0.05, **p<0.01).

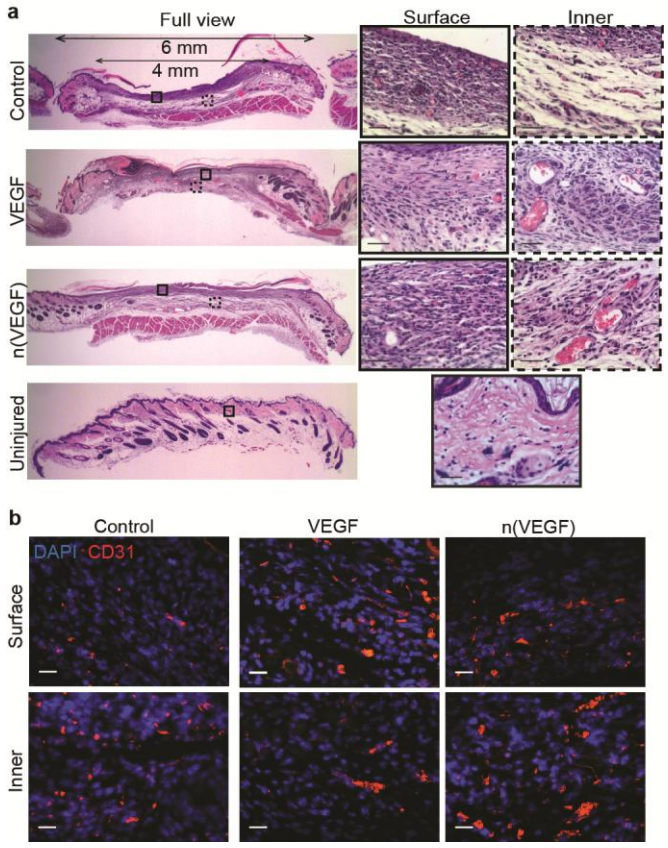

Figure 29 Histological analysis of wound areas on 11-day post surgery. a. Hematoxylin and eosin stain of wounds 11 days after dressing with fibrin matrices, macroscopic full view and high-magnification views of scaffolds closer to the surface (full line rectangular) and deeper into the wound beds (dash line rectangular) (scale bar 50 µm). b. Immunohistological staining of angiogenesis marker CD31+ on 11-day skin samples (scale bar 20 µm).

Although faster wound closure was observed with n(VEGF) supplemented fibrin dressing than plain or naked VEGF supplemented fibrin dressings at day 5, nanocapsules with 100% l-peptide crosslinkers did not achieve vascularization or wound healing differences by day 14 compared to bolus delivery; this result is likely because 100% L-chiral peptide n(VEGF) would

be largely consumed at the onset and early stage of angiogenesis considering the ample amount of proteolytic activity in the wound environment.

d-Peptide nanocapsules modulate slow VEGF release in vivo and enhance vascularization at wound sites.

By substituting some plasmin-sensitive nanocapsules for plasmin-resisting nanocapsules built with d-peptide, we expected to modulate the VEGF release rate to achieve a sustained delivery in vivo. Therefore, in an improved splinted wound healing model, a factor XIII supplemented fibrin dressing containing one of the following components was in situ injected into wound beds: (i) no exogenous VEGF, (control), (ii) 200 ng of VEGF, (iii) a combination of 100% l-peptide crosslinked n(VEGF) (100 ng) and 75% d-peptide crosslinked n(VEGF) (100 ng), denoted "n(VEGF) slow" release, (iv) a combination of 100% l-peptide crosslinked n(VEGF) (100 ng) and 50% d-peptide crosslinked n(VEGF) (100 ng), denoted "n(VEGF) medium" release, and (v) 200 ng of 100% l-peptide crosslinked n(VEGF), denoted "n(VEGF) fast" release rate. At 7 days post wounding, all nanocapsule treatment groups showed larger numbers of proliferating cells (BrdU positive) at wound beds compared to VEGF or control group. In particular, d-peptide incorporated nanocapsules for slow released VEGF resulted in statistically significantly larger density of vessels per mm^2 compared to n(VEGF) medium, n(VEGF) fast, naked VEGF or no-VEGF control (Figure 30). At 14 days post wounding, erythrocyte-filled blood vessels with coverage of smooth muscle cells or myoepithelial cells, as well as large diameter vessels (>18μm) were observed in nanocapsules-treated groups but not in naked VEGF or control groups (Figure 30).

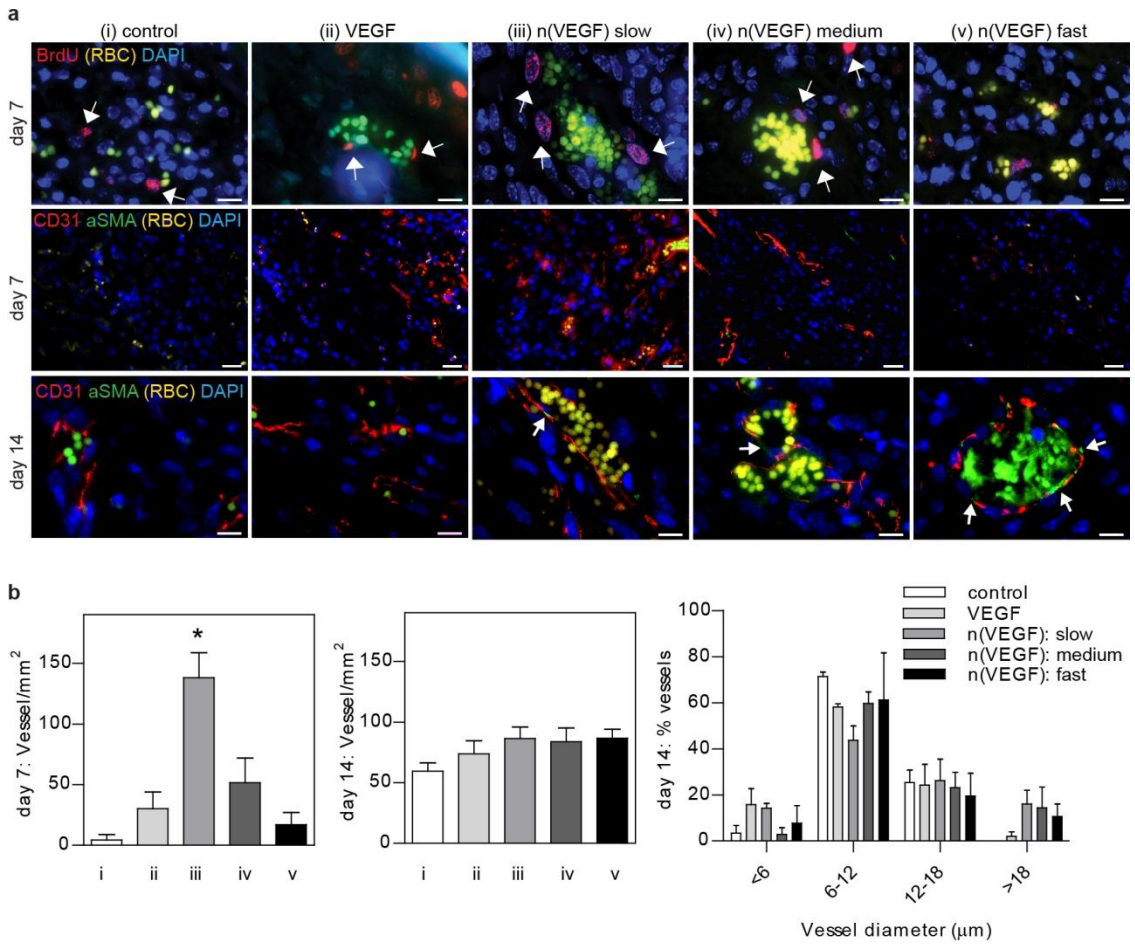

Figure 30 Angiogenesis from sustained delivered VEGF from engineered plasmin-responsive nanocapsules in skin wounds at 7-day and 14-day post surgery. a. Immunohistological staining of proliferating cell marker (BrdU+), angiogenesis marker (CD31+), perivascular cell marker (α-smooth muscle actin, α-SMA) and the auto-fluorescence red blood cells (RBC). Within fibrin dressing there were: (i) no exogenous VEGF (control), (ii) 200 ng native VEGF, (iii) 100 ng of 100% L-chiral n(VEGF) and 100 ng of 25% L(meaning 75% D)-chiral n(VEGF), ("n(VEGF) medium"), (iv) 100 ng 100% L-chiral n(VEGF) and 100 ng 50% L (meaning 50% D)-chiral n(VEGF), ("n(VEGF) slow"), and (v) 200 ng of 100% L-chiral n(VEGF), ("n(VEGF) fast"). Scale bar = 10 μm (BrdU staining), 20 μm (CD31 staining at day 7), 10 μm (CD31 staining at day 14). b. Quantifications of the vessel density and diameter. The results are the mean ± s.e.m. of four animals (three animals for control), with each data point being the

average of nine view of images representing three sections (50~100 μm apart) of each wound. *$p < 0.05$, **$p < 0.01$, ***$p < 0.001$, Kruskal-Wallis test with Dunns post test.

6.4 CONCLUSIONS

In conclusion, these studies demonstrate that the physical presentation of VEGF, in this case slowly released with time, can affect its molecular mechanism of actions resulting in differences in therapeutic benefit. With protease-labile peptides as the crosslinker in the nanogel, the delivery of VEGF using these nanocapsules was mediated by proteases. It achieved enhanced vascular sprouting in vitro and in vivo from a differential receptor activation profile compared to bolus delivered VEGF.

Looking forward, the enhancement in angiogenesis would further benefit from a pro-maturation factor such as platelet derived growth factor or angiopoietin-2 [87]. Nevertheless, the protease-modulated single-protein nanocapsule system shown here identifies from the molecular to cellular ramifications of a cell-demanded and adaptive VEGF delivery strategy.

CHAPTER 7:

SELF-ASSEMBLED HYDROGEL FOR DELIVERY OF HYDROPHOBIC AGENTS

7.1 INTRODUCTION OF SELF-ASSEMBLED HYDROGELS

Self-assembling hydrogels were previously studied in the formation of shear-thinnable, three-dimensional networks for the injectable delivery of protein biologics and stem cell therapy.[164,165] Polypeptide hydrogels rely on the association of ß-strands and the coiling of helices to self-assemble, giving rise to injectable hydrogels with inherent biofunctionality. [166] However, they do not necessarily dissolve hydrophobic drugs, while the addition of organic solvents can induce significant conformational changes to the polypeptide network.[167] Synthetic block copolymers on the other hand rely on the hydrophobic-hydrophilic interactions to form gels at high concentrations. While many studies have focused on linear block copolymers, i.e. triblock composed of ethylene glycol as core and propylene sulfide as ends[168], and triblock composed of hydroxybutyrate as core and ethylene oxide as ends[169], they readily form micelles but require dense polymer constituents in order to form gel network, which challenges the biocompatibility and degradability in vivo.

7.2 DELIVERY OF BIOACTIVE AGENTS VIA SELF-ASSEMBLED HYDROGELS

In the current paradigm of medicine, the majority of active substances are small molecules that help regulate a biological process. Specifically, hydrophobic functional groups are an essential component of the active ingredients of drugs for targeted protein-drug interactions.[170] However, it also renders the hydrophobicity of many compounds that do not readily dissolve in an aqueous environment. For example, major anti-infectious agents are composed of aromatic rings and, sometime, fused with cycloalkane rings, including Tetracycline. Without being sufficiently solubilized, drug candidates may result in crystallization and acute toxicity.[19] On the other hand, local interactions between small molecules and tissues rely on the proximate bioavailability of these drugs to induce cells in the three-dimensional milieu. Penicillin, for example, was shown more effective when applied locally than via systemic intramuscular administration in the treatment of corneal microbial infections, due to the localized concentration of the drug reached at the infection site. [20]

In order to deliver hydrophobic molecules in a locally concentrated, yet uniform, sustained dosage, carrier materials such as micelles[171,172], micro-/nano-spheres[173], emulsion gels/creams[174] and patches have been attempted. In the former two strategies of micelles and microspheres, amphiphlic polymers enable the solubilization of hydrophobic drugs in an injectable vehicle for minimally invasive dosing and good *surface* distribution of drugs. [172,175] However, the particulate sizes of these drug carriers do not provide the structural support or the delayed dosage profile in a tissue cavity, due to their immediate exposure to cells covering the cavity surface. In the latter two approaches of emulsion gels and transdermal patches, a uniform appearance of hydrophobic drugs within the carriers is enabled as well as extended release. Despite containing the desired physical consistency, these latter carriers either lack the

injectability for delivery into internal organs or are limited by the high surfactant concentration for good biocompatibility. It remains highly challenging to construct an injectable material that homogeneously delivers hydrophobic molecules in a cell-supporting structure for concurrent dosing and tissue remodeling.

We previously demonstrated the branched, 4-arm block copolymer, $(PEG_{113}\text{-}b\text{-}PPS_5)_4$ self-assembles through physically association to form gels at as low as 2.66 w/v%, which exceptionally allows for stem cell cultivation and transplantation to stroke area.[176] Here, we varied the hydrophobicity of $(PEG_{113}\text{-}b\text{-}PPS_x)_4$ (where x = 2.5, 5 or 16) to study its potential as a carrier for hydrophobic molecules and concurrently as a scaffold for injectable wound dressing. Additionally, we examined the oxidation and reduction-induced structural changes of this self-assembled hydrogel, as a potential means for environment-responsive scaffolds.

7.3 Materials and Methods

7.3.1 Materials

All chemicals were purchased from Sigma Aldrich unless otherwise noted.

7.3.2 Synthesis of branched poly(ethylene glycol)-b-poly(propylene sulfide)

The synthesis of PEG-PPS follows a three-step reaction, primarily described in previous publication with slight modifications.[177] Briefly in the first step, 10 g four-arm poly(ethylene glycol) (PEG) (MW 20,000, 2 mmol arms)) was dissolved in 120 mL dried tetrahydrofuran (THF) (pretreated with activated molecular sieves for overnight) and refluxed under argon gas at 90 °C for 4 hours (Figure 31). After the flask was cooled down, 0.6 g sodium hydride (8x excess

over arms = 16 mmol) was slowly added to the dissolved PEG and stirred for 15 min under argon. Subsequently 1.6 mL allyl bromide (10x excess over arms = 20 mmol) was injected into the mixture and the reaction was stirred under argon for overnight. To purify the reaction product of PEG-allyl ether, the reaction mixture was filtered under vacuum and the filtrate was dried to remove excess solvent. The viscous sample was redissolved in a small amount of dichloromethane and precipitated out in 200 mL ice-cold ethyl ether for two times. The precipitant was collected and dried under vacuum for overnight and subsequently stored in argon at -20 °C. NMR was used to characterize the final sample for modification. [178] ^{1}H NMR (400 MHz, $CDCl_3$): 3.39-3.89 (broad, PEG chain protons), 5.85-5.98 (m, 1H, -$CH_2OCH_2C\mathbf{H}=CH_2$), 5.15-5.30 (m, 2H, -$CH_2OCH_2CH=C\mathbf{H}_2$).

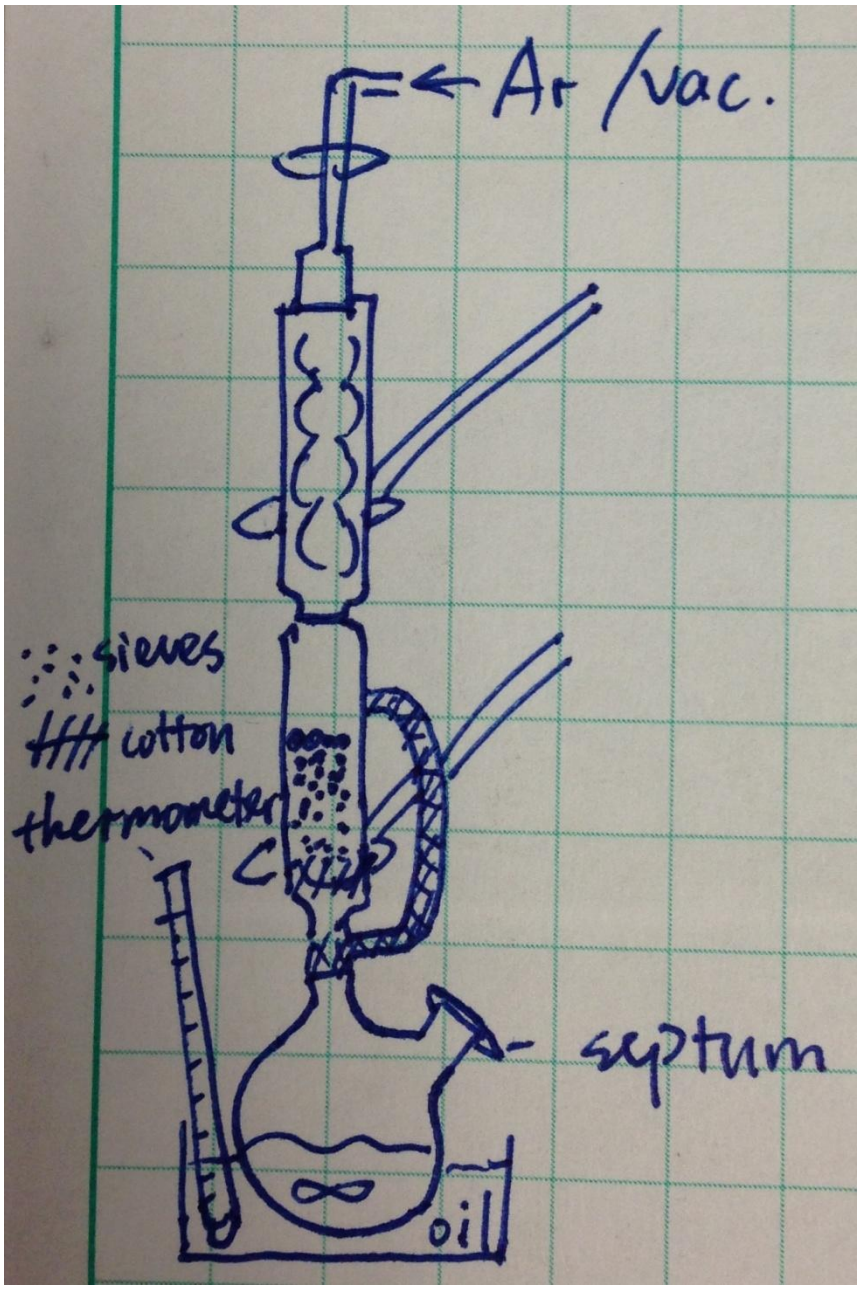

Figure 31 The reaction set-up for the synthesis of PEG-allyl. The round-bottom flask, the reflux vessel and the condenser are assembled and sealed with vacuum grease.

Second, PEG-allyl ether (3.78 g, 0.73 mmol arms) was dissolved in 130 mL anhydrous toluene with stirring and warming below 45 °C in a schlenk tube. The solution subsequently underwent freeze-pump-thaw degassing cycles until no bubbles were seen in the thawing step

(Figure 32). The radical initiator 2,2′-Azobis(2-methylpropionitrile) (AIBN) (1.5 g, 9 mmol) was freshly activated via recrystallization in methanol. Recrystalized AIBN and 2 mL thioacetic acid (26 mmol) dissolved in 20 mL anhydrous toluene were added to PEG-allyl ether solution in five aliquots over one day. The reaction was carried out at 80 °C for 72 hours in argon with aliquots of AIBN/thioacetic acid added at an interval of 2-3 hours. The reaction product of PEG-thioacetate was dried and precipitated in ice-cold ethyl ether. NMR was used to characterize the final sample for modification. ^{1}H NMR (400 MHz, $CDCl_3$): 1.81-1.9 (q, 2H, -$OCH_2C\mathbf{H}_2CH_2S$-), 2.35 (s, 3H, -$SCOC\mathbf{H}_3$), 2.92-2.97 (t, 2H, -$OCH_2CH_2C\mathbf{H}_2S$-), 3.39-3.89 (broad, PEG chain protons).

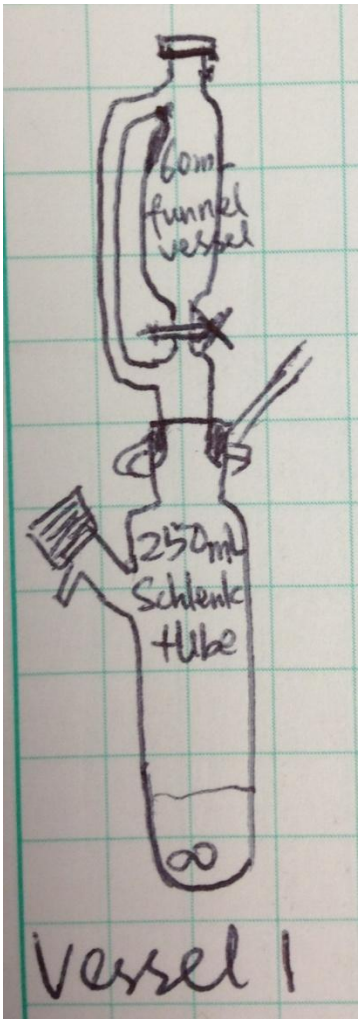

Figure 32 The reaction set-up for the synthesis of PEG-S-Ac. The schlenk tube (containing PEG-allyl dissolved in toluene) and the funnel vessel (containing AIBN and thiol acetic acid in tolune) are assembled and sealed with vacuum grease.

Third, PEG-thiolacetate (0.78 g, 0.153 mmol arms) was dissolved in freshly distilled THF (Figure 33). Sodium methoxide (83 mg, 10x excess over arms = 1.53 mmol) was added to PEG-thiolacetate/THF under argon and stirred for 30 min at room temperature. Subsequently specific amounts of propylene sulfide (2.5x, 5x and 16x molar equiv. of PEG arms) was added under argon and the reaction mixture was stirred for one hour. The end-capping reagent 2,2'-dithioldipyridine (168 mg, 5x excess over arms = 0.77 mmol) was later added and the reaction

mixture was stirred under argon for overnight. The sample of PEG-PPSx was later dried via rotary evaporator and dialyzed extensively against water. Lastly, the sample was lyophilized and stored under argon at -20 °C. NMR was used to characterize the final sample for modification. ^{1}H-NMR (in $CDCl_3$): 1.35-1.45 (d, CH3 in PPS chain), 1.81-1.9 (broad q, 2H, -OC**H**$_2$CH$_2$CH$_2$S), 3.6-3.7 (broad PEG chain protons).

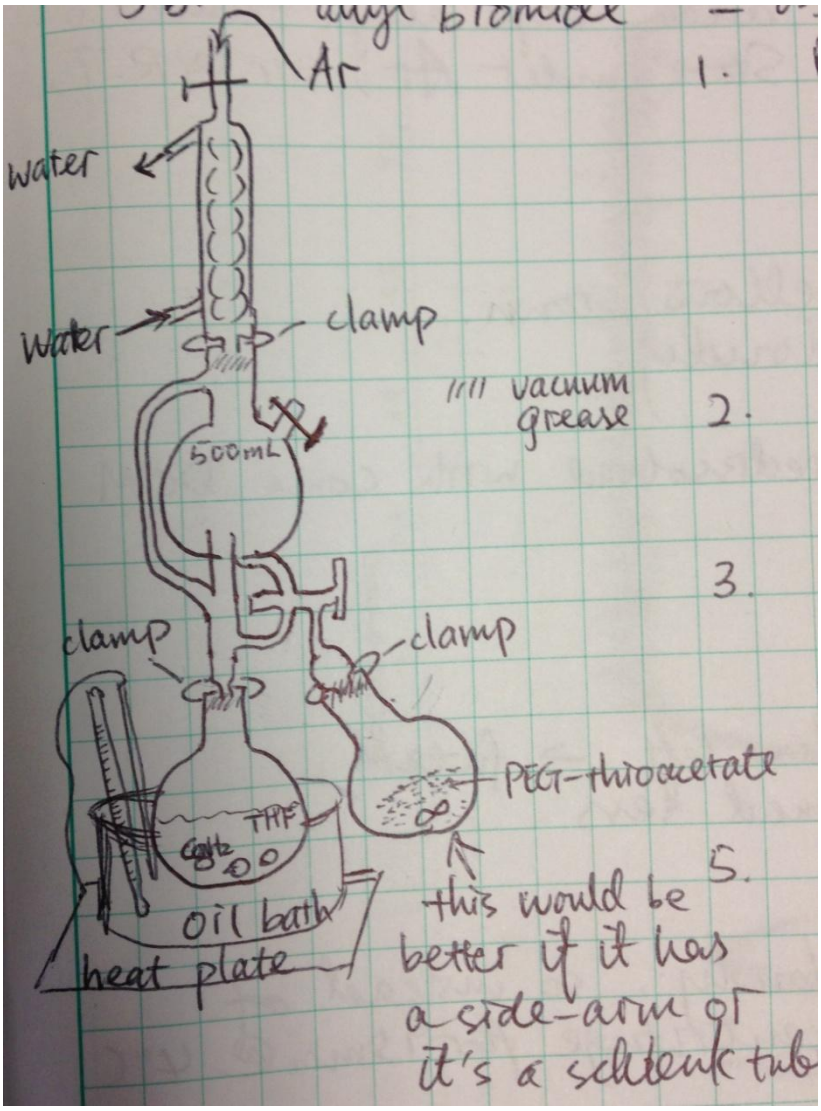

Figure 33 The reaction set-up for the final step of the synthesis of PEG-PPS. The distillation of tetrahydrofuran (THF) and the transfer of distilled THF to a reaction flask containing the reactant, PEG-S-Ac were set up together.

7.3.3 Rheological measurements of solvated PEG-PPS

PEG-PPS hydrogels were allowed to self-assemble overnight before transferred to an 8 mm plate-to-plate rheometer (Physica MCR 301, Anton Paar, Ashland, VA). An evaporation blocker system was used during measurements. For frequency sweep, the data were collected for the modulus with a frequency range of 0.1–100 rad/s under a 1% constrain at 37 °C. For amplitude sweep, the data were collected for the modulus with a frequency of 20 rad/s under a constrain range of 0.1-100% at 37 °C.

Water content measurements: Hydrated self-assembled PEG-PPS hydrogels were weighed for the wet mass (W_{wet}). Subsequently they were stored in a vacuum oven for two days until the mass did not change. The dried polymers were weighed (W_{dry}). Water content (%) was calculated as $(W_{wet} - W_{dry})/W_{wet}*100\%$.

7.3.4 Dissolution of hydrophobic molecules in PEG-PPS hydrogel

The dissolution of hydrophobic molecules, i.e. BrdU, vancomycin and tigecycline (used in Chapter 7), was generally carried out in the following manner.

The desired amounts of the powder form of the hydrophobic agents and the polymer were mixed in an eppendorf tube. Subsequently, a solvent or solution of choice was added to dissolve the mixture with vortexing and incubation at 37 °C for 4-12 hours.

7.3.5 Oxidation and reduction modifications of PEG-PPS

The oxidation experiment was performed by dissolved PEG-PPS (solid) into a 5 (v/v)% H_2O_2 aqueous solution.

The reduction modification on PEG-PPS was performed in two steps. The first step was to use Ellman's assay to determine all the available thiol groups on a certain percentage of aqueous solution of PEG-PPS. The second step was to use stoichiometric amounts of TCEP to treat PEG-PPS, resulting in various degrees of disulfide-crosslinked PEG-PPS.

7.3.6 Topical delivery of hydrophobic drugs in PEG-PPS hydrogel at wound site

Animal procedures were performed in accordance with the US National Institutes of Health Animal Protection Guidelines and the University of California Los Angeles Chancellor's Animal Research Committee. UV sterilized PEG-$PPS_{2.5}$ (at 10 w/v%) and PEG-PPS_5 (at 6 w/v%) were incubated with 500 μM Acetyl-GCGYGRGDSPG-NH_2, an adhesive peptide (RGD) containing a Cystein amino acid, and BrdU (at 10 mg/mL) in sterile phosphate buffer saline for overnight. The excisional splinted wound protocol was an established protocol previously reported by others and in details by our previous publication.[156] Detailed procedure of surgery can be found in Chapter 6.2.3.

On day 3 and day 7 post surgery, animals were euthanized and wounded tissues were punched out and cut in halves, where one half was fixed with 1% paraformaldehyde (PFA) for 16-18 hours at 4°C before paraffin embedding and the other half was freshly frozen in Tissue-Tek® *O.C.T.* Compound. Paraffin sections were sliced into 5 μm thickness for hematoxylin and eosin (H&E) stain. Cryo sections of skin cross-sections were sliced as 20 μm for immunohistochemistry staining. The primary antibodies used included rat anti-CD31 (1:100), rabbit anti-NG-2 (Millipore, 1:100), rat anti-F4/80 (eBioscience, 1:100), rat anti-BrdU (Abcam, 1:100), rabbit anti-Ki 67 (1:100). Alexa Fluor conjugated matching secondary antibodies (Life Technologies) were used. Three slides (50~100 μm apart) and each with designated fields of

view (Region I, II, III for wound center, wound/granulation tissue, and normal wounds) were imaged using a Nikon C2 confocal microscope. A full wound scan was also performed. Images were quantified in Image J for positive signal areas and averaged across four different wounds for statistical analysis.

7.4 Results and Discussion

7.4.1 NMR of branched $(PEG_{113}\text{-}PPS_x)_N$

The synthesis of $(PEG_{113}\text{-}b\text{-}PPS_x)_4$ follows a three-step reaction (Figure 34 The reaction schematics for the synthesis of branched block copolymer, PEG-PPS.Figure 34). First, 4-arm poly(ethylene glycol) is modified to with an allyl group. Subsequently the branched polymer is reacted to generate a protected thiolate ending group. By adjusting the molar mass of propylene sulfide added, the anionic ring-opening polymerization in the final step allows for controlling the length of the PPS block. As characterized by NMR, three different lengths of the hydrophobic block, namely $(PEG_{113}\text{-}b\text{-}PPS_{2.5})_4$, $(PEG_{113}\text{-}b\text{-}PPS_5)_4$ and $(PEG_{113}\text{-}b\text{-}PPS_{16})_4$, were synthesized (Figure 35).

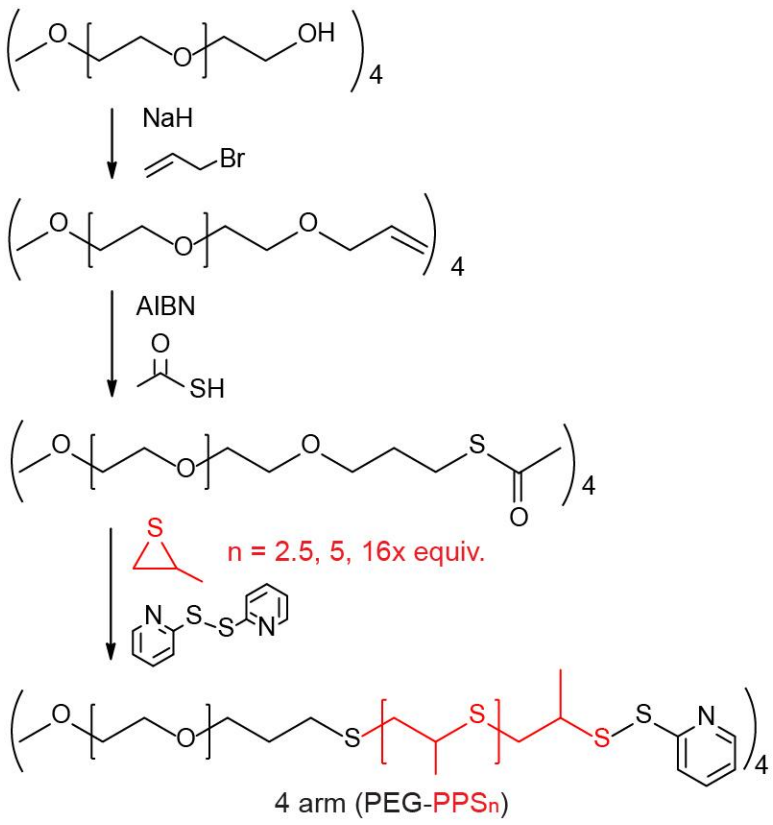

Figure 34 The reaction schematics for the synthesis of branched block copolymer, PEG-PPS.

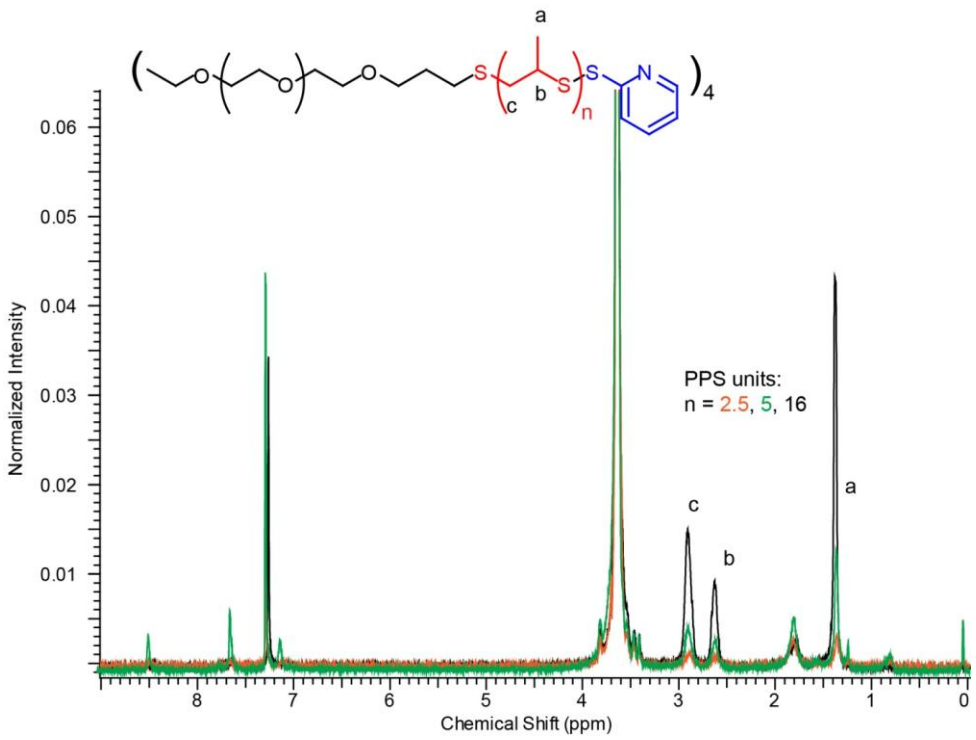

Figure 35 The NMR spectra PEG-$PPS_{2.5}$, PEG-PPS_5, and PEG-PPS_{16} in $CDCl_3$. All polymers were dissolved in $CDCl_3$ at 20 mg/mL.

7.4.2 Shear-thinning and self-healing properties of PEG-PPS hydrogel

When water was used to solvate PEG-PPS, a transition from a solution state to the gel state was observed from $(PEG_{113}$-*b*-$PPS_{2.5})_4$ to $(PEG_{113}$-*b*-$PPS_5)_4$ and $(PEG_{113}$-*b*-$PPS_{16})_4$ (all at 10 w/v%). When another solvent methanol was used, it immediately solubilized $(PEG_{113}$-*b*-$PPS_{2.5})_4$ whereas $(PEG_{113}$-*b*-$PPS_{16})_4$ at the same concentration became a very elastic gel (Figure 36**a**). The observed variations in the physical property of $(PEG_{113}$-*b*-$PPS_x)_4$ was confirmed in the rheological measurements (Figure 36**b**). With a longer hydrophobic block in the branched amphiphilic polymer, a stronger physical interaction (the hydrophobic-hydrophilic segregation) was shown to lead to a stiffer hydrogel.

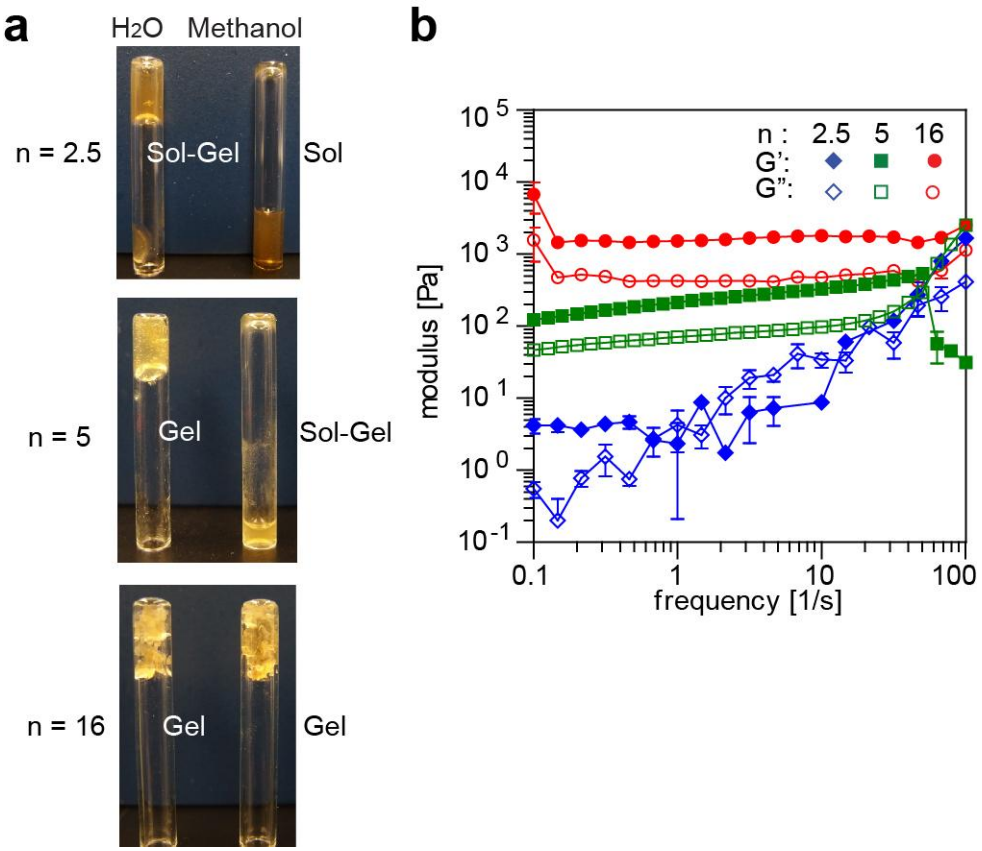

Figure 36 The sol-gel transition of PEG-PPS polymers from less to more hydrophobicity in aqueous and methanol solvents. a. When resuspended in water at 10 w/v%, PEG-$PPS_{2.5}$ exhibits sol-gel transition, PEG-PPS_5 is fully hydrated and PEG-PPS_{16} is partially hydrated with pockets of water not absorbed. When resuspended in methanol, PEG-$PPS_{2.5}$ flows under gravity, PEG-PPS_5 exhibits sol-gel transitioning and PEG-PPS_{16} is mostly hydrated as hydrogel. b. The rhelogical property of 10 w/v % PEG-$PPS_{2.5}$ (in water), PEG-PPS_5 (in water) and PEG-PPS_{16} (in methanol).

The effect of polymer mass on the hydrogel network (solvated in aqueous saline buffer) for this polymer was further studied using $(PEG_{113}$-*b*-$PPS_5)_4$. First, we looked at the behavior of the polymer under increasing shear force, which mimics injection processes. As the oscillatory deformation increased from 0.1% to 100% at a constant frequency, $(PEG_{113}$-*b*-$PPS_5)_4$ yields at similar strains of 33% ± 4 %, 27% ± 6% and 20% ± 8% for 5 w/v%, 7.5 w/v% and 10 w/v% respectively (p = 0.11). Upon the cessation of deformation and as the shearing resumed, (PEG_{113}-

b-$PPS_5)_4$ repeatedly began and remained as a solid-like state (G'>G") until yielding at the threshold strains (Figure 37a). This yielding behavior of the amphiphilic polymer network was previously observed in other systems where the polymer "breaks" (flows) under high shear force and "heals" (gels) once the shear force is ceased.[179] (PEG_{113}-*b*-$PPS_5)_4$ hydrogel remained as semi-transparent microscopically, and all three concentrations had a water content over 90 w/w % (Figure 37b). Additionally although a higher polymer concentration led to greater elastic and viscous moduli, (PEG_{113}-*b*-$PPS_5)_4$ hydrogel tested from 3 w/v % to 10 w/v % all exhibited a time (frequency)-dependent shear thinning property (Figure 37c).

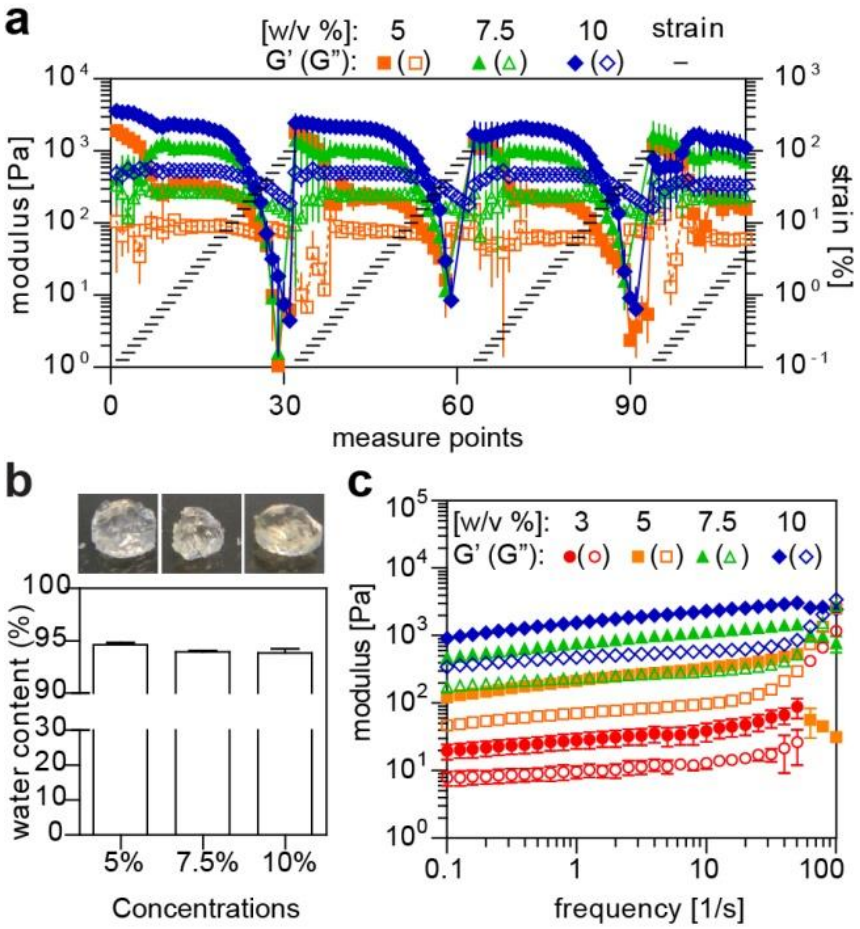

Figure 37 The shear-thinning, self-healing, redox responsiveness properties of PEG-PPS_5. a. The yielding and healing behaviors of different concentrations of PEG-PPS_5 in aqueous environment. b. Images of

PEG-PPS_5 hydrogels and the quantification for their water content as a percentage of total mass. c. The rheological moduli of PEG-PPS_5 hydrogels of different concentration under 1% strain.

7.4.3 DISPERSION OF HYDROPHOBIC DRUGS

Using bromodeoxyuridine (BrdU) as a model molecule, the ability of PEG-PPS to solubilize hydrophobic compounds was tested. BrdU is a commonly used agent to label proliferating cells due to its structural similarity to thymidine, which can be incorporated into newly formed DNA. However it has a poor solubility in water at room temperature, which results in general practices of either pre-dissolving in an organic solvent, such as dimethyl sulfoxide, prior to dilutions in aqueous solution, or taking up to a few hours at 37°C to dissolve a moderate amount (i.e. 1-5 mg/mL). As expected, BrdU in water (at 10 mg/mL) did not completely dissolve after 30 minutes of vortexing at room temperature. In contrast, BrdU in the aqueous suspension of $(PEG_{113}$-*b*-$PPS_{2.5})_4$ (10 w/v%) after minutes of gentle vortexing was homogeneously dissolved and no crystal structures could be observed under microscope (Figure 38a).

As expected, water or branched PEG itself dissolved in aqueous solution did not entirely solubilize BrdU via vortexing at room temperature, whereas $(PEG_{113}$-*b*-$PPS_5)_4$ did homogeneously dissolute BrdU (Figure 38b) as did $(PEG_{113}$-*b*-$PPS_{2.5})_4$ shown previously.

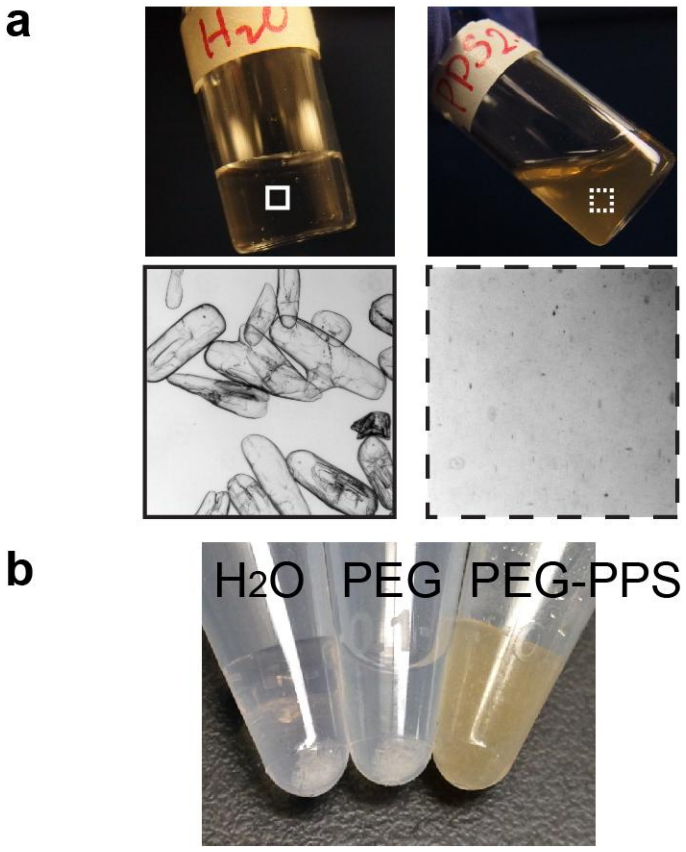

Figure 38 The dissolution of a small molecule, BrdU, in PEG-$PPS_{2.5}$ or PEG-PPS_5 as compared to water. a. The dissolution of BrdU (at 10 mg/mL) in PEG-$PPS_{2.5}$ in comparison to in water at room temperature for 30 minutes with vortexing, with the microscopic images of residual undissolved BrdU below. b. Images of BrdU (20 mg/mL) suspended in water (left, crystals of BrdU remain visible), PEG solution (middle, crystals of BrdU remain visible) and PEG-PPS_5 (right, no remaining crystals of BrdU visible).

7.4.4 Structural changes of PEG-PPS after oxidation and reduction modifications

Thus far the primary mode of $(PEG_{113}$-*b*-$PPS_5)_4$ association in forming hydrogel is the physical interaction between the hydrophobic and the hydrophilic blocks through molecular self-assembly. We further looked at other possible mechanisms in altering the structural basis of PEG-PPS hydrogel. Since the end-capping group of the branched polymer is pyridyl disulfide, we suspect the addition of a reducing agent, tris(2-carboxyethyl)phosphine (TCEP), would result

in the removal of pyridinethion and the exposure of free thiol groups, which could facilitate the disulfide crosslinking between polymers. When 0.5x equivalence of TCEP to the total amount of polymer arms was added, the elastic moduli of $(PEG_{113}\text{-}b\text{-}PPS_5)_4$ increased from 100 Pa to 300 Pa, and remained as such for the 30 minutes tested (Figure 39a). However a small, 0.1x equivalence of TCEP did not stiffen the mechanical property (data not shown), suggesting that this conversion from physical to chemical crosslinks requires a certain amount of thiol groups being available. Other than reduction-mediated chemical crosslinks, the polymer can also undergo dissociation in an oxidative environment. With 5 v/v % hydrogen peroxide, the viscosity of the polymer aqueous solution quickly decreased (Figure 39b), which suggested of a potential rapid release of cargos in conditions where reactive oxygen species are present.

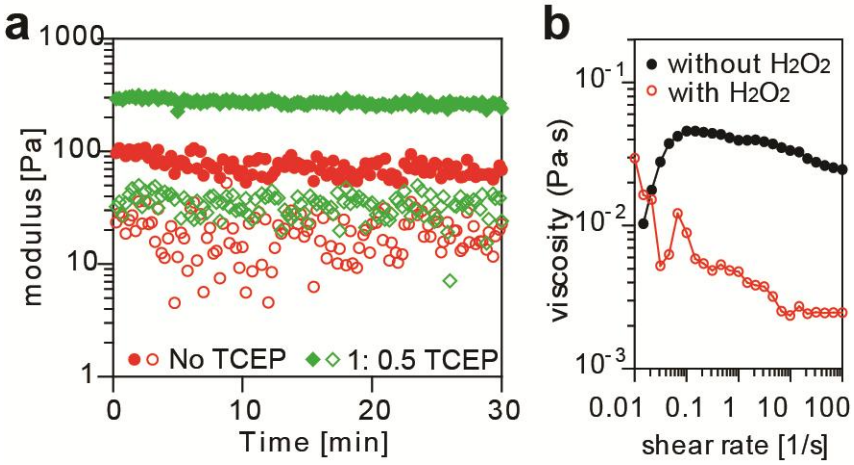

Figure 39 The rheological properties of reduced and oxidized 4 arm PEG-PPS_5. **a**. Reducing agent, TCEP, increases the stiffness of PEG-PPS_5 hydrogel (n(Polymer arm) : n(TCEP) = 1 : 0.5). Polymers were at 4.75 w/v%, and measured under 1% strain. **b**. Hydrogen peroxide (5 v/v%) decreases the viscosity of PEG-PPS_5 (3 w/v%).

7.4.5 PEG-PPS RETAINS BRDU FOR LONG-TERM IN VIVO DELIVERY

Topical administration of chemotherapeutics has been limited by the lack of appropriate mediums for the hydrophobicity of different active ingredients of small compounds. Non-polar solvents such as DMSO was used for such purposes, however it is irritating and toxic in high quantities.[180] We propose that the self assembled, amphiphilic PEG-PPS hydrogel would be a good medium to retain and slowly deliver hydrophobic molecules and to be injected at skin wounds, where it also serves as a compatible scaffold for endogenous cells to infiltrate. To compare the efficacy of retaining hydrophobic drugs in vivo, $(PEG_{113}\text{-}b\text{-}PPS_5)_4$ and $(PEG_{113}\text{-}b\text{-}PPS_{2.5})_4$ of similar viscosity properties were used to deliver BrdU at 10 mg/mL topically (Figure **40**). As expected, water or aqueous PEG solution did not entirely solubilize BrdU via vortexing at room temperature (Figure 38b), whereas $(PEG_{113}\text{-}b\text{-}PPS_5)_4$ did homogeneously dissolute BrdU as did $(PEG_{113}\text{-}b\text{-}PPS_{2.5})_4$ shown previously.

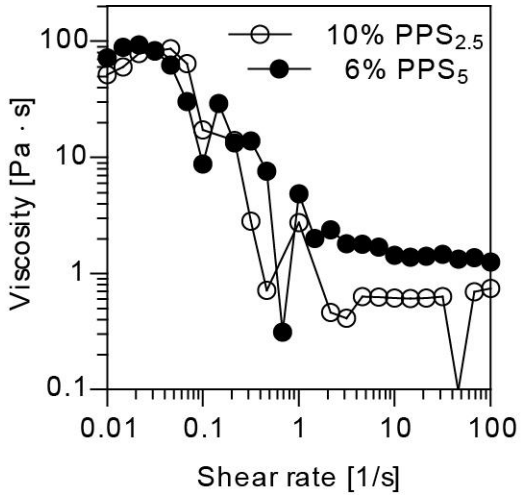

Figure 40 PEG-PPS_5 (6 w/v% in PBS) and PEG-$PPS_{2.5}$ (10 w/v% in PBS) show a similar viscosity and injectability.

A splinted excisional skin wound mouse model was utilized where PEG-PPS hydrogel containing BrdU was injected to a biopsy-punched skin wound and the wound was covered with sutured splints for 3 and 7 days.

For the delivery of BrdU via PEG-PPS to the cells in the wound bed, an antibody against BrdU+ cells was used, and the entire wound was scanned to identify the location of these cells (Figure 41).

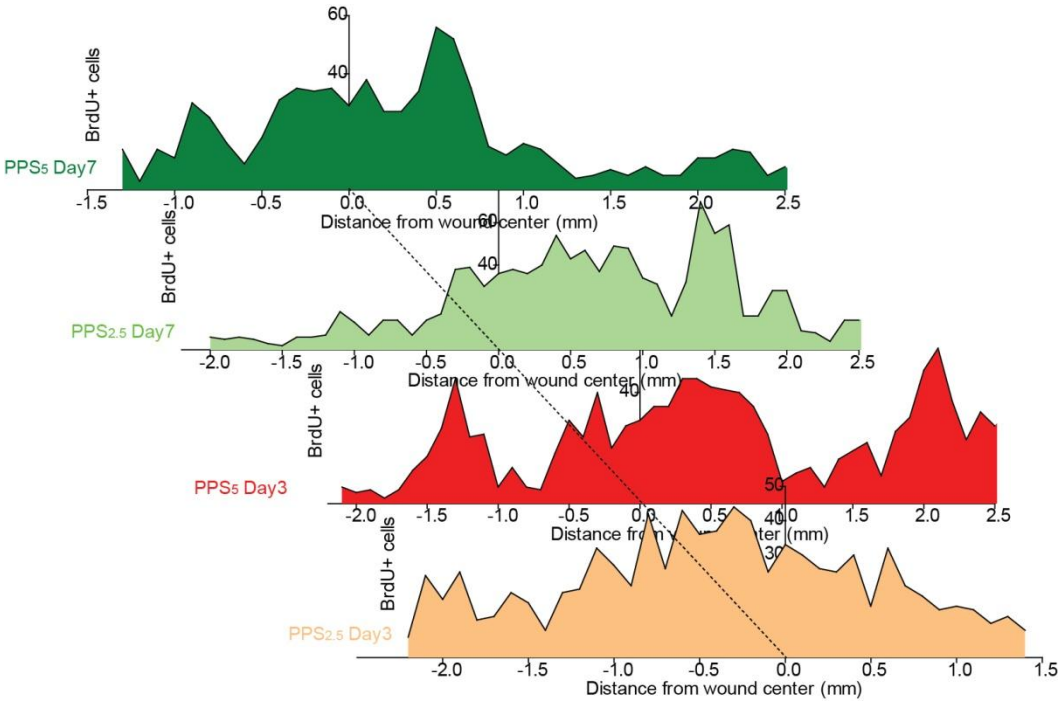

Figure 41 Counts of BrdU+ cells at wound beds on post operative day 3 and day 7.

Since during wound healing the collective migration of cells is primarily wound directed [181], the diffusion of BrdU, if any, from PEG-PPS dressing will allow proliferating cells at the periphery or beyond the wound edge to uptake BrdU and become positive. For the comparison of retaining BrdU between $(PEG_{113}\text{-}b\text{-}PPS_5)_4$ and $(PEG_{113}\text{-}b\text{-}PPS_{2.5})_4$, the wound was divided into three regions where the center of the wound bed (region I), the granulation tissue close to the boundary of the wound (region II) and the unwounded tissue surrounding the wound (region III)

were individually quantified (Figure 42a). Specifically, another general proliferating cell marker, Ki-67, was used to normalize the BrdU+ proliferating cells in order to eliminate the factor of different PEG-PPS materials allowing for different cell proliferations in general. The delivery of BrdU via $(PEG_{113}\text{-}b\text{-}PPS_5)_4$ resulted in a statistically significant amount of BrdU+ cells in the center of the wound (Region I) than $(PEG_{113}\text{-}b\text{-}PPS_{2.5})_4$ at day 3 and day 7 (Figure 42b and c). This observation indicated that the longer the hydrophobic block, PPS, is in the amphiphilic block copolymer, the better it is to retain hydrophobic cargos, which enables more sustained drug induction on cells that are infiltrating through this self-assembled scaffold. Noticeably in contrast to organic solvents or micro-sized micelles that achieve wound surface coverage and some penetration, PEG-PPS scaffolds allows for z-directional BrdU delivery due to its self-assembled three-dimensional network that can fill in the cavity of tissues.

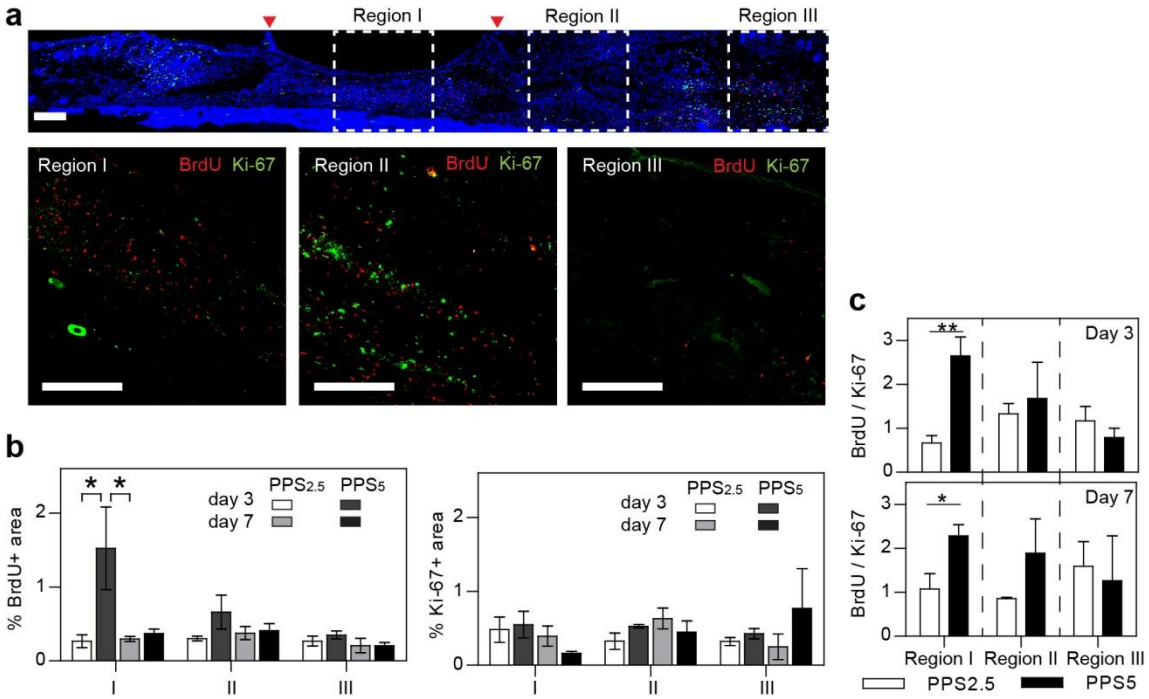

Figure 42 Delivery of a hydrophobic model molecule, BrdU, in two lengths of PEG-PPS hydrogel retains the molecules in wound dressings where the hydrogel was applied. **a**. Full-length scan of

immunohistochemically stained wounds for the delivered molecules (BrdU), proliferating cells (Ki-67) and nuclei (DAPI) including regions at the center of wound beds (I), the granulation tissue at the edge of the border of original skin wound (II), and the skin tissues outside of wound (III). b. Quantifications of BrdU+ area and Ki-67+ area in different regions at wounds. **c**. The quantification of the ratio of BrdU+ area to Ki-67+ area in Regions I, II, and III for wounds at day 3 and day 7 shows that PEG-PPS_5 results in statistically more BrdU delivery at the center of wound than PEG-$PPS_{2.5}$. (Scale bar = 100 μm (a). One-way ANOVA, * $p < 0.05$, ** $p < 0.01$).

7.4.6 PEG-PPS BIOCOMPATIBILITY IN SKIN WOUND ENVIRONMENT

The inflammatory response was examined of wounds that were dressed with PEG-PPS. Specifically the pan macrophage marker F4/80, leukocyte marker CD45 and neutrophils marker Ly6G were stained. From day 3 to day 7, the level of macrophages and leukocytes subsided which indicated the polymer did not deter normal inflammatory response (Figure 43a). When compared with wounds dressed with natural fibrin matrices, PEG-PPS material had a lower neutrophil infiltration at day 7 than fibrin (Figure 43b).

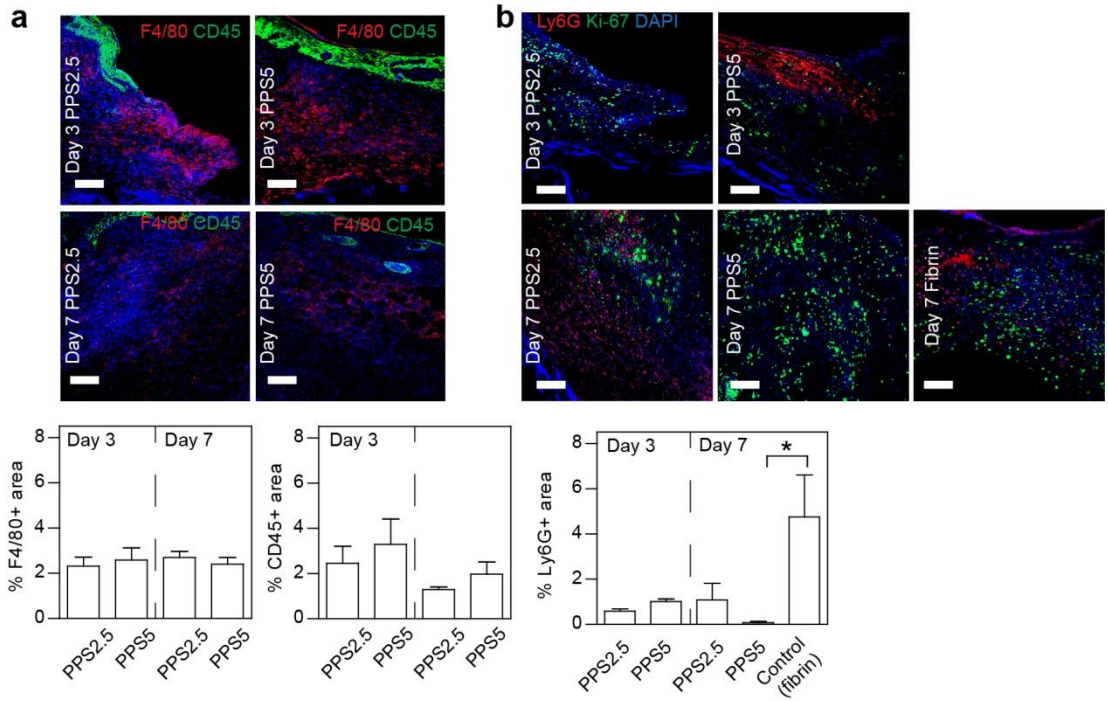

Figure 43 The inflammatory response of mouse skin wound to PEG-PPS as dressing materials. a. Immunohistochemical staining and quantification of macrophage marker (F4/80) and leukocyte marker (CD45) within the granulation tissue at day 3 and day 7 post surgery. b. Immunohistochemical staining and quantification of neutralphil marker (Ly6G) within the granulation tissue dressed with PEG-PPS relative to fibrin matrices at day 3 and day 7 post surgery. Scale bar = 20 μm.

Angiogenesis, another hallmark event of the wound healing process, was examined via endothelial cell marker (CD31) and pericyte marker (NG-2), which showed similar areas of staining among $(PEG_{113}\text{-}b\text{-}PPS_5)_4$, $(PEG_{113}\text{-}b\text{-}PPS_{2.5})_4$, and fibrin dressing in 7 days post surgery (Figure 44). Interestingly on day 3 post wounding, the antibody of NG-2 seemingly stained positive for big round "circles", where around some endothelial cells were present. Since these "circle" disappear in day 7, it was likely that the NG-2 antibody at day 3 non-specifically bound to the outside of the PEG-PPS polymer, or perhaps a factor from the blood was non-specifically binding to the polymer, which was picked up by NG-2, an antibody against chondroitin sulfate proteoglycan.

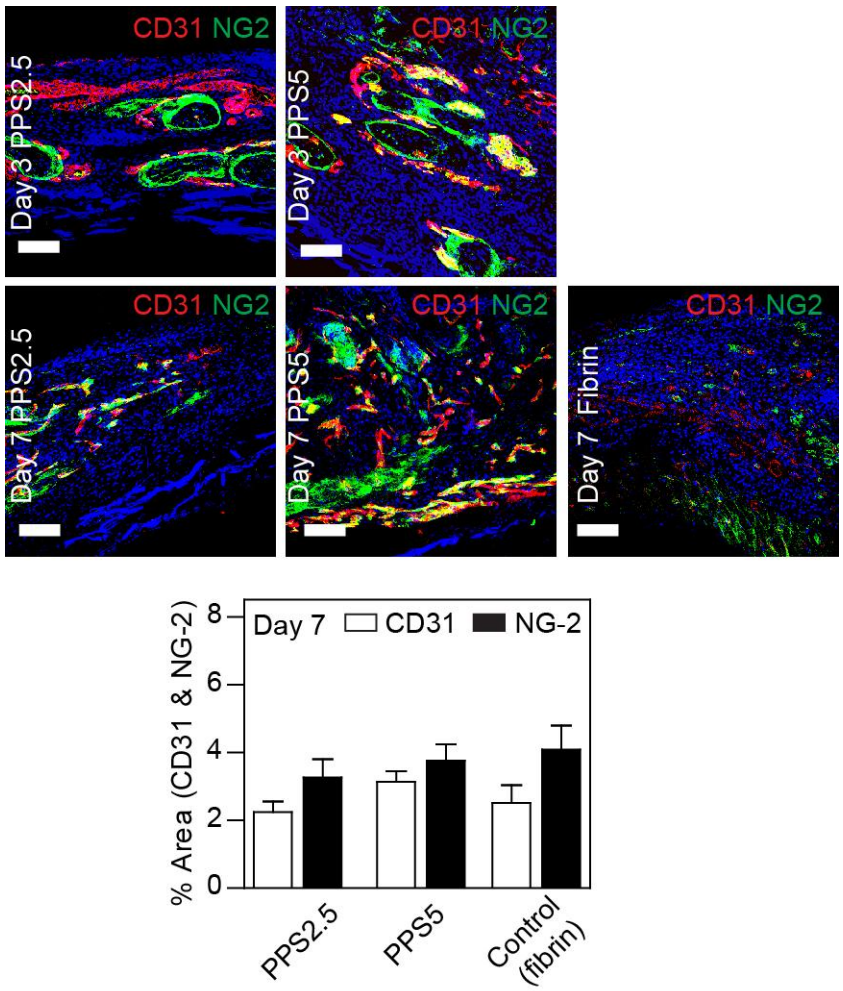

Figure 44 PEG-PPS hydrogel supports the angiogenesis response in mouse skin wound similarly to fibrin matrices. Immunohistochemical staining of endothelial marker (CD31) and pericyte marker (NG-2) within the granulation tissue at day 3 and day 7 post surgery. Scale bar = 20 μm.

7.5 CONCLUSIONS

In conclusion, we have demonstrated a general self-assembled hydrogel platform for the delivery of hydrophobic molecules in a three-dimensional network whose hydrophobicity and injectability can be synthetically tuned. Unlike solvent-form drug carriers such as DMSO or hydrophobic/amphiphilic particles, the branched PEG-PPS block copolymer solubilizes hydrophobic molecules in its self-assembled bulk environment which allows for cell infiltration

and tissue remodeling in three dimensions. This self-assembled branched block copolymer also is sensitive to the oxidative and reducing alterations of its structural and mechanical properties, providing an adaptive scaffold material and drug carrier for medicinal and tissue engineering purposes.

CHAPTER 8:

DELIVERY OF ANTIBIOTICS FROM SELF-ASSEMBLED PEG-PPS HYDROGEL AS THIN-FILM COATINGS ON ORTHOPAEDIC IMPLANTS

8.1 INTRODUCTION OF ORTHOPAEDIC SURGERY-RELATED INFECTION

Periprosthetic joint infection remains a devastating complication of total joint arthroplasty. Despite advances in sterile surgical technique and the use of perioperative antibiotics, post-arthroplasty joint infection continues to affect between from 1% and 7% of total joint arthroplasties [182-187]. It has been projected that 572,000 primary total hip arthroplasties and 3.48 million primary total knee arthroplasties will be performed annually by 2030, resulting in 38,000 to 270,000 annual joint infections [188]. Post-arthroplasty infection leads to increased patient disability, morbidity, and even mortality. Patients require prolonged intravenous antibiotics, multiple revision surgeries including extensive debridement and implant removal, and often end up with diminished functional use of their extremity [189,190].

The concept of local delivery of antimicrobial therapy to maximize local efficacy while minimizing systemic effects is not a new one, and has been available for decades in the form of solutions, ointments and creams. Local antimicrobial therapies considered for arthroplasty have

ranged from adding antibiotics to irrigation solution to use of vancomycin powder [191,192]. While these techniques have showed mixed results, the presence of antibiotic levels in the soft tissue around the implant is short lived and no antibiotic barrier is present on the implant itself protecting it from bacterial colonization [193]. The concept of coating implants has been suggested as a method to remedy these concerns. Currently antimicrobial coatings are clinically available as antibiotic impregnated cement (PMMA) in the US, iodine coating in Japan and nanosilver coating in Europe [194]. However, these coatings each have fundamental drawbacks as PMMA is an inert, permanent vehicle with unknown release kinetics, and both iodine and nanosilver have questionable toxicity profiles leaving halogen or metallic ions in the bloodstream, as well us unknown release kinetics. All existing coatings also act via passive release of antimicrobial agent so there is a broad local effect initiated on implantation independent of the presence of bacteria.

In the current study, we devised a novel non-toxic, biodegradable poly (ethylene glycol)-propylene sulfide (PEG-PPS) polymer coating that can be used as a vehicle to deliver antibiotics locally through both a passive and active mechanism. The active release is driven by the reactive oxygen cascade initiated by the presence of bacteria, allowing the "smart" polymer to release antibiotic where it is needed most. This therefore targets bacterial-rich environments and diffuses antibiotic down gradient toward the bacterial challenge. As the polymer is completely biodegradable, no additional foreign body is retained in the body once the antibiotic is completely eluted off the implant. We examine the in vitro release properties of this novel coating and use a validated longitudinal model of post-arthroplasty infection to test in vivo efficacy of the coating as a vehicle to eradicate infection and prevent biofilm formation. Based on previous work, this study used vancomycin and tigecycline as the antibiotics of choice as they

showed optimal efficacy against *Staphylococcus aureus (S. aureus)*, the causative organism in approximately 70% of arthroplasty infections [195-197]. The efficacy of this coating in preventing infection was then tested using an established *S. aureus in vivo* mouse model of post-arthroplasty infection.

8.2 Materials and Methods

8.2.1 Metal substrate modifications

Titanium Kirschner (K) wires (0.8 mm in diameter) were cleaned with sandpaper and underwent oxygen plasma treatment at 200 mTorr, 200 W for 15 min. Subsequently 1% (v/v) (3-mercaptopropyl) trimethoxysilane was reacted with the K-wires in toluene at 90 °C with stirring overnight followed by sonication in chloroform (5 times), acetone (2 times), methanol (5 times), and by milliQ water (5 times). The K-wires were then heated at 50 °C for at least 30 minutes to dry.

8.2.2 Antibiotics dispersion in PEG-PPS hydrogel and coating on titanium implants

PEG-PPS polymer was dissolved in phosphate buffer saline (PBS) to make either a 3% or a 6 % (w/v) solution, which was used to dissolve either tigecycline or vancomycin at a concentration of 20 mg/ml. The K-wires were submerged in the antibiotic-encapsulated PEG-PPS solution or PEG-PPS solution alone at 4 °C for 1 hour and later dried at 50 °C for 1 hour. This wet-dry cycle was continued for a total of 10 times. To aid in visualization, rhodamine was also coated on the titanium pins via encapsulation in PEG-PPS solution.

8.2.3 SEM-EDS ANALYSIS

The microstructure and surface compositional changes of the implant due to polymer coating was examined using Nova 230 Nano scanning electron microscopy (SEM) and energy dispersive spectroscopy (EDS). Representative images were acquired under standard operation, and EDS analysis was performed under 10.0kV voltage and at 35.3 degree take off angle.

8.2.4 IN VITRO RELEASE OF ANTIBIOTICS

In vitro release of coated antibiotics, vancomycin and tigecycline, from PEG-PPS on the K-wires was performed. This was conducted by submerging the K-wires in 200 µL of PBS and kept at 37 °C. As a control, PEG-PPS coated pins were also assayed for release in PBS. The buffer was refreshed daily for at least one week, and the amount of released vancomycin and tigecycline was quantified by high-performance liquid chromatography (HPLC). The column used in HPLC was Luna C18, 100*2.00mm, 5 um. The method used was 5-95% acetonitrile/water in 0.1% trifluoroacetic acid over 25 min, 0.1 mL/min, UV 280 nm detection. Tigecycline was detected at UV 245 nm.

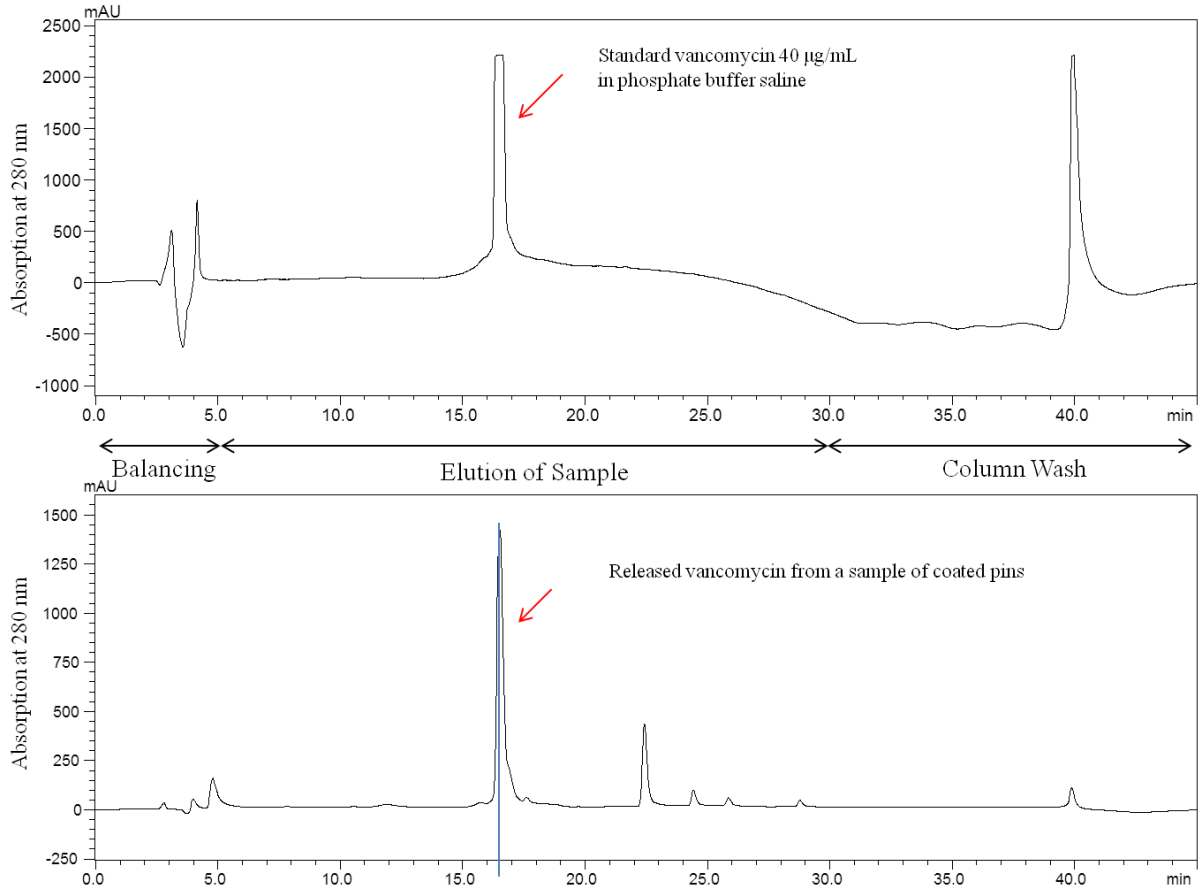

Figure 45 HPLC traces of the calibration vancomycin (upper) and the release sample (lower). Each run is 45-minute long, including the balance period (0 to 5 min), the elution of specimens from the column period (5 to 30 min) and the column wash period (30 to 45 min). Under this method, vancomycin is eluted at 16 – 17 minute. The calibration curve, peak area vs vancomycin concentration, was generated for reference.

8.2.5 JOINT INFECTION MOUSE MODEL

The following description was provided by Dr. Nick Bernthal's group in a joint manuscript with Dr. Segura and me.

"The bioluminescent *Staphylococcus aureus* Xen36 strain is derived from the bacteremia isolate ATCC 49525. It contains a bioluminescent operon construct integrated into a stable

bacterial plasmid which naturally produces a blue-green light that is emitted only by metabolically active bacteria [198,199]. This strain of bioluminescent *S. aureus* has been previously used in this established mouse model of arthroplasty infection [189,200]. ”

“Xen36 bacteria were streaked onto tryptic soy agar plates (tryptic soy broth, TSB, plus 1.5% bacto agar (BD Biosciences, Franklin Lakes, NJ)) and grown at 37°C overnight as previously described [201-203]. Single bacterial colonies of Xen36 were cultured in TSB and grown overnight in a shaking incubator (240 rpm) (MaxQ 4450; Thermo Fisher Scientific, Waltham, MA) at 37°C. Mid-logarithmic phase bacteria were obtained after a 2 hour subculture of a 1/50 dilution of the overnight culture. Bacterial cells were pelleted, resuspended and washed three times in PBS. Bacterial inocula (1×10^3 CFU) in 2µl PBS were estimated by measuring the absorbance at 600 nm at which an absorbance of 0.66 is equivalent to $2e \times 10^8$ colony forming units (CFU) (Biomate 3; Thermo Fisher Scientific). CFU were verified after overnight culture on plates.”

The establishment of this surgical model was demonstrated in previous publications[204,205]. Specifically, the surgical procedures and the post operation analysis are shown below, which were provided by Dr. Nick Berthal’s group in a joint manuscript with Dr. Segura and me.

“12 week old male C57BL/6 wild type mice were used in all experiments (Jackson Laboratories). All procedures were approved by the UCLA Animal Research Committee. Mice were anesthetized via inhalation isoflurane (2%). To model an orthopaedic implant infection, a medical-grade 0.8 mm diameter K-wire titanium implant, pre-coated with PEG-PPS, Vanc, or Tig, was surgically placed into the right distal femur of mice as previously described [189]. Briefly, a skin incision was made over the right knee and the distal right femur was accessed through a medial parapatellar arthrotomy with lateral displacement of the quadriceps-patellar complex.

After locating the femoral intercondylar notch, the femoral intramedullary canal was manually reamed with a 25 gauge needle for entry into the canal and further reamed with a 23 gauge needle. The coated titanium implant was surgically placed in a retrograde fashion with 1 mm of the end protruding into the joint space. An inoculum of Xen36 (1×10^3 CFU in 2 µl PBS) was pipetted onto the tip of the end of the implant in the joint space using a micropipette. The quadriceps-patellar complex was then reduced to its anatomic position and the surgical site was closed using 5-0 Vicryl sutures."

"Sustained-release buprenorphine (2.5 mg/kg) (ZooPharm, WY) was administered at the time of surgery and every 3 days postoperatively. For i*n vivo* bioluminescence, the mice were followed for 21 days postoperatively. CFU of bacteria adherent to the implant were determined on POD 21. "

Quantification of in vivo S. aureus postoperatively (in vivo bioluminescence imaging)

"Mice were anesthetized via inhalation of isoflurane (2%) and *in vivo* bioluminescence imaging was performed by using the Xenogen *in vivo* imaging system (Xenogen IVIS®; Caliper Life Sciences) [206-208]. Data are presented on color scale overlaid on a grayscale photograph of mice and quantified as maximum radiance (photons per second) within a circular region of interest (1×10^3 pixels) using Living Image® software (Xenogen). The bioluminescence signals were measured on POD 0, 1, 3, 5, 7, 10, 14, and 21."

Quantification of S. aureus postoperatively (culturing bacteria adherent to implant and bone and joint tissue)

"To confirm that the bioluminescence signals corresponded to the bacterial burden *in vivo,* bacteria adherent to the implants were quantified by detaching the bacteria from the implant by sonication in 1 ml 0.3% Tween-80 in TSB for 10 minutes followed by vortexing for 5 minutes

following the last day of imaging postoperative day 21 [199,201,209]. In addition, bacteria in the surrounding joint tissue were confirmed by culturing the homogenized bone and joint tissue on day 21 (Pro200® Series homogenizer; Pro Scientific) as previously described [199,201]. The number of bacterial CFU that were adherent to the implant and in the joint tissue was determined by counting CFU after overnight culture of plates and was expressed as total CFU harvested from the implant and joint tissue."

Visualization of osteolysis

"Radiographs were performed post-operatively, then on POD 7, 14, and 21 to qualitatively assess osseointegration and bone resorption. All radiographs were performed using a Faxitron® LX-60 Cabinet radiography system with a variable kV point projection X-ray source and digital imaging system (Qados, Cross Technologies plc, Berkshire, United Kingdom)."

8.2.6 FEMUR OPEN FRACTURE INFECTION MOUSE MODEL

The description of the open fracture femur infection model can be seen on a Conference Abstracted submitted by Dr. Jared Niska in collaboration with Dr Segura and me.

"The surgical procedure for this open fracture model was approved by the Animal Research Committee and was adapted from the surgical procedure for prosthetic joint infection as previously described. A medial parapatellar knee arthrotomy was made and a medical-grade titanium Kirschner-wire (K-wire) (8 mm) coated with PEG-PPS alone, PEG-PPS containing vancomycin, or PEG-PPS containing tigecycline was implanted into the femoral intramedullary canal in a retrograde fashion. A separate incision was made 1cm proximal to the joint space on the lateral thigh and a 2mm femoral defect created at the level of the midshaft femur. A micropipette was used to inoculate Xen36 ($1x10^8$ CFUs in 2µl saline) into the surgically created

open fracture site. The two surgical wounds were closed using 5-0 vicryl sutures. Analgesia (2.5 mg/kg sustained-release buprenorphine was administered at the time of surgery as well as every 3 days postoperatively. X-rays were obtained on POD 0 and any mice determined to have improper placement were euthanized and excluded from the study, which accounts for differences in sample size among groups."

8.3 Results and Discussion

8.3.1 Surface morphology and elemental analysis of coated metal implants

The successive oxygen plasma and silanization treatments functionalize metallic surfaces with a organosulfur (thiol) group, which would conjugate with PEG-PPS polymer via a disulfide exchange reaction with the end-capping group of pyridyl-disulfide. The branched, amphiphilic polymer PEG-PPS self-assemble in aqueous solution via physical interactions. Rhodamine molecules entrapped in the polymer during the coating process resulted in a dark (red) color on the final dried implants (Figure 46).

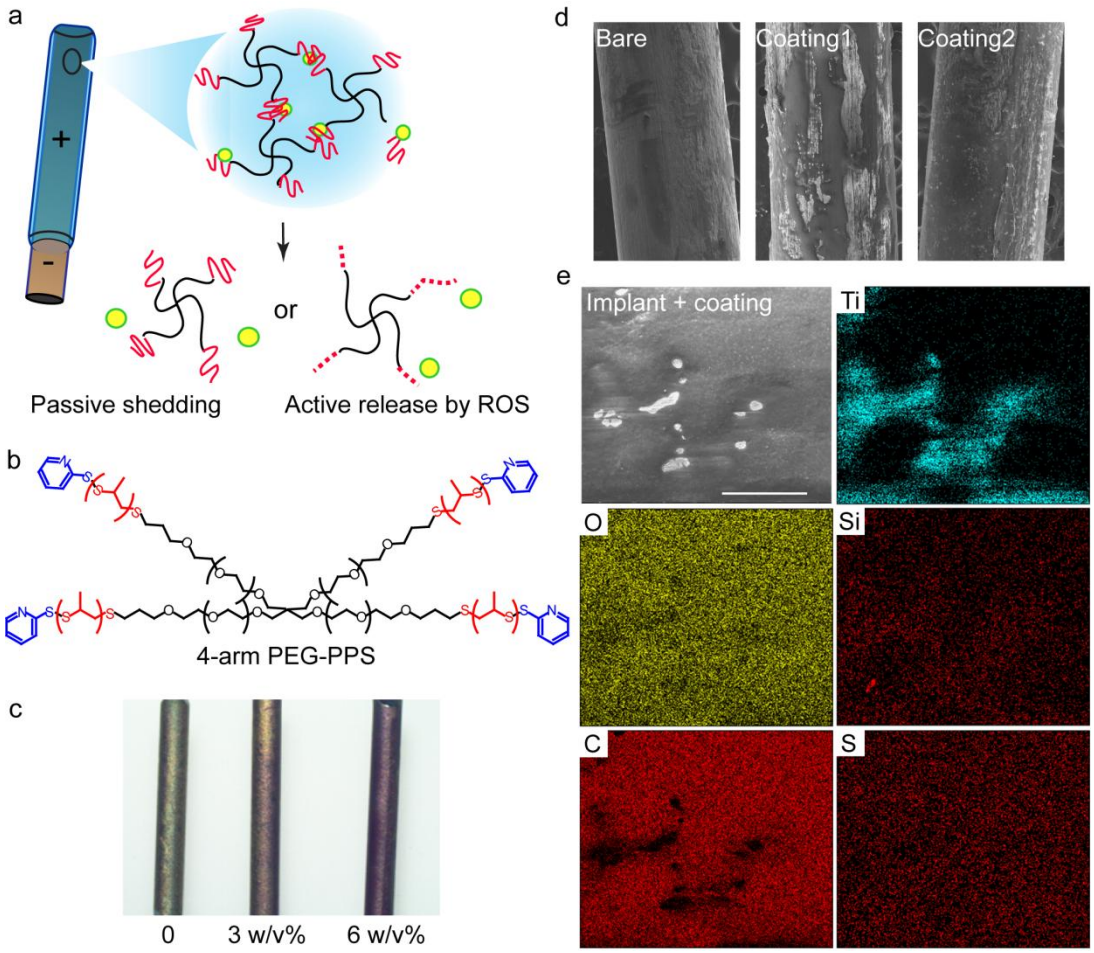

Figure 46 Schematics of antibiotic coatings of PEG-PPS polymer on metal implants. a. The release is either via passive elution or triggered by reactive oxygen species (ROS) for active release of antibiotics. b. The structure of PEG-PPS polymer used to coat metal implants. c. The visualization of the polymer coating is demonstrated by a model molecule, rhodamine, which was dispersed in the PEG-PPS coating solution prior to coating. (-, bare titanium pin; + 3(w/v)% PEG-PPS coated pin containing rhodamine; ++, 6(w/v) % PEG-PPS coated pin containing rhodamine). d. Scanning electron microscopic (SEM) images of the surfaces of a bare titanium pin (8-mm in diameter), a titanium pin coated with PEG-PPS containing vancomycin and a titanium pin coated with PEG-PPS containing tigecycline. e. A higher magnification of the surface morphology and the X-ray microanalysis of available elements on the surface of a PEG-PPS-coated titanium pin.

Scanning electron microscopy, Nova 230 Nano SEM, confirmed a uniform coating on the surfaces of the titanium pin (K-wire, 8 mm in diameter); and X-ray elemental analysis of titanium pins at different stages of modifications confirmed the sequential incorporation of multiple compounds. Silicon amount increases from naught on raw titanium substrate (composed of 88.8 atom% titanium and 11.2% aluminum) to 1.13 atom% on trimethoxysilane-reacted substrates (composed of 88.7 atom% titanium, 10.2 atom% aluminum and 1.13 atom% silicon). Figure 46 d and e showed the surface elemental composition of the implant with the polymer coating. Distinctive elements (i.e. sulfur, silicon) as a result of the silanization treatment as well as the polymer coating are found fairly homogenously on the surface of the implant. Specifically, the surface of substrates showed a great increase in the carbon and oxygen atoms (61.1 atom% and 28.7atom% respectively) and the appearance of sulfur atoms (0.87 atom%) owing to the composition of the polymer; whereas the surface titanium and aluminum amounts reduced (to 3.27 atom% and 0.52 atom% respectively). The detection beam penetrates to a surface depth on the order of single digit micrometers, which is indicative of the minimum thickness of the polymer coating.

8.3.2 In vitro elution of antibiotics from implant coating

As the polymer concentration increased from 3 to 6 (w/v)% , the amount of releasable payloads increased for both titanium and stainless steel substrates, although more from titanium than stainless steel (Figure 47a). This result suggests that the drug loading capacity increases with the amount of polymer, which indicates a denser assembly network from a higher concentration of polymer. The daily release of vancomycin and tigecycline off titanium and

stainless steel was above the minimum inhibition concentration (MIC) of both vancomycin and tigecycline (2 µg/ml) for the seven days.

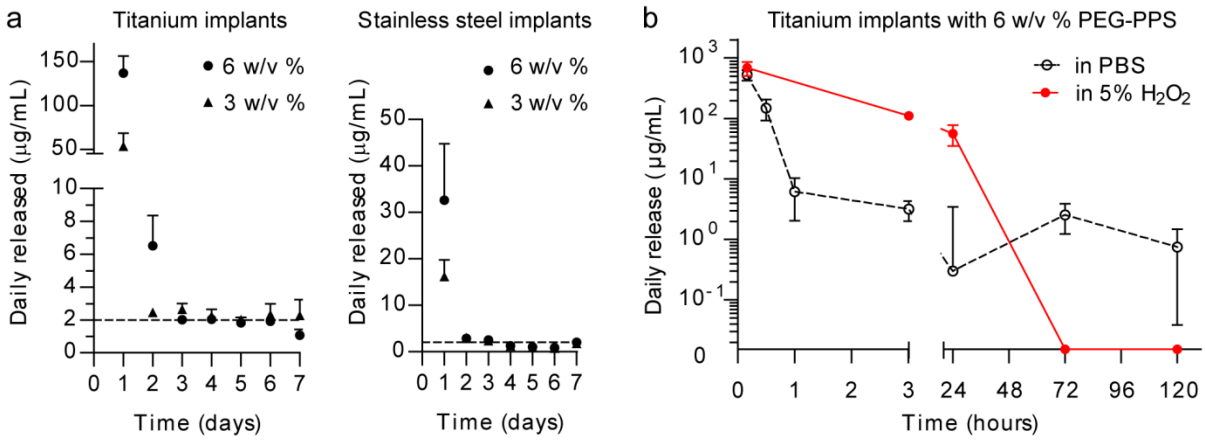

Figure 47 *In vitro* passive and active release of vancomycin from polymers coated on different substrates. a, quantified via HPLC, the daily release of vancomycin per pin over 7 days showed a much higher loading efficiency from 6 (w/v) % PEG-PPS than 3 (w/v) % on both titanium and stainless steel implants. (The concentration of 2µg/mL was labeled in a dash line.) b, daily released vancomycin per pin showed a "burst" release from loosely bound polymer and a sustained release from cross-linked polymer. (N = 3, Mean ± SEM)

The release of payload drugs from PEG-PPS coating can also be promoted in a reactive oxygen species (ROS), periprosthetic infection-mimicking environment. Vancomycin-loaded PEG-PPS coatings in phosphate buffer saline slowly released vancomycin from day 1 to day 7, whereas identical coatings in 5 (v/v)% hydrogen peroxide solution quickly released all vancomycin in 24 hours (Figure 47b). This result is indicative of the "smart" polymer design to actively release payload in an oxidative environment, because the hydrophobic block, poly(propylene sulfide), is oxidized to a hydrophilic element of poly(propylene sulfone), which reduces the physical interaction among molecules and ultimately disintegrates the coating network.

8.3.3 IN VIVO ANTIMICROBIAL EFFECTS OF IMPLANT COATING

The results presented below are in 2 joint manuscripts by the Dr. Bernthal's and Dr. Segura's labs, where the figures were plotted by me and the text was co-authored.

8.3.3.1 Model 1

In vivo bioluminescence signals following knee post-arthroplasty infection

The bioluminescence signal was similar between groups on POD 0 imaging (immediately after surgery and inoculation of bacteria) (Figure 48). On every other imaging time point postoperatively however, the bioluminescent signal was lower for both Vanc and Tig groups in comparison to the PEG-PPS group. This difference was statistically significant for the Vanc group on POD1, 3, 5, and 7. The mean Tig signal was statistically significantly lower on all days ($p<0.05$) (Figure 49a). A final experiment to control for an antimicrobial effect of the PEG-PPS polymer itself was performed comparing PEG-PPS pins to naked, uncoated pins in vivo. This confirmed no difference between the groups.

E*x vivo* bacterial counts

CFU quantification of both implant and surrounding tissue on POD21 showed a decreased number of CFU cultured from both the Vanc and Tig groups in comparison to the PEG-PPS group and historical controls with no coating at all [205]. While all implants from the PEG-PPS grew out bacteria (mean 264 CFUs), only 60% of the Vanc group pins grew out bacteria (mean 9 CFUs). All of the Tig-coated pins were completely without bacterial growth ($p<0.05$) (Figure 49c). As for the surrounding soft tissue, both the Vanc and PEG-PPS groups all had viable bacteria present (mean 5862 and 4291 CFUs, respectively), whereas only 60% of the Tig group had any viable bacteria in the surrounding tissue (mean 117 CFUs) ($p<0.05$) (Figure

49b). In sum, a statistically significant reduction of bacteria on the implant and in the surrounding tissue was seen in both the Vanc and Tig groups, with the Tig group showing 100% aseptic metal and 40% aseptic soft tissue.

Effect of bacterial and coating on osteointegration

Implants coated with PEG-PPS alone showed a dramatic degree of periprosthetic osteolysis becoming evident by POD7 and progressively severe over time. Tig-impregnated PEG-PPS implants, in comparison, coating showed no radiographic periprosthetic osteolysis (Figure 48), consistent with the finding of zero viable bacteria on the implant.

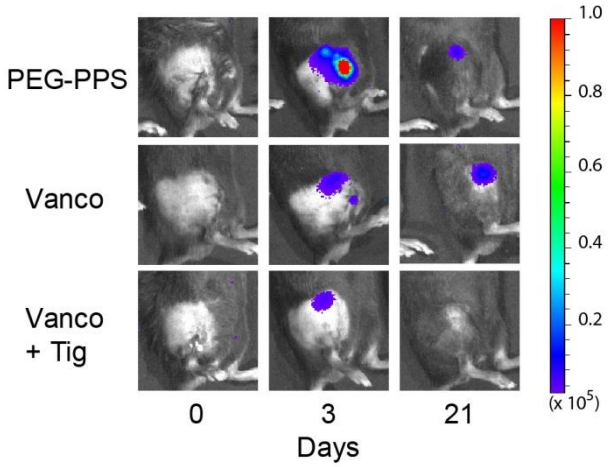

Figure 48 Representative radiographs of *in vivo* bioluminescence images on postoperative day 0, 3 and 21. First row is control (PEG-PPS coating only); second row is vancomycin-containing PEG-PPS coating; third row is tigecycline-containing PEG-PPS coating.

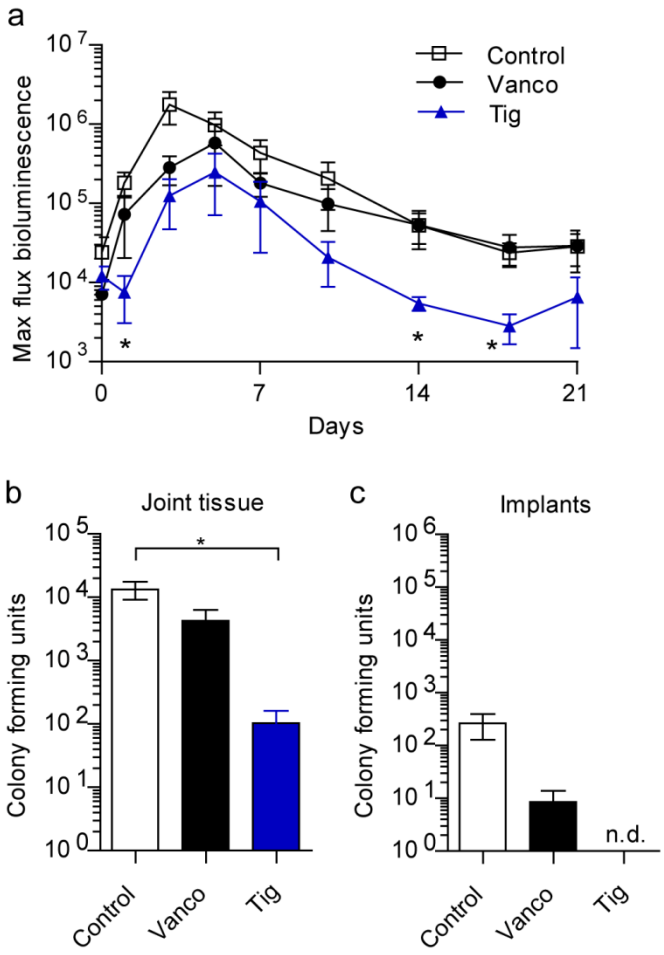

Figure 49 Quantification of bioluminescent signals and the colony forming units cultured from the surrounding tissue and the pins on postoperative day 21. a. Postoperative *in vivo S. aureus* bioluminescence signals (logarithmic scale) from day 0 to 21. b and c. Colony forming units cultured from the surrounding tissue (b) and on the pins (c). (n.d. none detected.)

8.3.3.2 Model 2: Femur open fracture

Effect of antibiotic coatings on X-ray imaging

An experienced orthopaedic surgeon evaluated the high resolution X-ray images (Figure 50) to determine whether vancomycin or tigecycline coated implants had any impact on bony architecture and implant stability at 3 and 6 weeks. The evaluator was blinded to the treatment

groups and assessed implant stability, osteolysis, and appearance of osteomyelitis or involucrum. Mice treated with PEG-PPS alone displayed more osteolysis and imaging findings suggestive of implant loosening compared to mice treated with vancomycin or tigecycline coatings. In addition, mice treated with PEG-PPS alone had significant bony destruction consistent with osteomyelitis and involucrum formation. As a whole, the high resolution X-rays demonstrated that both vancomycin and tigecycline coatings prevent radiologic changes observed in the setting of implant infection and osteomyelitis.

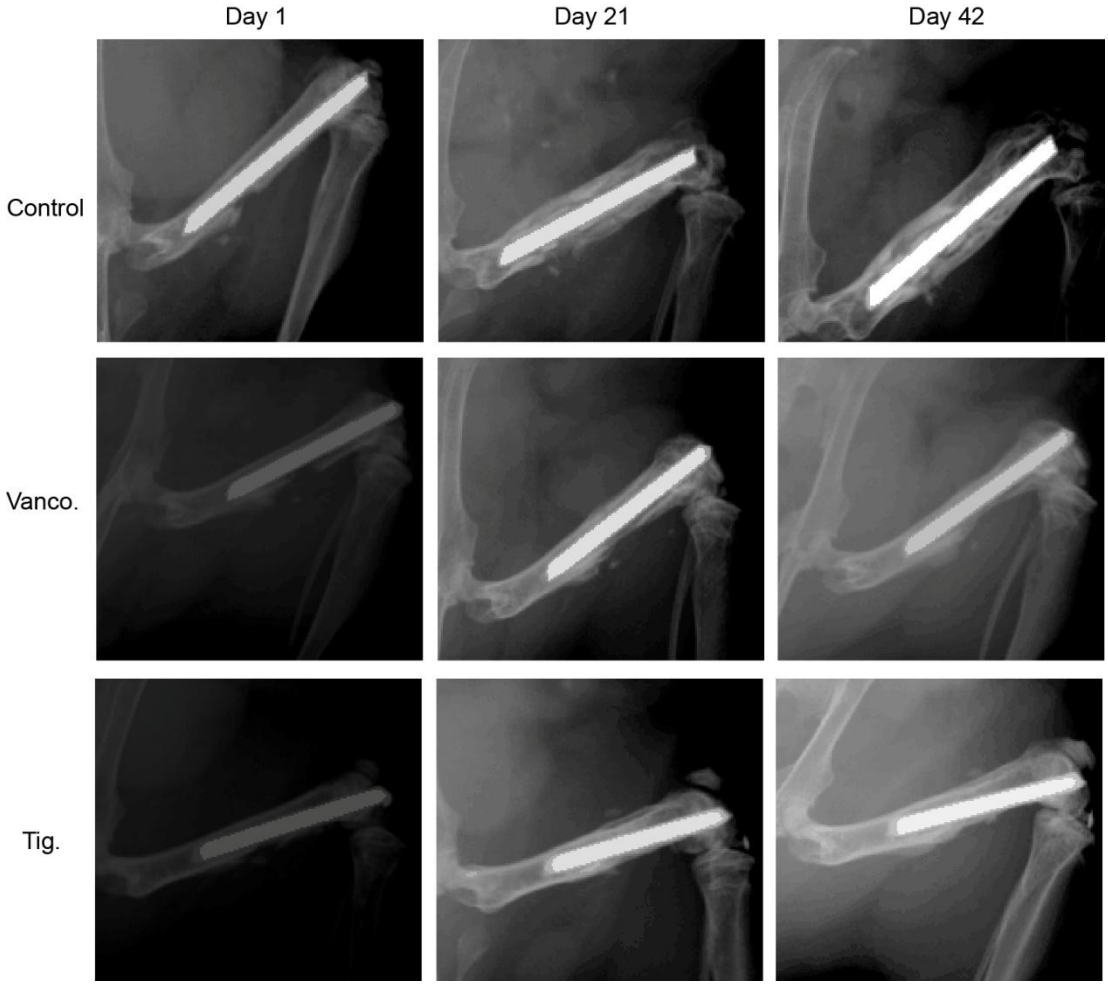

Figure 50 Representative X-ray images of open fractured femur with titanium implants on postoperative day 1, 21 and 42. The implants were coated with PEG-PPS polymer (Control), PEG-PPS polymer containing dispersed vancomycin (Vanco), or PEG-PPS polymer containing dispersed tigecycline (Tig).

Effect of antibiotic coatings on *in vivo* bioluminescent signals

Bioluminescence signals peaked on day 7 ($5.7x10^6 \pm 7.4x10^6$ photons/s/cm^2/sr) in the mice treated with PEG-PPS alone and signals remained above $2.4x^5$ photons/s/cm^2/sr throughout the 42-day experiment, indicating a chronic infection (Figure 51a). Vancomycin coatings resulted in a statistically significant reduction in bioluminescence signals on days 14, 28 and 42 (25-, 9-, and 4-fold respectively). Tigecycline coatings also resulted in a statistically significant reduction in bioluminescence signals on days 14, 28 and 42 (19-, 8-, and 4-fold respectively) compared with PEG-PPS alone. There was no difference in bioluminescence signals between vancomycin and tigecycline treatment groups after 42 days.

Effect of antibiotic coatings on *ex vivo* bacterial counts

Implants and surrounding soft tissue and bone from the fracture site were harvested at the completion of the experiment (day 42) and ex vivo CFUs determined. (Figure 51b). Mice implanted with PEG-PPS alone had $3.7 \pm 1.1 \times 10^5$ CFUs isolated from the peri-implant tissue and $2.8 \pm 1.5 \times 10^2$ CFUs isolated from the implants. Vancomycin and tigecycline coated pins both resulted in a significant reduction in bacterial CFUs after the 42-day experiment. Vancomycin coated pins grew out 2 ± 2 CFUs (139-fold reduction) and zero CFUs in the peri-implant tissue. Tigecycline coated pins resulted in $1.8 \pm 1.8 \times 10^1$ CFUs from the implants (15-fold reduction) and $6.3 \pm 4.5 \times 10^1$ CFUs isolated from the peri-implant tissue (5991-fold reduction).

The homogenized samples were then cultured in TSB for an additional 48 hours at 37º C to confirm the presence or absence of bacteria. Vancomycin coatings resulted in bacteria present in 1 of 5 implant cultures and 1 of 5 peri-implant tissue cultures. The tigecycline group had

bacteria present in 2 of 5 of the *ex vivo* peri-implant tissue cultures and 1 of 5 of the *ex vivo* implant cultures.

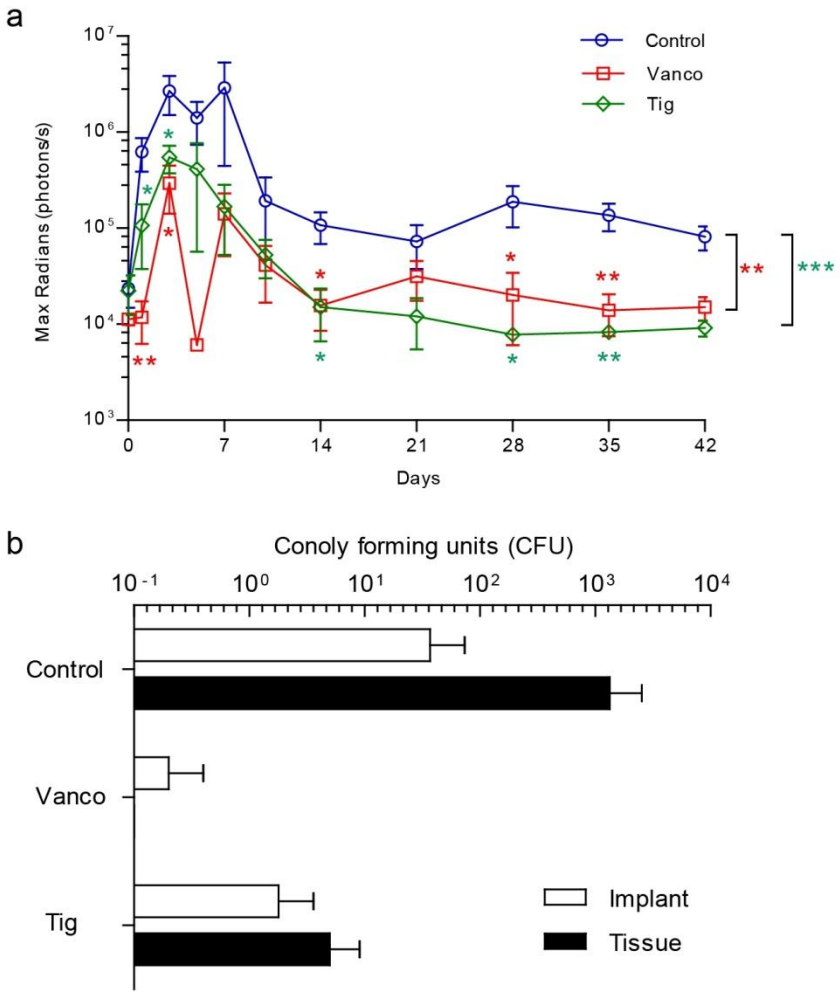

Figure 51 Quantification of bioluminescent signals and the colony forming units cultured from the surrounding tissue and the pins on postoperative day 42 in the femur open fracture model. a. Postoperative *in vivo S. aureus* bioluminescence signals (logarithmic scale) from day 0 to 21. B. Colony forming units cultured on the pins and from the surrounding tissue (b).

8.4 CONCLUSIONS

This novel PEG-PPS implant coating is an effective tool to deliver various antibiotics or even combinations of antibiotics locally during the perioperative period. This coating is versatile in that it can be loaded with many different antibiotics or antimicrobials, it can be optimized to be easily applied at the time of surgery, it is "smart" in that it responds to the presence of bacteria with increased antibiotic deposition, it has highly consistent release kinetics to ensure levels above the desired MIC to prevent the formation of resistance, it is completely biodegradable, and it can be easily applied to implants of all shapes and sizes. In sum, smart antimicrobial implant coatings, such as the one described in this study, have great potential in minimizing the incidence of postoperative infection following arthroplasty.

Additionally, the open fracture mouse model presented in this study demonstrated a therapeutic benefit of vancomycin and tigecycline coated implants against a local *S. aureus* infection. This study provides important preclinical evidence in support of a novel antibiotic coating to prevent biofilm formation and release antibiotics into bone and soft tissue to decrease infection associated with open fractures. In particular, this coating allows for one-stage fracture fixation without the need for a second surgery to remove the antibiotic delivery vehicle (i.e. cement beads), which has potential to improve clinical outcomes. Taken together, the findings suggest that this mouse model of open fracture could serve as a valuable preclinical *in vivo* model to evaluate and optimize the treatment of open fractures before further studies in humans.

CHAPTER 9:
CONCLUSIONS AND FUTURE DIRECTIONS

9.1 INTRODUCTION

The goal of the research presented in this dissertation was to promote wound healing via different strategies, namely controlled delivery of protein biologics and the application of injectable amphiphilic hydrogel for the delivery of small molecules. Through the work in our lab and collaboration with Dr. Carmichael's lab in the Department of Neurology and Dr. Bernthal's lab in the Department of Orthopaedic Surgery, these proposed strategies have been tested in a full-thickness skin wound repair model, a permanent focal ischemic stroke model and two anthroplasty models in mice. The following section re-visits the proposed specific aims and hypotheses, followed by the major conclusions and possible future experimental directions.

9.2 SPECIFIC AIM 1

This aim developed protease-sensitive protein nanocapsules with engineered peptide chirality in the shell for sustained delivery of one protein and sequential delivery of two proteins in vitro and in vivo. Although VEGF nanocapsules were previously shown to allow for controlled enzyme-responsive release through the balanced crosslinker mixture of plasmin-labile peptide (L-chiral form) and non-degradable compound methylene-bisacrylamide, it was not clear if in vivo protease would be able to metabolize such nanocapsules. By proposing D-chiral peptide in substitution for methylene-bisacrylamide, it is expected that all encapsulated proteins

would eventually be released; and multiple proteins can be fabricated to form nanocapsules that enable kinetically ordered release. Still, we had two major considerations: (1) does the D-chiral peptide get incorporated as effectively as L-chiral peptide to form the nanocapsule shell, especially in the presence of L-chiral peptide? (2) does the technique to enable protease-responsiveness of nanocapsules be easily transferable from plasmin to other proteases such as MMPs? Can we form MMP-2-labile protein nanocapsules? (3) Given that different proteases in wound have differential expression profiles, which mechanism to trigger multiple protein release is better – a shared protease-specificity but researcher-determined L/D chirality (therefore release rate), or two or more types of protease selectivites to allow the wound to dictate when to release a protein, or a combination of both?

Hypothesis 1: Protein nanocapsules with shells that are crosslinked by D-chiral peptides will slow down the protease-mediated degradation of nanocapsules compared to L-chiral nanocapsules, thus delaying the release of proteins. By mixing protein nanocapsules of different surface chirality, the enzyme responsive sustained and sequential delivery of proteins can be achieved.

By carefully choosing the right buffer (pH) and charged monomer relative to the isoelectric points of proteins, nanocapsules delivering proteins from 23 kD to 110kD to 440 kD were formed through the initial surface adsorption process to associate the monomers/crosslinkers (prior to polymerization to form the shell) and the core. Even when the peptide crosslinker was of a different sequence, protein naoncapsules could be formed in the same manner (but with variation in the ratios of monomers to proteins). Besides, L- and D- chiral form of plasmin-sensitive peptide crosslinkers were equally effective in getting incorporated into the formation of protein nanocapsules. These enantiomeric peptides share the same sequence,

therefore net charges and polymerization kinetics; and this technique can be generally applied to form a library of protein nanocapsules for various purposes. Last but not least, being able to release therapeutic proteins according to protease trigger opens the door to microenvironment-instructed protein delivery. An underlying assumption to this argument is that the expressed proteases in wounds are relatively "long-lasting" to be able to metabolize the D chiral nanocapsules and necessarily non-diffusive to be able to localize the release of proteins. Moreover in the case of two or more protease selectivity, it is rarely possible that any one of the two (or more) associated proteases (upregulated in the same wound in similar or differential temporal scales) is entirely naught or non-expressed. Besides, it remains possible that some proteases cross-degrade, to some extent, the substrates of other proteases [133].

To verify whether the assumptions mentioned above are true, future studies should include nanocapsule stability assays in wound fluid (in vitro or in vivo), immobilizing agents such as factor XIII as a co-delivered agent to make sure delivered nanocapsule resides in its original position, and the mapping of the locality and duration of expressed proteases.

9.3 SPECIFIC AIM 2

This aim investigated sustained released VEGF in comparison to bolus delivered VEGF for conveying differential receptor responses to endothelial cells and how the sustained VEGF delivery can lead to enhanced angiogenesis in murine dermal wounds.

Hypothesis 2: Sustained released VEGF, either by pipetting in small quantities of naked VEGF over time or through the use of our bioengineered VEGF nanocapsules, is capable of maintaining receptor activation over time. This extended receptor activation is associated with the sprouting of endothelial cells in vitro and angiogenesis in vivo.

With western blot analysis on receptor activation and downstream signaling events, sustained released VEGF elicits differential signaling responses to endothelial cells compared to bolus delivery providing an alternative mechanism for the observed improvements. Furthermore, our bioengineered VEGF nanocapsules can be tuned for different release rates in vivo, resulting in therapeutic benefit in cutaneous wound healing with 100-fold less dosage than bolus delivery of the factor.

Looking forward, it is desirable to perform a titer testing of naked VEGF to see at what concentration naked VEGF (resupplied) can induce significant angiogenesis; and to identify the amount of $n(VEGF)_{x\%}$ (one-dose) is comparable to that concentration of resupplied VEGF. This way the equation can be established linking the nanocapsule system and the naked protein, which may shed more light on the best mode and amount of dosing. Additionally the enhancement in angiogenesis would further benefit from a pro-maturation factor such as platelet derived growth factor or angiopoietin-2 [87].

9.4 SPECIFIC AIM 3

This aim studied the shear-thinning properties and the capability to solubilize hydrophobic compounds of 4-arm branched $(PEG\text{-}PPS_x)_4$. Therefore the potential of this self-assembled hydrogel was assessed as a depot for drug release in the forms of a wound dressing filler material and thin films for orthopaedic implant coatings. Utilizing the feature of hydrophobic propylene sulfide being converted to hydrophilic propylene sulfone by oxidation, smart fast release can be realized in areas of bacterial infection and with an abundance of reactive oxidation species.

Hypothesis 3: By increasing the x from 2.5 to 16, $(PEG\text{-}PPS_x)_4$ becomes more hydrophobic and it forms stiffer hydrogel when solvated in aqueous solution. It can also solubilize and retain hydrophobic drugs within the hydrogel in vitro and in vivo.

Hypothesis 4: Drug-impregnating $(PEG\text{-}PPS_x)_4$ can be chemically grafted and physically self-assembles on titanium surfaces, which releases the antimicrobial drugs via both passive elution and active oxidation-accelerated mode.

With detailed rheological analysis of $(PEG\text{-}PPS_x)_4$, we verified the injectability of this hydrogel, which could self-assemble into a three-dimensional network whose hydrophobicity and injectability can be synthetically tuned. This self-assembled branched block copolymer also is sensitive to the oxidative and reducing alterations of its structural and mechanical properties, providing an adaptive scaffold material and drug carrier for medicinal and tissue engineering purposes. In future studies, it will be beneficial to compare this branched $(PEG\text{-}PPS_x)_4$ with branched Pluronics of similar molecular weight and block lengths to identify if the oxidation-responsive feature of PEG-PPS would be therapeutically necessary for delivery of hydrophobic drugs. Besides, growth factor nanocapsules stimulating vascularization or other tissue regeneration can be combined in this hydrogel where anti-infectious agents are delivered.

In regards to the coating applications with orthopaedic implants, we have evaluated the efficacy of the self-assembled coating for the delivery of single antibiotics against *S. aureus*. Certain limitations exist in the study, including (1) the burst release and relatively short sustained release, (2) the bond of the hydrogel coating is relatively loose (therefore leading to burst release) and (3) the quantitative coating vs loading relation is not clear. Therefore in future studies, it will be beneficial to incorporate certain layers of covalently-crosslinked PEG-PPS (i.e. by the addition of dithiol crosslinkers) in order to create a denser network for more stable and

slower releasing coatings. It is also worth comparing or combining two-arm, four-arm and eight-arm block PEG-PPS for the potential benefits of creating higher ordered network and enabling more sustained release of drugs.

REFERENCES

1. Kumar, T.R., Soppimath, K. & Nachaegari, S.K. Novel delivery technologies for protein and peptide therapeutics. *Curr Pharm Biotechnol* **7**, 261-276 (2006).

2. Langer, R. & Folkman, J. Polymers for the sustained release of proteins and other macromolecules. *Nature* **263**, 797-800 (1976).

3. Richardson, T.P., Peters, M.C., Ennett, A.B. & Mooney, D.J. Polymeric system for dual growth factor delivery. *Nat Biotechnol* **19**, 1029-1034 (2001).

4. Hsu, B.B., *et al.* Ordered and kinetically discrete sequential protein release from biodegradable thin films. *Angew Chem Int Ed Engl* **53**, 8093-8098 (2014).

5. Henry, T.D., *et al.* The VIVA trial: Vascular endothelial growth factor in Ischemia for Vascular Angiogenesis. *Circulation* **107**, 1359-1365 (2003).

6. Ropper, A.H., *et al.* Vascular endothelial growth factor gene transfer for diabetic polyneuropathy: a randomized, double-blinded trial. *Ann Neurol* **65**, 386-393 (2009).

7. He, X. & Jabbari, E. Material properties and cytocompatibility of injectable MMP degradable poly(lactide ethylene oxide fumarate) hydrogel as a carrier for marrow stromal cells. *Biomacromolecules* **8**, 780-792 (2007).

8. Adelow, C., Segura, T., Hubbell, J.A. & Frey, P. The effect of enzymatically degradable poly(ethylene glycol) hydrogels on smooth muscle cell phenotype. *Biomaterials* **29**, 314-326 (2008).

9. Zisch, A.H., *et al.* Cell-demanded release of VEGF from synthetic, biointeractive cell ingrowth matrices for vascularized tissue growth. *FASEB J* **17**, 2260-2262 (2003).

10. Park, Y., Lutolf, M.P., Hubbell, J.A., Hunziker, E.B. & Wong, M. Bovine primary chondrocyte culture in synthetic matrix metalloproteinase-sensitive poly(ethylene glycol)-based hydrogels as a scaffold for cartilage repair. *Tissue Engineering* **10**, 515-522 (2004).

11. Vorvolakos, K., Isayeva, I.S., Luu, H.M., Patwardhan, D.V. & Pollack, S.K. Ionically cross-linked hyaluronic acid: wetting, lubrication, and viscoelasticity of a modified adhesion barrier gel. *Med Devices (Auckl)* **4**, 1-10 (2011).

12. Yokoyama, F., Masada, I., Shimamura, K., Ikawa, T. & Monobe, K. Morphology and Structure of Highly Elastic Polyvinyl-Alcohol) Hydrogel Prepared by Repeated Freezing-and-Melting. *Colloid Polym Sci* **264**, 595-601 (1986).

13. Mathur, A.M., Hammonds, K.F., Klier, J. & Scranton, A.B. Equilibrium swelling of poly(methacrylic acid-g-ethylene glycol) hydrogels - Effect of swelling medium and synthesis conditions. *Journal of Controlled Release* **54**, 177-184 (1998).

14. Pawar, G.M., *et al.* Injectable Hydrogels from Segmented PEG-Bisurea Copolymers. *Biomacromolecules* **13**, 3966-3976 (2012).

15. Wong Po Foo, C.T., Lee, J.S., Mulyasasmita, W., Parisi-Amon, A. & Heilshorn, S.C. Two-component protein-engineered physical hydrogels for cell encapsulation. *Proc Natl Acad Sci U S A* **106**, 22067-22072 (2009).

16. Lee, J., *et al.* A mechanical metamaterial made from a DNA hydrogel. *Nature Nanotechnology* **7**, 816-820 (2012).

17. Wojtecki, R.J., Meador, M.A. & Rowan, S.J. Using the dynamic bond to access macroscopically responsive structurally dynamic polymers. *Nature Materials* **10**, 14-27 (2011).

18. Bloom, G.P. & Grillo, H.C. The influence of tetracycline and chloramphenicol on the healing of cutaneous wounds. *J Surg Res* **10**, 1-5 (1970).

19. Williams, H.D., *et al.* Strategies to Address Low Drug Solubility in Discovery and Development. *Pharmacological Reviews* **65**, 315-499 (2013).

20. Leopold, I.H., Holmes, L.F. & LaMotte, W.O. Local versus systemic penicillin therapy of rabbit corneal ulcer produced by gram-negative rod. *Arch Ophthalmol-Chic* **32**, 193-195 (1944).

21. Oh, K.T., Bronich, T.K. & Kabanov, A.V. Micellar formulations for drug delivery based on mixtures of hydrophobic and hydrophilic Pluronic block copolymers. *J Control Release* **94**, 411-422 (2004).

22. Leung, D.W., Cachianes, G., Kuang, W.J., Goeddel, D.V. & Ferrara, N. Vascular Endothelial Growth-Factor Is a Secreted Angiogenic Mitogen. *Science* **246**, 1306-1309 (1989).

23. Schmidt, C., *et al.* Scatter Factor/Hepatocyte Growth-Factor Is Essential for Liver Development. *Nature* **373**, 699-702 (1995).

24. Nakamura, T., *et al.* Molecular-Cloning and Expression of Human Hepatocyte Growth-Factor. *Nature* **342**, 440-443 (1989).

25. Ostman, A., Andersson, M., Betsholtz, C., Westermark, B. & Heldin, C.H. Identification of a cell retention signal in the B-chain of platelet-derived growth factor and in the long splice version of the A-chain. *Cell Regul* **2**, 503-512 (1991).

26. Robinson, C.J. & Stringer, S.E. The splice variants of vascular endothelial growth factor (VEGF) and their receptors. *J Cell Sci* **114**, 853-865 (2001).

27. Heldin, C.H. & Westermark, B. Mechanism of action and in vivo role of platelet-derived growth factor. *Physiol Rev* **79**, 1283-1316 (1999).

28. Villegas, G., Lange-Sperandio, B. & Tufro, A. Autocrine and paracrine functions of vascular endothelial growth factor (VEGF) in renal tubular epithelial cells. *Kidney Int* **67**, 449-457 (2005).

29. Eldor, A., Polliack, G., Vlodavsky, I. & Levy, M. Effects of Dipyrone on Prostaglandin Production by Human-Platelets and Cultured Bovine Aortic Endothelial-Cells. *Thromb Haemostasis* **49**, 132-137 (1983).

30. Soma, Y., Dvonch, V. & Grotendorst, G.R. Platelet-Derived Growth Factor-Aa Homodimer Is the Predominant Isoform in Human Platelets and Acute Human Wound Fluid. *Faseb Journal* **6**, 2996-3001 (1992).

31. Abou-Khalil, R., *et al.* Autocrine and paracrine angiopoietin 1/Tie-2 signaling promotes muscle satellite cell self-renewal. *Cell Stem Cell* **5**, 298-309 (2009).

32. Pellaud, J., Schote, U., Arvinte, T. & Seelig, J. Conformation and self-association of human recombinant transforming growth factor-beta3 in aqueous solutions. *J Biol Chem* **274**, 7699-7704 (1999).

33. Oshimori, N. & Fuchs, E. Paracrine TGF-beta signaling counterbalances BMP-mediated repression in hair follicle stem cell activation. *Cell Stem Cell* **10**, 63-75 (2012).

34. Vlodavsky, I., Fridman, R., Sullivan, R., Sasse, J. & Klagsbrun, M. Aortic Endothelial-Cells Synthesize Basic Fibroblast Growth-Factor Which Remains Cell Associated and Platelet-Derived Growth Factor-Like Protein Which Is Secreted. *Journal of Cellular Physiology* **131**, 402-408 (1987).

35. Rifkin, D.B. & Moscatelli, D. Recent developments in the cell biology of basic fibroblast growth factor. *J Cell Biol* **109**, 1-6 (1989).

36. La Rosa, S., *et al.* Expression of acidic fibroblast growth factor (aFGF) and fibroblast growth factor receptor 4 (FGFR4) in breast fibroadenomas. *Journal of Clinical Pathology* **54**, 37-41 (2001).

37. Taylor, J.M., Mitchell, W.M. & Cohen, S. Epidermal Growth-Factor - Physical and Chemical Properties. *Journal of Biological Chemistry* **247**, 5928-& (1972).

38. Singh, A.B. & Harris, R.C. Autocrine, paracrine and juxtacrine signaling by EGFR ligands. *Cell Signal* **17**, 1183-1193 (2005).

39. Corral, C.J., *et al.* Vascular endothelial growth factor is more important than basic fibroblastic growth factor during ischemic wound healing. *Arch Surg-Chicago* **134**, 200-205 (1999).

40. Infanger, M., *et al.* Vascular endothelial growth factor serum level is strongly enhanced after burn injury and correlated with local and general tissue edema. *Burns* **30**, 305-311 (2004).

41. Springer, M.L., *et al.* Localization of vascular response to VEGF is not dependent on heparin binding. *FASEB J* **21**, 2074-2085 (2007).

42. Beer, H.D., Longaker, M.T. & Werner, S. Reduced expression of PDGF and PDGF receptors during impaired wound healing. *Journal of Investigative Dermatology* **109**, 132-138 (1997).

43. Amiram, M., Luginbuhl, K.M., Li, X., Feinglos, M.N. & Chilkoti, A. Injectable protease-operated depots of glucagon-like peptide-1 provide extended and tunable glucose control. *Proc Natl Acad Sci U S A* **110**, 2792-2797 (2013).

44. Martino, M.M., *et al.* Engineering the growth factor microenvironment with fibronectin domains to promote wound and bone tissue healing. *Sci Transl Med* **3**, 100ra189 (2011).

45. Gao, W.P., *et al.* In situ growth of a stoichiometric PEG-like conjugate at a protein's N-terminus with significantly improved pharmacokinetics. *P Natl Acad Sci USA* **106**, 15231-15236 (2009).

46. Gao, W., Liu, W., Christensen, T., Zalutsky, M.R. & Chilkoti, A. In situ growth of a PEG-like polymer from the C terminus of an intein fusion protein improves pharmacokinetics and tumor accumulation. *Proc Natl Acad Sci U S A* **107**, 16432-16437 (2010).

47. Tolstyka, Z.P., *et al.* Chemoselective Immobilization of Proteins by Microcontact Printing and Bio-orthogonal Click Reactions. *Chembiochem* **14**, 2464-2471 (2013).

48. Nguyen, T.H., *et al.* A heparin-mimicking polymer conjugate stabilizes basic fibroblast growth factor. *Nat Chem* **5**, 221-227 (2013).

49. Keefe, A.J. & Jiang, S.Y. Poly(zwitterionic)protein conjugates offer increased stability without sacrificing binding affinity or bioactivity. *Nat Chem* **4**, 60-64 (2012).

50. Trabbic-Carlson, K., Liu, L., Kim, B. & Chilkoti, A. Expression and purification of recombinant proteins from Escherichia coli: Comparison of an elastin-like polypeptide fusion with an oligohistidine fusion. *Protein Sci* **13**, 3274-3284 (2004).

51. Wen, J., *et al.* Controlled Protein Delivery Based on Enzyme-Responsive Nanocapsules. *Adv Mater* (2011).

52. Weis, S., Lee, T.T., del Campo, A. & Garcia, A.J. Dynamic cell-adhesive microenvironments and their effect on myogenic differentiation. *Acta Biomaterialia* **9**, 8059-8066 (2013).

53. Zisch, A.H., Schenk, U., Schense, J.C., Sakiyama-Elbert, S.E. & Hubbell, J.A. Covalently conjugated VEGF--fibrin matrices for endothelialization. *J Control Release* **72**, 101-113 (2001).

54. Whitmire, R.E., *et al.* Self-assembling nanoparticles for intra-articular delivery of anti-inflammatory proteins. *Biomaterials* **33**, 7665-7675 (2012).

55. Zhao, Y., Lord, M.S. & Stenzel, M.H. A polyion complex micelle with heparin for growth factor delivery and uptake into cells. *J Mater Chem B* **1**, 1635-1643 (2013).

56. Soontornworajit, B., Zhou, J., Zhang, Z. & Wang, Y. Aptamer-functionalized in situ injectable hydrogel for controlled protein release. *Biomacromolecules* **11**, 2724-2730 (2010).

57. Koria, P., *et al.* Self-assembling elastin-like peptides growth factor chimeric nanoparticles for the treatment of chronic wounds. *P Natl Acad Sci USA* **108**, 1034-1039 (2011).

58. Moon, J.J., *et al.* Interbilayer-crosslinked multilamellar vesicles as synthetic vaccines for potent humoral and cellular immune responses. *Nat Mater* **10**, 243-251 (2011).

59. Li, A.V., *et al.* Generation of effector memory T cell-based mucosal and systemic immunity with pulmonary nanoparticle vaccination. *Sci Transl Med* **5**, 204ra130 (2013).

60. Biswas, A., *et al.* Endoprotease-mediated intracellular protein delivery using nanocapsules. *ACS Nano* **5**, 1385-1394 (2011).

61. Zhao, M., *et al.* Redox-responsive nanocapsules for intracellular protein delivery. *Biomaterials* **32**, 5223-5230 (2011).

62. Zhao, M.X., *et al.* Degradable polymeric nanocapsule for efficient intracellular delivery of a high molecular weight tumor-selective protein complex. *Nano Today* **8**, 11-20 (2013).

63. Gu, Z., *et al.* Glucose-Responsive Microgels Integrated with Enzyme Nanocapsules for Closed-Loop Insulin Delivery. *ACS Nano* (2013).

64. Wei, W., *et al.* Construction of robust enzyme nanocapsules for effective organophosphate decontamination, detoxification, and protection. *Adv Mater* **25**, 2212-2218 (2013).

65. Liu, Y., *et al.* Biomimetic enzyme nanocomplexes and their use as antidotes and preventive measures for alcohol intoxication. *Nat Nanotechnol* **8**, 187-192 (2013).

66. Yan, M., *et al.* Single siRNA nanocapsules for enhanced RNAi delivery. *J Am Chem Soc* **134**, 13542-13545 (2012).

67. Cho, C.H., *et al.* COMP-Ang1: a designed angiopoietin-1 variant with nonleaky angiogenic activity. *Proc Natl Acad Sci U S A* **101**, 5547-5552 (2004).

68. Petrie, T.A., *et al.* Multivalent Integrin-Specific Ligands Enhance Tissue Healing and Biomaterial Integration. *Science Translational Medicine* **2**(2010).

69. Myung, J.H., Gajjar, K.A., Saric, J., Eddington, D.T. & Hong, S. Dendrimer-Mediated Multivalent Binding for the Enhanced Capture of Tumor Cells. *Angew Chem Int Edit* **50**, 11769-11772 (2011).

70. Wall, S.T., *et al.* Multivalency of Sonic hedgehog conjugated to linear polymer chains modulates protein potency. *Bioconjugate Chem* **19**, 806-812 (2008).

71. Conway, A., *et al.* Multivalent ligands control stem cell behaviour in vitro and in vivo. *Nat Nanotechnol* (2013).

72. Anderson, S.M., Siegman, S.N. & Segura, T. The effect of vascular endothelial growth factor (VEGF) presentation within fibrin matrices on endothelial cell branching. *Biomaterials* **32**, 7432-7443 (2011).

73. Roberts, R., *et al.* Heparan sulphate bound growth factors: a mechanism for stromal cell mediated haemopoiesis. *Nature* **332**, 376-378 (1988).

74. Hubbell, J. Matrix-bound growth factors in tissue repair. *Swiss Med Wkly* **136**, 387-391 (2006).

75. Li, G., *et al.* The dose of growth factors influences the synergistic effect of vascular endothelial growth factor on bone morphogenetic protein 4-induced ectopic bone formation. *Tissue Eng Part A* **15**, 2123-2133 (2009).

76. Banfi, A., *et al.* Therapeutic angiogenesis due to balanced single-vector delivery of VEGF and PDGF-BB. *Faseb Journal* **26**, 2486-2497 (2012).

77. Chen, T.T., *et al.* Anchorage of VEGF to the extracellular matrix conveys differential signaling responses to endothelial cells. *Journal of Cell Biology* **188**, 595-609 (2010).

78. Anderson, S.M., *et al.* VEGF internalization is not required for VEGFR-2 phosphorylation in bioengineered surfaces with covalently linked VEGF. *Integr Biol (Camb)* **3**, 887-896 (2011).

79. Wylie, R.G. & Shoichet, M.S. Three-dimensional spatial patterning of proteins in hydrogels. *Biomacromolecules* **12**, 3789-3796 (2011).

80. Aizawa, Y., Wylie, R. & Shoichet, M. Endothelial cell guidance in 3D patterned scaffolds. *Adv Mater* **22**, 4831-4835 (2010).

81. Wylie, R.G., *et al.* Spatially controlled simultaneous patterning of multiple growth factors in three-dimensional hydrogels. *Nat Mater* **10**, 799-806 (2011).

82. Leslie-Barbick, J.E., Shen, C., Chen, C. & West, J.L. Micron-scale spatially patterned, covalently immobilized vascular endothelial growth factor on hydrogels accelerates endothelial tubulogenesis and increases cellular angiogenic responses. *Tissue Eng Part A* **17**, 221-229 (2011).

83. McBeath, R., Pirone, D.M., Nelson, C.M., Bhadriraju, K. & Chen, C.S. Cell shape, cytoskeletal tension, and RhoA regulate stem cell lineage commitment. *Dev Cell* **6**, 483-495 (2004).

84. Tay, C.Y., *et al.* Micropatterned matrix directs differentiation of human mesenchymal stem cells towards myocardial lineage. *Exp Cell Res* **316**, 1159-1168 (2010).

85. Baker, B.M., Trappmann, B., Stapleton, S.C., Toro, E. & Chen, C.S. Microfluidics embedded within extracellular matrix to define vascular architectures and pattern diffusive gradients. *Lab on a Chip* **13**, 3246-3252 (2013).

86. Vulic, K. & Shoichet, M.S. Tunable growth factor delivery from injectable hydrogels for tissue engineering. *J Am Chem Soc* **134**, 882-885 (2012).

87. Brudno, Y., Ennett-Shepard, A.B., Chen, R.R., Aizenberg, M. & Mooney, D.J. Enhancing microvascular formation and vessel maturation through temporal control over multiple pro-angiogenic and pro-maturation factors. *Biomaterials* **34**, 9201-9209 (2013).

88. Johnston, K.P., *et al.* Concentrated Dispersions of Equilibrium Protein Nanoclusters That Reversibly Dissociate into Active Monomers. *ACS Nano* **6**, 1357-1369 (2012).

89. Lee, J., *et al.* Trehalose Glycopolymers as Excipients for Protein Stabilization. *Biomacromolecules* **14**, 2561-2569 (2013).

90. King, N.P., *et al.* Computational Design of Self-Assembling Protein Nanomaterials with Atomic Level Accuracy. *Science* **336**, 1171-1174 (2012).

91. Lai, Y.T., Cascio, D. & Yeates, T.O. Structure of a 16-nm Cage Designed by Using Protein Oligomers. *Science* **336**, 1129-1129 (2012).

92. Schroeder, A., *et al.* Remotely Activated Protein-Producing Nanoparticles. *Nano Letters* **12**, 2685-2689 (2012).

93. Sharei, A., *et al.* A vector-free microfluidic platform for intracellular delivery. *Proc Natl Acad Sci U S A* **110**, 2082-2087 (2013).

94. Gu, Z. & Tang, Y. Enzyme-assisted photolithography for spatial functionalization of hydrogels. *Lab Chip* **10**, 1946-1951 (2010).

95. Nguyen, D.H., *et al.* Biomimetic model to reconstitute angiogenic sprouting morphogenesis in vitro. *Proc Natl Acad Sci U S A* **110**, 6712-6717 (2013).

96. Tang, R., *et al.* Direct delivery of functional proteins and enzymes to the cytosol using nanoparticle-stabilized nanocapsules. *ACS Nano* **7**, 6667-6673 (2013).

97. Romer, J., *et al.* Impaired wound healing in mice with a disrupted plasminogen gene. *Nat Med* **2**, 287-292 (1996).

98. Saarialho-Kere, U.K., *et al.* Interstitial collagenase is expressed by keratinocytes that are actively involved in reepithelialization in blistering skin disease. *J Invest Dermatol* **104**, 982-988 (1995).

99. Grainger, D.J., Kemp, P.R., Liu, A.C., Lawn, R.M. & Metcalfe, J.C. Activation of transforming growth factor-beta is inhibited in transgenic apolipoprotein(a) mice. *Nature* **370**, 460-462 (1994).

100. Shen, Y., *et al.* Mice Deficient in Urokinase-Type Plasminogen Activator Have Delayed Healing of Tympanic Membrane Perforations. *PLoS One* **7**(2012).

101. Li, W.Y., Chong, S.S., Huang, E.Y. & Tuan, T.L. Plasminogen activator/plasmin system: a major player in wound healing? *Wound Repair Regen* **11**, 239-247 (2003).

102. Zhang, X. & Nothnick, W.B. The role and regulation of the uterine matrix metalloproteinase system in menstruating and non-menstruating species. *Front Biosci* **10**, 353-366 (2005).

103. Wysocki, A.B., Kusakabe, A.O., Chang, S. & Tuan, T.L. Temporal expression of urokinase plasminogen activator, plasminogen activator inhibitor and gelatinase-B in chronic wound fluid switches from a chronic to acute wound profile with progression to healing. *Wound Repair Regen* **7**, 154-165 (1999).

104. Wall, S.J., *et al.* Differential expression of matrix metalloproteinases during impaired wound healing of the diabetes mouse. *J Invest Dermatol* **119**, 91-98 (2002).

105. Ozawa, C.R., *et al.* Microenvironmental VEGF concentration, not total dose, determines a threshold between normal and aberrant angiogenesis. *Journal of Clinical Investigation* **113**, 516-527 (2004).

106. von Degenfeld, G., *et al.* Microenvironmental VEGF distribution is critical for stable and functional vessel growth in ischemia. *Faseb Journal* **20**, 2657-+ (2006).

107. Galiano, R.D., *et al.* Topical vascular endothelial growth factor accelerates diabetic wound healing through increased angiogenesis and by mobilizing and recruiting bone marrow-derived cells. *Am J Pathol* **164**, 1935-1947 (2004).

108. Greenhalgh, D.G., Sprugel, K.H., Murray, M.J. & Ross, R. PDGF and FGF stimulate wound healing in the genetically diabetic mouse. *Am J Pathol* **136**, 1235-1246 (1990).

109. Park, S.Y., *et al.* Dual Delivery of rhPDGF-BB and Bone Marrow Mesenchymal Stromal Cells Expressing the BMP2 Gene Enhance Bone Formation in a Critical-Sized Defect Model. *Tissue Eng Part A* (2013).

110. Kolambkar, Y.M., *et al.* Spatiotemporal delivery of bone morphogenetic protein enhances functional repair of segmental bone defects. *Bone* **49**, 485-492 (2011).

111. Wang, Y., Cooke, M.J., Morshead, C.M. & Shoichet, M.S. Hydrogel delivery of erythropoietin to the brain for endogenous stem cell stimulation after stroke injury. *Biomaterials* **33**, 2681-2692 (2012).

112. Cooke, M.J., Wang, Y., Morshead, C.M. & Shoichet, M.S. Controlled epi-cortical delivery of epidermal growth factor for the stimulation of endogenous neural stem cell proliferation in stroke-injured brain. *Biomaterials* **32**, 5688-5697 (2011).

113. Wang, Y., Cooke, M.J., Sachewsky, N., Morshead, C.M. & Shoichet, M.S. Bioengineered sequential growth factor delivery stimulates brain tissue regeneration after stroke. *J Control Release* **172**, 1-11 (2013).

114. Formiga, F.R., *et al.* Sustained release of VEGF through PLGA microparticles improves vasculogenesis and tissue remodeling in an acute myocardial ischemia-reperfusion model. *Journal of Controlled Release* **147**, 30-37 (2010).

115. Hanjaya-Putra, D., *et al.* Integration and Regression of Implanted Engineered Human Vascular Networks During Deep Wound Healing. *Stem Cell Transl Med* **2**, 297-306 (2013).

116. Johnson, P.J., Tatara, A., Shiu, A. & Sakiyama-Elbert, S.E. Controlled Release of Neurotrophin-3 and Platelet-Derived Growth Factor From Fibrin Scaffolds Containing Neural Progenitor Cells Enhances Survival and Differentiation Into Neurons in a Subacute Model of SCI. *Cell Transplantation* **19**, 89-101 (2010).

117. Lorentz, K.M., Yang, L.R., Frey, P. & Hubbell, J.A. Engineered insulin-like growth factor-1 for improved smooth muscle regeneration. *Biomaterials* **33**, 494-503 (2012).

118. Leader, B., Baca, Q.J. & Golan, D.E. Protein therapeutics: a summary and pharmacological classification. *Nat Rev Drug Discov* **7**, 21-39 (2008).

119. Gurtner, G.C., Werner, S., Barrandon, Y. & Longaker, M.T. Wound repair and regeneration. *Nature* **453**, 314-321 (2008).

120. Sinclair, R.D. & Ryan, T.J. Proteolytic enzymes in wound healing: the role of enzymatic debridement. *Australas J Dermatol* **35**, 35-41 (1994).

121. Ekaputra, A.K., Prestwich, G.D., Cool, S.M. & Hutmacher, D.W. The three-dimensional vascularization of growth factor-releasing hybrid scaffold of poly (epsilon-caprolactone)/collagen fibers and hyaluronic acid hydrogel. *Biomaterials* **32**, 8108-8117 (2011).

122. Seliktar, D., Zisch, A.H., Lutolf, M.P., Wrana, J.L. & Hubbell, J.A. MMP-2 sensitive, VEGF-bearing bioactive hydrogels for promotion of vascular healing. *J Biomed Mater Res A* **68**, 704-716 (2004).

123. Wen, J., *et al.* Controlled Protein Delivery Based on Enzyme-Responsive Nanocapsules. *Advanced Materials* **23**, 4549-+ (2011).

124. Shen, B.Q., *et al.* Conjugation site modulates the in vivo stability and therapeutic activity of antibody-drug conjugates. *Nat Biotechnol* **30**, 184-189 (2012).

125. Yan, M., *et al.* A novel intracellular protein delivery platform based on single-protein nanocapsules. *Nature Nanotechnology* **5**, 48-53 (2009).

126. Weng, D., Jiang, Z.K., Jin, J., Wu, L. & Lu, Y.F. Enhanced structural stability of adenovirus nanocapsule. *Prog Nat Sci-Mater* **24**, 171-174 (2014).

127. Biswas, A., Liu, Y., Liu, T.F., Fan, G.P. & Tang, Y. Polyethylene glycol-based protein nanocapsules for functional delivery of a differentiation transcription factor. *Biomaterials* **33**, 5459-5467 (2012).

128. Zhao, M.X., *et al.* Clickable Protein Nanocapsules for Targeted Delivery of Recombinant p53 Protein. *Journal of the American Chemical Society* **136**, 15319-15325 (2014).

129. Demidova-Rice, T.N., Hamblin, M.R. & Herman, I.M. Acute and impaired wound healing: pathophysiology and current methods for drug delivery, part 2: role of growth factors in normal and pathological wound healing: therapeutic potential and methods of delivery. *Adv Skin Wound Care* **25**, 349-370 (2012).

130. Liang, G., *et al.* Supramolecular hydrogel of a D-amino acid dipeptide for controlled drug release in vivo. *Langmuir* **25**, 8419-8422 (2009).

131. Nagy, K.J., Giano, M.C., Jin, A., Pochan, D.J. & Schneider, J.P. Enhanced mechanical rigidity of hydrogels formed from enantiomeric peptide assemblies. *J Am Chem Soc* **133**, 14975-14977 (2011).

132. Darnell, M.C., *et al.* Performance and biocompatibility of extremely tough alginate/polyacrylamide hydrogels. *Biomaterials* **34**, 8042-8048 (2013).

133. Chen, E.I., *et al.* A unique substrate recognition profile for matrix metalloproteinase-2. *J Biol Chem* **277**, 4485-4491 (2002).

134. Fudala, R., *et al.* Fluorescence detection of MMP-9. I. MMP-9 selectively cleaves Lys-Gly-Pro-Arg-Ser-Leu-Ser-Gly-Lys peptide. *Curr Pharm Biotechnol* **12**, 834-838 (2011).

135. West, J.L. & Hubbell, J.A. Polymeric biomaterials with degradation sites for proteases involved in cell migration. *Macromolecules* **32**, 241-244 (1999).

136. Patterson, J. & Hubbell, J.A. Enhanced proteolytic degradation of molecularly engineered PEG hydrogels in response to MMP-1 and MMP-2. *Biomaterials* **31**, 7836-7845 (2010).

137. Lei, Y., Gojgini, S., Lam, J. & Segura, T. The spreading, migration and proliferation of mouse mesenchymal stem cells cultured inside hyaluronic acid hydrogels. *Biomaterials* **32**, 39-47 (2011).

138. Lei, Y.G., Gojgini, S., Lam, J. & Segura, T. The spreading, migration and proliferation of mouse mesenchymal stem cells cultured inside hyaluronic acid hydrogels. *Biomaterials* **32**, 39-47 (2011).

139. Gao, F., *et al.* Hyaluronan oligosaccharides promote excisional wound healing through enhanced angiogenesis. *Matrix Biology* **29**, 107-116 (2010).

140. Lam, J. & Segura, T. The modulation of MSC integrin expression by RGD presentation. *Biomaterials* **34**, 3938-3947 (2013).

141. Salhia, B., *et al.* Expression of vascular endothelial growth factor by reactive astrocytes and associated neoangiogenesis. *Brain Research* **883**, 87-97 (2000).

142. Ferrara, N., Houck, K., Jakeman, L. & Leung, D.W. Molecular and biological properties of the vascular endothelial growth factor family of proteins. *Endocr Rev* **13**, 18-32 (1992).

143. Vemuri, S., *et al.* The stability of bFGF against thermal denaturation. *J Pharm Pharmacol* **46**, 481-486 (1994).

144. Lee, S., Jilani, S.M., Nikolova, G.V., Carpizo, D. & Iruela-Arispe, M.L. Processing of VEGF-A by matrix metalloproteinases regulates bioavailability and vascular patterning in tumors. *J Cell Biol* **169**, 681-691 (2005).

145. Rosengart, T.K., Johnson, W.V., Friesel, R., Clark, R. & Maciag, T. Heparin protects heparin-binding growth factor-I from proteolytic inactivation in vitro. *Biochem Biophys Res Commun* **152**, 432-440 (1988).

146. Zhang, J.C., Wojta, J. & Binder, B.R. Growth and fibrinolytic parameters of human umbilical vein endothelial cells seeded onto cardiovascular grafts. *J Thorac Cardiovasc Surg* **109**, 1059-1065 (1995).

147. Zhang, Z.G., *et al.* VEGF enhances angiogenesis and promotes blood-brain barrier leakage in the ischemic brain. *J Clin Invest* **106**, 829-838 (2000).

148. Ma, Y., Zechariah, A., Qu, Y. & Hermann, D.M. Effects of vascular endothelial growth factor in ischemic stroke. *J Neurosci Res* **90**, 1873-1882 (2012).

149. Frank, S., *et al.* Regulation of vascular endothelial growth factor expression in cultured keratinocytes. Implications for normal and impaired wound healing. *J Biol Chem* **270**, 12607-12613 (1995).

150. Xie, H., *et al.* PDGF-BB secreted by preosteoclasts induces angiogenesis during coupling with osteogenesis. *Nat Med* **20**, 1270-1278 (2014).

151. Kang, J., Lambert, O., Ausborn, M. & Schwendeman, S.P. Stability of proteins encapsulated in injectable and biodegradable poly(lactide-co-glycolide)-glucose millicylinders. *Int J Pharm* **357**, 235-243 (2008).

152. Kobsa, S. & Saltzman, W.M. Bioengineering approaches to controlled protein delivery. *Pediatr Res* **63**, 513-519 (2008).

153. van der Walle, C.F., Sharma, G. & Ravi Kumar, M. Current approaches to stabilising and analysing proteins during microencapsulation in PLGA. *Expert Opin Drug Deliv* **6**, 177-186 (2009).

154. Zhu, G., Mallery, S.R. & Schwendeman, S.P. Stabilization of proteins encapsulated in injectable poly (lactide- co-glycolide). *Nat Biotechnol* **18**, 52-57 (2000).

155. Hendel, R.C., *et al.* Effect of intracoronary recombinant human vascular endothelial growth factor on myocardial perfusion: evidence for a dose-dependent effect. *Circulation* **101**, 118-121 (2000).

156. Galiano, R.D., Michaels, J.t., Dobryansky, M., Levine, J.P. & Gurtner, G.C. Quantitative and reproducible murine model of excisional wound healing. *Wound Repair Regen* **12**, 485-492 (2004).

157. Fujio, Y. & Walsh, K. Akt mediates cytoprotection of endothelial cells by vascular endothelial growth factor in an anchorage-dependent manner. *J Biol Chem* **274**, 16349-16354 (1999).

158. Vinals, F. & Pouyssegur, J. Confluence of vascular endothelial cells induces cell cycle exit by inhibiting p42/p44 mitogen-activated protein kinase activity. *Mol Cell Biol* **19**, 2763-2772 (1999).

159. Rousseau, S., Houle, F., Landry, J. & Huot, J. p38 MAP kinase activation by vascular endothelial growth factor mediates actin reorganization and cell migration in human endothelial cells. *Oncogene* **15**, 2169-2177 (1997).

160. Gee, E., Milkiewicz, M. & Haas, T.L. p38 MAPK Activity Is Stimulated by Vascular Endothelial Growth Factor Receptor 2 Activation and Is Essential for Shear Stress-Induced Angiogenesis. *Journal of Cellular Physiology* **222**, 120-126 (2010).

161. Funahashi, Y., *et al.* Notch regulates the angiogenic response via induction of VEGFR-1. *J Angiogenes Res* **2**, 3 (2010).

162. Nakatsu, M.N., *et al.* Angiogenic sprouting and capillary lumen formation modeled by human umbilical vein endothelial cells (HUVEC) in fibrin gels: the role of fibroblasts and Angiopoietin-1. *Microvasc Res* **66**, 102-112 (2003).

163. Brooks, P.C., Clark, R.A.F. & Cheresh, D.A. Requirement of Vascular Integrin Alpha(V)Beta(3) for Angiogenesis. *Science* **264**, 569-571 (1994).

164. Lu, H.D., Charati, M.B., Kim, I.L. & Burdick, J.A. Injectable shear-thinning hydrogels engineered with a self-assembling Dock-and-Lock mechanism. *Biomaterials* **33**, 2145-2153 (2012).

165. Silva, D., *et al.* Synthesis and characterization of designed BMHP1-derived self-assembling peptides for tissue engineering applications. *Nanoscale* **5**, 704-718 (2013).

166. Deming, T.J. Polypeptide hydrogels via a unique assembly mechanism. *Soft Matter* **1**, 28-35 (2005).

167. Szyperski, T., *et al.* Pulmonary surfactant-associated polypeptide C in a mixed organic solvent transforms from a monomeric alpha-helical state into insoluble beta-sheet aggregates. *Protein Science* **7**, 2533-2540 (1998).

168. Velluto, D., Demurtas, D. & Hubbell, J.A. PEG-b-PPS diblock copolymer aggregates for hydrophobic drug solubilization and release: Cyclosporin A as an example. *Mol Pharmaceut* **5**, 632-642 (2008).

169. Li, J., *et al.* Self-assembled supramolecular hydrogels formed by biodegradable PEO-PHB-PEO triblock copolymers and alpha-cyclodextrin for controlled drug delivery. *Biomaterials* **27**, 4132-4140 (2006).

170. Ishikawa, M. & Hashimoto, Y. Improvement in aqueous solubility in small molecule drug discovery programs by disruption of molecular planarity and symmetry. *J Med Chem* **54**, 1539-1554 (2011).

171. Miura, Y., *et al.* Cyclic RGD-linked polymeric micelles for targeted delivery of platinum anticancer drugs to glioblastoma through the blood-brain tumor barrier. *ACS Nano* **7**, 8583-8592 (2013).

172. Trimaille, T., Mondon, K., Gurny, R. & Moller, M. Novel polymeric micelles for hydrophobic drug delivery based on biodegradable poly(hexyl-substituted lactides). *Int J Pharm* **319**, 147-154 (2006).

173. Martin-Banderas, L., *et al.* Functional PLGA NPs for oral drug delivery: recent strategies and developments. *Mini Rev Med Chem* **13**, 58-69 (2013).

174. Friedman, D.I., Schwarz, J.S. & Weisspapir, M. Submicron emulsion vehicle for enhanced transdermal delivery of steroidal and nonsteroidal antiinflammatory drugs. *J Pharm Sci* **84**, 324-329 (1995).

175. Shimizu, T., *et al.* Nanogel DDS enables sustained release of IL-12 for tumor immunotherapy. *Biochem Bioph Res Co* **367**, 330-335 (2008).

176. Zhang, J., *et al.* Physically associated synthetic hydrogels with long-term covalent stabilization for cell culture and stem cell transplantation. *Adv Mater* **23**, 5098-5103 (2011).

177. Zhang, J.J., *et al.* Physically Associated Synthetic Hydrogels with Long-Term Covalent Stabilization for Cell Culture and Stem Cell Transplantation. *Advanced Materials* **23**, 5098-5103 (2011).

178. Napoli, A., Tirelli, N., Wehrli, E. & Hubbell, J.A. Lyotropic behavior in water of amphiphilic ABA triblock copolymers based on poly(propylene sulfide) and poly(ethylene glycol). *Langmuir* **18**, 8324-8329 (2002).

179. Olsen, B.D., Kornfield, J.A. & Tirrell, D.A. Yielding Behavior in Injectable Hydrogels from Telechelic Proteins. *Macromolecules* **43**, 9094-9099 (2010).

180. Malten, K.E. & Denarend, J. Topical Toxicity of Various Concentrations of Dmso Recorded with Impedance Measurements and Water-Vapor Loss Measurements - Recording of Skin Adaptation to Repeated Dmso Irritation. *Contact Dermatitis* **4**, 80-92 (1978).

181. Chapnick, D.A. & Liu, X.D. Leader cell positioning drives wound-directed collective migration in TGF beta-stimulated epithelial sheets. *Molecular Biology of the Cell* **25**, 1586-1593 (2014).

182. Illingworth, K.D., *et al.* How to minimize infection and thereby maximize patient outcomes in total joint arthroplasty: a multicenter approach: AAOS exhibit selection. *J Bone Joint Surg Am* **95**, e50 (2013).

183. Lentino, J.R. Prosthetic joint infections: bane of orthopedists, challenge for infectious disease specialists. *Clin Infect Dis* **36**, 1157-1161 (2003).

184. Best, J.T. Revision total hip and total knee arthroplasty. *Orthop Nurs* **24**, 174-179; quiz 180-171 (2005).

185. Blom, A.W., *et al.* Infection after total knee arthroplasty. *J Bone Joint Surg Br* **86**, 688-691 (2004).

186. Bozic, K.J., *et al.* The epidemiology of revision total hip arthroplasty in the United States. *J Bone Joint Surg Am* **91**, 128-133 (2009).

187. Jafari, S.M., Coyle, C., Mortazavi, S.M.J., Sharkey, P.F. & Parvizi, J. Revision Hip Arthroplasty Infection is the Most Common Cause of Failure. *Clin Orthop Relat R* **468**, 2046-2051 (2010).

188. Kurtz, S., Ong, K., Lau, E., Mowat, F. & Halpern, M. Projections of primary and revision hip and knee arthroplasty in the United States from 2005 to 2030. *J Bone Joint Surg Am* **89**, 780-785 (2007).

189. Del Pozo, J.L. & Patel, R. Clinical practice. Infection associated with prosthetic joints. *N Engl J Med* **361**, 787-794 (2009).

190. Zimmerli, W., Trampuz, A. & Ochsner, P.E. Prosthetic-joint infections. *N Engl J Med* **351**, 1645-1654 (2004).

191. Kruckenhauser, E.M., Nogler, M. & Coraca-Huber, D. Use of lavage fluids in arthroplasty to prevent postoperative infections. *Drug Res (Stuttg)* **64**, 166-168 (2014).

192. Qadir, R., *et al.* Establishing a role for vancomycin powder application for prosthetic joint infection prevention-results of a wear simulation study. *J Arthroplasty* **29**, 1449-1456 (2014).

193. Alijanipour, P., Heller, S. & Parvizi, J. Prevention of Periprosthetic Joint Infection: What Are the Effective Strategies? *J Knee Surg* **27**, 251-258 (2014).

194. Shirai, T., *et al.* Antimicrobial megaprostheses supported with iodine. *J Biomater Appl* **29**, 617-623 (2014).

195. Fulkerson, E., *et al.* Antibiotic susceptibility of bacteria infecting total joint arthroplasty sites. *Journal of Bone and Joint Surgery-American Volume* **88A**, 1231-1237 (2006).

196. Salgado, C.D., Dash, S., Cantey, J.R. & Marculescu, C.E. Higher risk of failure of methicillin-resistant Staphylococcus aureus prosthetic joint infections. *Clin Orthop Relat R*, 48-53 (2007).

197. Walls, R.J. Surgical site infection with methicillin-resistant Staphylococcus aureus after primary total hip replacement Reply. *Journal of Bone and Joint Surgery-British Volume* **90B**, 1536-1537 (2008).

198. Howden, B.P., Davies, J.K., Johnson, P.D.R., Stinear, T.P. & Grayson, M.L. Reduced Vancomycin Susceptibility in Staphylococcus aureus, Including Vancomycin-Intermediate and Heterogeneous Vancomycin-Intermediate Strains: Resistance Mechanisms, Laboratory Detection, and Clinical Implications. *Clin Microbiol Rev* **23**, 99-+ (2010).

199. Aslam, S., Trautner, B.W., Ramanathan, V. & Darouiche, R.O. Combination of tigecycline and N-acetylcysteine reduces biofilm-embedded bacteria on vascular catheters. *Antimicrob Agents Ch* **51**, 1556-1558 (2007).

200. Cafiso, V., Bertuccio, T., Spina, D., Purrello, S. & Stefani, S. Tigecycline inhibition of a mature biofilm in clinical isolates of Staphylococcus aureus : comparison with other drugs. *FEMS Immunol Med Microbiol* **59**, 466-469 (2010).

201. Cai, Y., Wang, R., Liang, B., Bai, N. & Liu, Y. Systematic review and meta-analysis of the effectiveness and safety of tigecycline for treatment of infectious disease. *Antimicrob Agents Chemother* **55**, 1162-1172 (2011).

202. Brand, A.M., de Kwaadsteniet, M. & Dicks, L.M.T. The ability of nisin F to control Staphylococcus aureus infection in the peritoneal cavity, as studied in mice. *Lett Appl Microbiol* **51**, 645-649 (2010).

203. Faust, N., Varas, F., Kelly, L.M., Heck, S. & Graf, T. Insertion of enhanced green fluorescent protein into the lysozyme gene creates mice with green fluorescent granulocytes and macrophages. *Blood* **96**, 719-726 (2000).

204. Bernthal, N.M., *et al.* A mouse model of post-arthroplasty Staphylococcus aureus joint infection to evaluate in vivo the efficacy of antimicrobial implant coatings. *PLoS One* **5**, e12580 (2010).

205. Pribaz, J.R., *et al.* Mouse model of chronic post-arthroplasty infection: noninvasive in vivo bioluminescence imaging to monitor bacterial burden for long-term study. *J Orthop Res* **30**, 335-340 (2012).

206. John, A.K., *et al.* Efficacy of Daptomycin in Implant-Associated Infection Due to Methicillin-Resistant Staphylococcus aureus: Importance of Combination with Rifampin. *Antimicrob Agents Ch* **53**, 2719-2724 (2009).

207. Saginur, R., *et al.* Multiple combination bactericidal testing of staphylococcal biofilms from implant-associated infections. *Antimicrob Agents Chemother* **50**, 55-61 (2006).

208. Saleh-Mghir, A., Muller-Serieys, C., Dinh, A., Massias, L. & Cremieux, A.C. Adjunctive Rifampin Is Crucial to Optimizing Daptomycin Efficacy against Rabbit Prosthetic Joint Infection Due to Methicillin-Resistant Staphylococcus aureus. *Antimicrob Agents Ch* **55**, 4589-4593 (2011).

209. Lora-Tamayo, J., *et al.* A large multicenter study of methicillin-susceptible and methicillin-resistant Staphylococcus aureus prosthetic joint infections managed with implant retention. *Clin Infect Dis* **56**, 182-194 (2013).